Personalized neoantigen-targeting cancer vaccines in ovarian cancer: a phase 1 trial

MacLean C. Sellars[1,2], Jessica A. Frank[1, 2], Bohoon Shim[3], Allison Vanasse[4], Ruolin Liu[5], Cleo Forman[1, 3], Chloe R. Tu[1, 3], Kyohei K. Tabata[1], Antonia Kowelewski[2, 5], Su-Chun Cheng[3,6], Catherine Song[5], Kan Xiong[5], Pia Jain[5], Andjela Crnjac[5], Haley E. Sax[1], Vipheaviny Chea[4], Wesley Lu[4], J. Thomas Janes 3rd [4], Micah Rickles-Young[5], Amit Sud[1,7], Savni Sarolkar[1], Martin Hayes[1], Oriol Olive[1], Haley Greenslade[1], Carrie Cibulskis[5], Nir Hacohen[2, 5, 8], Edward F. Fritsch[1, 5], Shuqiang Li[4, 5], Kenneth J. Livak[4], Nabihah Tayob[3, 6], Elizabeth H. Stover[1, 2], Carolyn Krasner[1, 2], Rebecca Porter[1, 2], Ursula Matulonis[1,2], Gad Getz[5, 9, 10], Giacomo Oliveira[1, 2], Patrick A. Ott[1, 2, 5, 11, 12], Jeremy M. Simon[3, 6], Viktor A. Adalsteinsson[5], Derin B. Keskin[1, 2, 4, 5, 13, 14], Panagiotis A. Konstantinopoulos[1,2,15, *], Catherine J. Wu[1, 2, 5, 12,*]

*These authors contributed equally and are both corresponding authors
Corresponding Authors: Catherine_Wu@dfci.harvard.edu, Panogiotis_Konstantinopoulos@dfci.harvard.edu

Affiliations:
[1] Department of Medical Oncology, Dana-Farber Cancer Institute, Boston, MA, USA
[2] Harvard Medical School, Boston, MA, USA
[3] Department of Data Science, Dana-Farber Cancer Institute, Boston, MA, USA
[4] Translational Immunogenomics Laboratory, Dana-Farber Cancer Institute, Boston, MA, USA
[5] Broad Institute of MIT and Harvard, Cambridge, MA, USA
[6] Department of Biostatistics, Harvard T.H. Chan School of Public Health
[7] Centre for Immuno-Oncology, Nuffield Department of Medicine, University of Oxford, Oxford, UK
[8] Krantz Family Center for Cancer Research, Massachusetts General Hospital, Boston, MA, USA
[9] Department of Pathology, Massachusetts General Hospital, Boston, MA, USA
[10] Department of Pathology, Harvard Medical School, Boston, MA, USA
[11] Center for Immuno-Oncology, Dana-Farber Cancer Institute, Boston, MA, USA
[12] Department of Medicine, Brigham and Women's Hospital, Boston, MA, USA
[13] Section of Computational Biomedicine, Department of Medicine, Boston University School of Medicine
[14] Department of Medical Education and Biomedical Sciences, Methodist University CFVH School of Medicine, Fayetteville, North Carolina, USA
[15] Mellen and Eisenson Family Center for BRCA and Related Genes, Dana-Farber Cancer Institute, Boston, MA, USA

ABSTRACT

Personalized neoantigen-targeting cancer vaccines (PCV) in the adjuvant setting are of increasing interest across malignancies. Herein, we report the results of a first-in-disease phase I clinical trial testing the feasibility and safety of PCV for high-grade epithelial ovarian cancer (HGOC). 'NeoVax' consisted of pools of synthetic long peptides targeting patient-specific neoantigens admixed with the immunostimulant polyICLC, was combined with delayed administration of anti-PD-1 antibody, and was tested in 10 patients (one newly diagnosed patient (Cohort A) and 9 patients at first recurrence (Cohort B)) with platinum-sensitive OC following standard-of-care (SOC) platinum doublet chemotherapy. Nine of 12 evaluable Cohort B patients were vaccinated (75%, 90% CI 47-93%) and 1 of 9 Cohort A patients (11%, 90% CI 0.6 – 43%). No unexpected safety signals were encountered and no patients discontinued treatment due to toxicity. Across patients, >70% selected targets remained detectable by non-invasive cell-free DNA analysis despite a median of 6.5 months from the time of diagnostic biopsy to vaccine administration, during which patients received SOC chemotherapy. Biomarker analysis was suggestive of biologic activity of the vaccine in 6 of 10 patients and this was associated with broader tumor and vaccine-specific immune responses in blood and tumor following vaccination. Resistant tumor clones reflected diverse mechanisms affecting antigen presentation, indicative of immune-selective pressure exerted by vaccination. Overall, the interplay between the repertoire of antigens presented by the tumor and the breadth of induced immunity appeared to dictate clinical efficacy following vaccination. ClinicalTrials.gov Identifier: NCT04024878

INTRODUCTION

Epithelial ovarian cancers, 90% of which are *TP53* mutant, high grade serous type, were among the first malignancies for which the frequency of CD8 tumor infiltrating lymphocytes (TIL) and their ratio to regulatory T cells (Treg) were associated with overall survival[1,2]. However, OC has largely not benefited from modern cancer immunotherapy. Anti PD-(L)1 monotherapy induces objective responses in <10% of patients with ovarian cancer[3,4] and the addition of immune checkpoint blockade (ICB) to standard cytotoxic therapy has only recently received FDA approval[5], after multiple negative trials. Underlying reasons include tumor heterogeneity, low tumor mutation burden (TMB)[6], systemic immune suppression[7], and an immunosuppressive microenvironment, characterized by suppressive myeloid populations[8], Tregs[2,9] and stromal cells[8]. Furthermore, most OC tumors exhibit immune desert or immune excluded immunopathology[10], likely reflecting poor priming of endogenous immune responses.

The rate of HGOC missense mutations arising from single nucleotide variants (SNVs) and short insertions and deletions (INDELs) is similar to other low TMB malignancies in which PCVs have generated vaccine-specific immunity[11-13]. We hypothesized that PCVs in the adjuvant setting following SOC therapy would directly address tumor heterogeneity and overcome deficiencies in immune priming, allowing anti-tumor T cell responses to be initiated, amplified, and diversified. Moreover, PCV administration after chemotherapy (and in select cases, surgery) at a time of low tumor burden, could potentially provide consolidating therapy and prevent recurrence. We thus conducted an phase 1 study integrating PCV into SOC therapy for platinum-sensitive HGOC.

RESULTS

Integrating a PCV with standard-of-care treatment for ovarian cancer

The study enrolled patients with newly diagnosed disease (cohort A), or with first platinum-sensitive recurrence (cohort B) (NCT04024878). Adjuvant NeoVax was administered as 5 priming doses over 3 weeks followed by booster doses at 12 and 20 weeks, with ICB (nivolumab) starting at week 14 (**Fig. 1a, Methods**). All patients underwent a tissue biopsy prior to starting SOC chemotherapy; newly diagnosed patients received interval cytoreductive surgery after 3 cycles. Feasibility and safety were the primary endpoints; for feasibility, <45% of prescreening patients achieving vaccination was defined as unacceptable (see **Supplementary Information** for full accounting of pre-defined endpoints). From November 20, 2020 to September 7, 2023, twenty-two patients consented to prescreening (**Fig 1b**); of these, 1 withdrew prior to prescreening biopsy and 9 subjects withdrew from the study before treatment consent (inadequate tissue from core needle biopsies [4], progression on SOC therapy [2], preference [2], and impaired performance status [1]). In total, 12 patients consented to treatment, and PCVs were designed and successfully synthesized for 11 patients (**Methods, Extended Data Fig. 1**); one patient withdrew consent prior to vaccine manufacture and one prior to treatment. In sum, nine of 12 evaluable Cohort B patients were successfully vaccinated (75%, 90% CI 47-93%) and one of 9 Cohort A patients (11%, 90% CI 0.6 – 43%) (**Fig 1b**).

Amongst the 10 vaccinated patients (**Fig. 1b**), their tumors harbored a median of 103 missense mutations (SNV and INDELs; range 51-150) (**Fig. 1c-top, Supplementary Table 1**), corresponding to a median TMB of 2.8 (range 1.4-4.1). Of these mutations, a median of 86.5 (range 45-127) encoded neoepitopes predicted to bind at least weakly (rank<2.0 by either class

I epitope prediction tools HLAthena[14] or NetMHCpanv4.0[15]) to the personal study subject HLA alleles **(Supplementary Table 2)**. Vaccines targeted a median of 14 mutations (range 7-15), consisting of a median of 15 peptides (range 8–18), 17-32 amino acids long (median: 23), that were allocated to 1 of 4 peptide pools (A-D) per patient **(Fig. 1d, Supplementary Table 3),** and administered subcutaneously/intradermally (sc/id) at each of 4 injection sites.

Median follow up after vaccination initiation was 6.3 months (range 3.9-21.3) at the time of the data cutoff (December 31, 2025). The median platinum-free interval (PFI) prior to sample collection for the 9 patients with recurrent disease was 19.7 months (range 7.9-51.5). Six patients entered into the clinical trial following progression through first-line maintenance therapy (PARP inhibitor [5], bevacizumab [1] [**Table 1, Fig. 1e**]); two others previously completed first-line maintenance PARPi therapy without progression. Four patients exhibited rising CA125 prior to starting vaccination (P106, P108, P114, P117), suggesting emergence of platinum refractory/resistant disease; three others exhibited signs of recurrence between priming (days 1-21) and the first booster dose at day 78 (P113 by imaging; P116 by rising CA125; P111 by both). Per protocol, treatment was allowed post-progression, if deemed that patients were deriving clinical benefit, progression was not rapid, treatment was tolerated, and continued treatment did not delay intervention to prevent serious complications of disease.

The study regimen was well-tolerated, without unexpected treatment-related adverse events (AEs, **Table 2**). The most common NeoVax-associated AEs were injection site reactions (70%), myalgias (50%), chills (50%) and neutropenia (50%); two grade 3 AEs occurred in one patient each (allergic reaction, neutropenia). In one patient (P111), grade 3 abdominal pain and

diarrhea were associated with Nivolumab. The primary safety endpoint was to report the percentage of patients who complete vaccine therapy without discontinuation due to toxicity. Nine of 10 vaccinated patients received all planned vaccine doses. P111's G3 ICB-associated diarrhea occurred in the context of progression on post-progression Nivolumab treatment, and was not considered the primary factor in discontinuing therapy (**Supplementary Information**). Thus, all evaluable, treatment-consented patients completed NeoVax and Nivolumab without discontinuation for toxicity (Cohort A: 1 of 1 [90% CI: 5-100%], Cohort: B 8 of 8 [90% CI: 69-100%]).

In the intervening months between the vaccine design biopsy (B1), and vaccine priming (median of 6.5 months; range 6.0-7.6), patients received SOC chemotherapy +/- surgery. As an *ad hoc* analysis, we interrogated the extent to which somatic mutations encoding neoantigens were still present at the start of vaccination via bespoke cell-free DNA (cfDNA) analysis ('MRD Tracker'[16], **Methods**). We detected > 50% of vaccine target SNV mutations for 7 of 10 subjects at priming (D1 or D15), and for an 8th, prior to the last NeoVax boost (D140). In aggregate, 56.5% and 73.1% of target SNV mutations were detected at priming and by the last boost, respectively (**Fig 1f**), indicating that vaccines remained relevant to tumor mutations present at the time of vaccine administration, despite intervening treatment.

Patterns of tumor biomarker and vaccine immune responses following NeoVax plus nivolumab

Progression-free survival (PFS) after vaccination was highly variable (median 3.3 months, range 1-NR). We used blood-based CA125 and cfDNA-based assays to indirectly track tumor

burden across organ sites over time. Nine of 10 patient tumors expressed plasma CA125 (all except P113); all subjects were analyzable with bespoke MRD Tracker assays, using a median of 900 (range 160-950) coding and non-coding SNV mutations, to assess average tumor variant allele frequencies (VAFs) and limits of detection by time point (**Fig 2a-c**; **Extended Data Fig 2**).

We observed three patterns of tumor-burden response (see **Methods**). First, four patients were "progressors" (P111, P113, P114, P117), exhibiting progression by RECIST criteria prior to vaccine boosting *and* steep and unabated rises in CA125 and/or cfDNA VAF following vaccination. In the case of P114, an early stabilization of cfDNA was attributed to palliative radiation of a residual, symptomatic vaginal cuff lesion in week 5, followed by rising biomarkers (**Fig. 2a)**.

A second group also exhibited early rising CA125 and cfDNA (P106 and P108 prior to starting priming; P116 prior to first boost), but in contrast to the trend for progressors, both measures concordantly leveled-off or decreased around the first booster dose (D78+/-7), before eventually rising again (**Fig. 2b**), suggesting "transient control" of disease. For P106 and P108, the timing of biomarker-measured control before the start of nivolumab (D92+/-7)) was consistent with an effect from vaccination. For P116, the CA125 and cfDNA declines occurred following nivolumab administration and while on SOC PARPi maintenance therapy.

Finally, three patients exhibited prolonged disease control (P118, P119, P122), in which CA125 remained consistently low following vaccination (**Fig. 2c**). P118 exhibited a partial response to

SOC chemotherapy, with normalization of CA125, but residual disease by imaging; P119 and P122 were in complete response (CR) following SOC chemotherapy. Strikingly, despite persistently low CA125 levels, all three patients exhibited dynamic cfDNA changes between D15 and D300, suggesting episodes of tumor growth and regression, with vaccination and nivolumab as the only interventions. For P122, cfDNA levels peaked at D140 and then decreased to below the limit of detection (D274), with the patient remaining disease free through to data cut off (Day 650) (**Fig. 1e, Fig. 2c; Extended Data Fig. 2)**.

Overall, these *ad hoc* serologic tumor burden analyses reveal dynamic changes in serum biomarkers for 6 of 10 patients, which may be consistent with on target immunologic activity from combined NeoVax with nivolumab.

Peripheral immune responses following NeoVax

To define the extent to which NeoVax followed by nivolumab elicited circulating vaccine peptide-specific T cell responses and whether these differed amongst the biomarker subgroups, we performed exploratory *ex vivo* IFN-γ ELISpot assays on pre- and serially collected post-vaccine PBMC, using treatment pools of full-length 17-32-mer immunizing peptides. In 8 of 10 patients, we detected *ex vivo* IFN-γ reactivity[17] to at least one vaccine pool, most commonly peaking after the week 12 boost (**Fig. 2d, Extended Data Fig. 3a**). To define the immunogenicity of individual peptides, we further tested each immunizing peptide for its ability to stimulate IFNγ reactivity using post-boost PBMCs (after first ['week 14', W14] or second boost ['week 22', W22]) that were expanded *in vitro* against vaccine peptide pools. Overall, 85 of 144 (59.0%) peptides were immunogenic (**Extended Data Fig. 4)**. A median of 7 peptides (range 4-15), from

a median of 7 mutations (range 4-13) were immunogenic, per patient. Of note, the vaccines of the 6 patients with transient or prolonged disease control induced immune responses to a larger number of vaccine target mutations than for progressors (mean 9.3 vs. 5.5 mutations; $P = 0.029$) (**Fig. 2e**); there was also a trend towards an increased number of targeted mutations for transient and prolonged controllers (mean 14.3 vs. 10.5 mutations; $P = 0.132$; **Fig. 2f**). No differences were found between the serum biomarker-defined groups in relation to immunogenicity rate, missense mutation burden, PFI (**Fig. 2g-i**), or frequency of recurrence on active PARPi treatment prior to prescreening consent ($P = 0.77$ [Chi Square]).

To identify vaccine- and nivolumab-induced TCR clonotypes, we assessed peripheral TCRβ chain dynamics in $CD3^+$ PBMC across the vaccination course for all subjects (**Methods**; **Extended Data Fig. 3b-c**). A median of 82.5 (range 7-150) NeoVax-, and 96.5 (range 18-650) post-nivolumab-expanded clonotypes **(**Fisher's exact test $P < 0.05$; **Extended Data Fig. 3b)** were detected. In two transient controllers (P108, P116) for whom TCRβ clonotypes at a later timepoint (~ W40) could be assessed, post-NeoVax- and post-nivolumab-expanded clonotypes were long-lived, comprising a similar frequency of the TCR repertoire at W40 as at W14 and W22 (**Extended Data Fig. 3c**), consistent with T cell memory responses.

Identification of immune populations in NeoVax patient biopsies

We collected and processed fresh tumor biopsies from 6 of 10 patients for single cell (sc) RNA- and TCR- sequencing (**Fig. 3a**). These included biospecimens collected at individual time points (B1, B2, and B3) for three disease progressors (P117, P111, P114), and paired pre- and post-vaccine time points for one progressor (P113) and two transient controllers (P108, P116).

To increase resolution of cell type identification, a pre-vaccine sample was included for one additional patient who did not proceed with vaccination due to progression (P112). We obtained 25,103 high-quality single-cell transcriptomes (median 7,371 UMI/cell, 3,045 genes/cell). By unsupervised clustering, we identified 16 clusters comprised of diverse immune and non-immune cells (e.g. tumor, fibroblasts) **(Fig. 3b, Extended Data Fig. 5a**). Progressors exhibited a trend towards higher intratumoral fractions of monocyte/macrophages (**Fig. 3b-c**), which expressed inhibitory receptors (e.g. *VSIR*, *TNFRSF14*, *LGALS9*, *SIRPA*; **Supplementary Fig. 1a**), consistent with a suppressive role. In contrast, higher fractions of T/NK and B cell populations were detected in transient controllers than in progressors (**Fig. 3b-c**).

To better understand the interaction between the intratumoral T cell compartment and treatment with NeoVax with nivolumab, we re-clustered T cell populations (**Extended Data Fig. 5b-c, Supplementary Fig. 1b**). Progressor tumor biopsies contained higher fractions of exhausted T cells (CD4.TTE, CD8.TTE) and Tregs (CD4.TReg, CD4.NR4A1.TReg), as well as a trend towards lower CD8:CD4 ratio **(Fig. 3d**). We observed a higher Shannon diversity index amongst T cell clonotypes in transient controller biopsies (**Fig 3e**; two tailed Mann Whitney test, P = 0.004). Progressor patient P113 uniquely displayed relatively larger numbers of TIL with expanded clonotypes, the majority of which represented T_{EX} phenotypes (**Extended Data Fig 5d-e**). While limited by the number of paired pre- and post-vaccine biopsies, we noted a trend toward higher Treg fractions amongst progressor patients, and increased intratumoral T cell clonotype diversity amongst transient controllers.

Assessment of TIL tumor and vaccine target reactivity following NeoVax

To discern the extent to which TIL might recognize tumor and vaccine target antigens, we analyzed the T cell responses of P108 (transient controller) and P113 (progressor), whose tumors had been profiled at single cell resolution over time and from which patient-derived organoids (PDO) had been generated. The source cells for P108 PDO (O108-B2; **Fig. 3f**) were obtained on D126, ~1 month after booster 1 and the initiation of nivolumab; we were unable to generate a PDO from pre-treatment cells (B1). For P108, 45 of 83 mutations were detected at the RNA level from the B1 biopsy, including 13 of 14 vaccine target mutations. All O108-B2 *TP53* reads mapped to the parental tumor's *TP53* mutation, reflecting pure tumor origin. However, only 13 of 83 somatic missense variants, and only 3 of 14 vaccine target mutations were expressed, consistent with either lost target antigen expression in the subclone represented in the biopsied recurrence or subclone selection during organoid generation. We observed less clonal evolution in the tumors from P113, from which we propagated PDO lines from 2 independent biopsies (**Fig 3g**): (i) the "pre-Vax" B1 biopsy procured prior to SOC chemotherapy from a left upper quadrant abdominal wall mass (O113-B1); and (ii) the "post-Vax" B2 biopsy, procured on D95, 17 days after booster 1 and 4 days after nivolumab initiation, from an abdominal wall lesion at the same site as B1 (O113-B2). All *TP53* RNAseq reads from the O113 lines represented the tumor variant allele, and >50% of B1 missense mutations were expressed (including 4 and 5 of 9 vaccine target mutations for O113-B1 and -B2, respectively); 58.4% (59 of 101) of the B1 mutations were expressed in the parental tumor RNA.

Expanded TIL clonotypes with an exhausted phenotype (T_{EX}) in solid tumors have been reported to be enriched for tumor-reactive cells[18,19], including a small series of TIL TCRs in ovarian cancer[20], whereas expanded effector memory (T_{EM}) TIL clonotypes are enriched for viral

specificity[18]. To confirm this in OC and in the PCV setting, we evaluated 14 expanded T_{EX} clonotypes (having ≥ 3 cells through the entire data set, majority from the CD8.TTE cluster) and 9 expanded T_{EM} clonotypes identified from the B1 and B2 biopsies of P108 (**Extended Data Fig 5e**; **Supplementary Table 4**). Thirteen of 14 T_{EX} clonotypes were present in the post-vaccine B2 biopsies and 11 of 14 were more highly represented in the post- vs. pre-vaccine biopsies, consistent with post-vaccine/nivolumab expansion. Cloning and specificity testing of individual clonotypes revealed that 9 (5 strong, 4 borderline) of 14 expanded T_{EX} clonotypes (but only 1 (borderline) of 9 T_{EM} TCRs) exhibited CD137 upregulation after co-culture with O108-B2 PDO (**Fig. 3h; Extended Data Fig. 6a-b**). Five of 9 T_{EM} TCRs exhibited reactivity against autologous EBV-immortalized lymphoblastoid cell lines (LCL). These data confirmed that the T_{EX} and T_{EM} TIL are enriched for tumor and viral reactivity, respectively[18]. We did not identify NeoVax-specific clonotypes amongst tested P108 TIL. As O108-B2 lacked expression of the majority of vaccine target antigens, we interpreted the presence of TIL tumor-reactivity in the absence of vaccine reactivity as potentially consistent with epitope spreading of T cell responses to non-vaccine target antigens.

Analogous evaluation of P113 revealed a strikingly different pattern of TIL reactivity. P113 biopsies B1, B2 and B3 captured more T cells than for P108, including a higher proportion of T_{EX} cells, and a larger number of expanded clonotypes (**Extended Data Fig. 5d-e**). We cloned and tested TCRs from 22 expanded T_{EX} clonotypes (in this case, each representing > 10 cells), including the top 6 expanded exhausted TCRs in each biopsy (**Extended Data Fig. 5e**; **Supplementary Table 4**). TCRs from 20 of 22 T_{EX} cells reacted strongly to Pre-Vax O113-B1, with the level of CD137 upregulation generally increased by PDO pretreatment with IFNγ (**Fig 3i, Extended Data Fig. 6a**

& c, Supplementary Table 4); 19 recognized Post-Vax O113-B2, but generally with lower levels of CD137 upregulation when compared to co-incubation with O113-B1 (**Fig. 3j**). Of the 3 expanded T_{EM} clonotypes (≥6 cells) tested, 2 recognized autologous EBV-LCL, again consistent with enrichment of viral antigen specificity in the T_{EM} compartment; 1 of these, exhibited reactivity to both B1 and B2 PDO. Overall, the majority of expanded T_{EX} TIL recognized autologous PDO, with the highest reactivity against the Pre-Vax PDO.

Pulsing of P113 autologous EBV-LCLs with vaccine peptide pools prior to co-incubation with cloned TIL-TCRs, revealed 4 T_{EX} TCRs (5, 6, 19 and 20), which recognized vaccine pool C. All four were reactive against the same DPP3 p.L658R epitope, LT**R**RDTVLL (**Fig 3j; Extended Data Fig 6e-f**). TCR6 had the highest avidity, followed by TCR20, TCR5 and TCR19 (**Fig 3k**). Only TCRs 5, 19, and 20 were present in B1, where they comprised ~15% of T_{EX} cells, and 12.5% of antigen-experienced, non-T_{Naive} T cells overall, with TCR5 dominating (**Extended Data Fig 5g**; **Fig 3l**), consistent with a pre-existing immune response. However, in the post-Vax recurrent tumor at B2, all 4 clonotypes were present (TCR 6 was newly detected), with over 80% of the DPP3 p.L658R specific TIL now represented by the two TCRs with highest avidity (6 and 20). The fraction of DPP3 p.L658R-specific, antigen experienced, non-T_{naive} TIL remained relatively stable across the vaccine booster doses, but was dominated by further expansion of the highest avidity TCR6 (**Fig 3l**). This shift was mirrored in the peripheral blood, where we detected circulating TCRβ chains matching TCR 5, 6 and 20 at W14 (after boost 1), with further increased fraction by W22 (**Fig 3m**). Although the distribution of DPP3 p.L658R-specific TIL with non-naïve, T_{TE}, T_{PE}, T_{Prol} and T_{EM} phenotypes was similar between B1 and B2, there was a shift towards $T_{PE,}$ T_{Prol}, and even T_{EM} phenotypes at B3, following booster dose 2 and ~ 6 weeks of nivolumab treatment (**Fig 3n**).

Altogether, these observations support the expansion of vaccine-reactive clonotypes in P113, especially a new high avidity clonotype, following vaccine boost and nivolumab, both in tumor and peripheral blood.

Mechanisms of tumor escape across study subjects

To dissect the potential immune selective pressure imposed by NeoVax with nivolumab, we first assessed if vaccination was linked to changes in tumor transcriptional programs. Bulk tumor RNAseq from B1 pre-vax biopsies revealed relatively similar class I and class II antigen presentation-related gene expression across tumors, with only progressor P117's tumor exhibiting a trend towards lower expression than other tumors (**Supplementary Fig. 2a)**. We next used GSEA analysis of pre- and post-vaccination biopsy scRNA-seq to assess tumor cell transcriptional programs. While this did not reveal any clear mechanisms of immune escape for post-vaccine tumor cells from P108 or P116, P113 post-vaccine and nivolumab (B2 and B3) tumor cells (but not T cells) exhibited significantly down-regulated gene sets related to TNFα, IFNα and IFNγ signaling compared to pre-vaccine (B1) (**Supplementary Fig. 2b; Fig. 4a**). Of note, O113-B2 genomic DNA harbored a chromosome 1 inversion structural variant (SV) at p31.3, affecting the 3rd intron of *JAK1* and an intergenic region ~1.6Mb away (*chr1:64,882,954::chr1:63,277,187* (hg19); **Extended Data Fig. 7a-d).** This breakpoint was not observed in genomic DNA from pre-vaccine B1 whole genome sequencing, nor detectable via PCR from B1-derived PDOs (**Extended Data Fig. 7c-d**), consistent with a treatment emergent SV. RNAseq from only the post-vaccine PDO showed a loss of poly-adenylated RNA derived from *JAK1* exons 4-25 (**Fig. 4b**). As expected, *JAK1* interruption in post-vaccination PDO was associated with abrogation of STAT1 phosphorylation and HLA-I upregulation following IFNγ stimulation compared to pre-vaccination

organoid (**Fig. 4b-c**); it was not associated with resistance to carboplatin and doxorubicin, the SOC chemotherapies received prior to vaccination (**Extended Data Fig. 7e**). Strikingly, re-introduction of *JAK1* cDNA into O113-B2 rescued STAT1 phosphorylation, HLA-I expression and DPP3 p.L558R vaccine-specific TIL TCR recognition (**Fig. 4d, Extended Data Fig. 7f-k)**. Thus, a *JAK1* SV mediating reduced antigen presentation was associated with escape from combined NeoVax with nivolumab therapy in P113.

We asked if there might have been pre-existing mechanisms of immune escape in any of our patients. Loss of heterozygosity (LOH) in the HLA loci on chromosome 6 (chr6) has been previously associated with immune escape[21] and has been reported at least 15% of OC tumors at the time of diagnosis[9,21]. We detected regions of chr6 LOH in tumor cells from B1 biopsies of 3 of 10 vaccinated patients, including 2 of 4 progressors (P111, P117; **Fig 4e** and **Extended Data Fig 8a**); WES data from 6 unvaccinated, prescreening consent patients, revealed 2 further cases of chr6 LOH in the HLA locus, (total 5 of 16 [31%]; **Extended Data Fig 8b**). For P111 and P117, such LOH was associated with loss of an entire haplotype covering HLA-A, B and C (**Extended Data Fig 9)**. Thus, the HLA alleles for a substantial fraction of the best predicted epitopes (by *HLAthena*) for vaccine mutations were lost (3 of 7 for P111; 6 of 16 for P117) and for mutations for which we could measure a peripheral immune response (2 of 4 for P111; 3 of 8 for P117). Taking into account all possible strong and weak binders, >45% of predicted epitopes contained in the immunizing peptides lost their predicted HLA binding allele (**Fig 4e**). Likewise, for the prolonged controller P118, the HLA alleles for the best epitope were lost for 10 of 14 target mutations and 10 of 13 immune response mutations. No new HLA LOH was evident by WES at progression in the 3 patients with a recurrence biopsy (P106, P108, P113), though tumor fraction

of < 20% in the samples tested for P108 and P106, limited sensitivity for LOH analysis. Altogether, across these three patients with chr6 LOH, the HLA alleles for the best predicted vaccine targets were lost for 19 of 36 mutations, constituting substantial baseline compromise of potential vaccine target epitope presentation in tumors. The difference in clinical outcome for P118 vs. P111 and P117, may be related to productive immune responses against an antigen(s) presented by retained HLA alleles, or potentially, other factors.

To better understand the importance of these observations in OC, we asked how allele specific HLA-loss intersects with important clinical ovarian cancer biomarkers: (i) homologous recombination deficiency (HRD) or HR proficiency, which defines the use of PARP inhibitors; and (ii) *CCNE1* amplification, which is enriched in HRP tumors[6], portends worse prognosis, and is an emerging target. Analysis of a TCGA ovarian cohort (n = 160) with paired RNA and WES data revealed a ~31% rate of loss of HLA diversity (25.6% rate of HLA-LOH, 5.6% as loss allele specific expression (ASE) at the RNA level, without detected LOH [data retrieved from Filip et al.[22]]). As high levels of genomic LOH are a defining characteristic of HRD status[23,24], we hypothesized that HLA LOH might be more frequently associated with HRD than HRP tumors. Indeed, across all TCGA tumors, HRD status[24] associated with increased HLA-LOH but not transcriptionally detected loss of HLA ASE. Within OC, however, there were similar levels of HLA-LOH, as well as -ASE, in both HRD and HRP tumors (**Extended Data Fig. 8c**). Similarly, we found no difference in the rate of HLA-LOH or -ASE loss[22] in *CCNE1* amplified vs. non-amplified tumors[25] (**Extended Data Fig. 8d**). These data highlight the broad importance, across biomarker subgroups, of considering HLA allele retention and expression for antigen-directed therapies in high grade OC.

Finally, we asked if there was evidence of immune selective pressure against vaccine target mutations in either recurrence biopsies or by cfDNA, independent of HLA LOH. We were able to generate WES data from recurrence biopsies for P106, P108 and P113; of note, we did not identify any mutations in genes which would be expected to contribute to immune escape (e.g. *TAP1/2*, *B2M*, *JAK/STAT*, etc). For transient controllers P106 and P108, we found 3 of 15 and 6 of 14 vaccine target mutations, respectively, that were lost in the recurrence biopsies (**Fig 4f**). This included the loss of one truncal mutation for P108 (Cancer Cell Fraction (CCF) = 1; *POLQ2* [p.R708G]) and 3 mutations with CCF > 0.5 (*FDFT1* [p.T275S]; *URB1* [p.A1107T]; *ACTR10* [p.A229G]); of note the *URB1* SNV was detected in cfDNA at priming, indicating that it was not lost during SOC chemotherapy prior to vaccination. For P108 we also noted decreased RNA expression of three vaccine target genes *TTC3, FLNA*, and *SRSF3* in B2 vs. B1 biopsy tumor cells by scRNAseq, consistent with transcriptional down-regulation of some vaccine targets, though we could not determine mutant allele expression (**Supplementary Fig. 2**). For P106, two mutations lost at recurrence were truncal (*ARHGAP27* [p.A509G] and *PLCB2* [p.E741Q]) and the third had CCF > 0.5 (*PPP1R12A* [p.R682T]). In contrast, P113, for whom *JAK1* loss globally decreased antigen presentation (**Fig. 3j, 4c-d**), only 1 of 9 vaccine target mutations was lost at recurrence (**Fig 4g**) and no vaccine target mutation genes exhibited decreased RNA expression (**Supplementary Fig. 2**).

To corroborate these results, we asked if we might see differences in cfDNA VAFs of vaccine target SNVs vs. non-target, missense SNVs. Although the small sample size limited our power to identify significant differences, for P106 and P108, we observed a trend towards lower mean VAFs for vaccine target mutations vs. non-target mutations at post-priming timepoints (**Fig 4f**). In

contrast for P113, vaccine target and non-target SNV mutation cfDNA VAFs were similar at all timepoints. In other patients, cfDNA VAFs did not clearly differ between target and non-target mutations (**Extended Data Fig 10**). Taken together, these data suggest differential selective pressure on vaccine target vs. non-target mutations in patients P106 and P108.

DISCUSSION

We report a first-in-disease clinical trial in the low TMB setting of High Grade OC of synthetic long peptide neoantigen vaccination combined with nivolumab as maintenance therapy following SOC chemotherapy +/- cytoreductive surgery. Consistent with efforts in other low TMB diseases[11-13,26], we generated personalized genomics-guided vaccines that induced robust immune responses in all patients.

Non-invasive tumor monitoring utilizing blood serum/plasma biomarkers enabled us to demonstrate vaccine targeting and activity. We confirmed that personalized approaches can be integrated around prolonged SOC treatments via cfDNA-based detection of the majority of vaccine target mutations (designed using pre-treatment biopsies) even after ~6 months of SOC therapy. Further, we demonstrated dynamic cfDNA changes in six of 10 patients, supported by CA125 dynamics, consistent with waves of on-target immune activity; in P122, cfDNA rose during the initial vaccine course, peaking at the time of the final NeoVax booster, before declining to below the LOD, with the patient remaining disease-free through data cut off (>12 months), potentially reflecting immune-mediated disease clearance. Importantly, observed biomarker responses were associated with broader immune responses highlighting the importance of a multi-targeted vaccine, presumably to better address tumor heterogeneity and/or maximize the likelihood of inducing effective on-tumor responses. These data also highlight the utility of cfDNA in adjuvant vaccination trials – allowing both an understanding of vaccine relevance to residual disease, and serving as a biomarker for response. With primary tissue often difficult to access, cfDNA will be a critical biomarker for future studies.

We identified several potential resistance mechanisms (either pre-existing or treatment-emergent) that point to the impact of immune selective pressure. Our analyses highlighted previously identified mechanisms of immune resistance in OC, including elevated T_{reg} fractions[2] and immunosuppressive macrophage/monocyte[10] populations in progression patients. However, the most robust link to therapy resistance in our study was loss of antigen presentation in tumors: two of four primary progressor patients exhibited loss of HLA haplotype heterozygosity prior to vaccination, likely rendering more than half of vaccine antigens off target, and a third subject's tumor revealed treatment-emergent deficiency in interferon signaling, severely abrogating antigen presentation. We further identified evidence of immune editing or suppression by cfDNA and WES in 2 of 3 transient controllers, though we cannot exclude clonal evolution during SOC chemotherapy. Combined with our observation that broader immune response induction correlates with clinical benefit, a common theme emerges around the balance of induced immune responses and the capacity of tumor cells to present immunogenic antigens. Considering that ~31% of tumors analyzed in both our cohort and TCGA ovarian tumors exhibit allele specific HLA loss due to either genomic deletion or transcriptional repression, our work strongly supports recent calls to take into account HLA LOH and mechanisms of antigen presentation loss in vaccine design[27], for example by integrating this information into antigen selection workflows[28].

Finally, our work highlights the importance of choosing an optimal setting for PCV trials. High tumor burden carries with it increased extent of tumor heterogeneity, the fuel for clonal evolution and therapeutic resistance. In this vein, 5 of 10 enrolled patients exhibited progressing tumors at the time of vaccination, largely associated with recurrence on PARP inhibitor at trial

enrollment. We speculate that actively growing tumors, with an established immunosuppressive microenvironment and greater heterogeneity, pose substantial barriers to immune control in a disease that is minimally responsive to PD-1 blockade alone. We assert that introducing PCVs with first line treatment, at times of truly minimal residual disease may be more beneficial. Our work thus argues for (i) early vaccine approaches to target low volume disease, (ii) improved vaccine antigen selection to obtain broad and balanced responses, and (iii) targeting of antigens that tumors retain the HLA machinery to present.

We acknowledge limitations to our study. We experienced accrual challenges to cohort A, due to limited tissue from core needle biopsies and the changing regulatory environment for 1L maintenance; both issues are easily addressed for future studies. Our cohort was small and heterogenous with regards to the degree of platinum sensitivity, limiting our ability draw strong conclusions about clinical efficacy. We have utilized several orthogonal analysis platforms to define clinical benefit and identify resistance mechanisms that point to immunologic efficacy. Nonetheless, deep characterization of resistance mechanisms and cfDNA analysis in future trials will assuredly provide clearer insights into how best to establish vaccine efficacy in difficult-to-treat tumors like HGOC.

Funding Statement

This work was supported by NCI Dana Farber / Harvard Cancer Center Ovarian Cancer SPORE (P50-CA240243-05; to U.A.M, P.A.K, C.J.W), the Mark Foundation Endeavor Award (to C.J.W), NIH/NCI award 5R01CA276865 (to C.J.W.), Breast Cancer Research Fund award (to U.A.M and P.A.K), Friends of Dana Farber (to M.C.S and R.J.P.), the Fund in Memory of Patty Klein, the Feldmann Ovarian Cancer Research Fund, and the Blavatnik Family Foundation. M.C.S. received support from the Lubin Family Foundation, the Dana Farber NIH Medical Oncology training grant (NIH T32CA009172**)** and the Ovarian Cancer Research Association**.** A.S. was supported by a Wellcome Trust Early Career Award (227000/Z/23/Z). S.L is supported by the NCI Research Specialist Award (R50CA251956). E.H.S is supported in part by NCI K08CA237871. G.O. received support from the Claudia Adams Barr Program for Innovative Cancer Research and an American Cancer Society Institutional Research Grant. D.B.K. is supported by U54-CA272688, R01-HL157174, R01-CA285308, R01-CA279391, R01-NS140967 and Alex's Lemonade Stand. P.A.O. is supported in part by NCI-1R01CA229261, the Francis and Adele Kittredge Family Immuno-Oncology and Melanoma Research Fund, the Fisher Family Fund, The Morgan Family Fund for Melanoma Research, the Susana and Bruce Hampton Research Fund and the Faircloth Family Research Fund. C.J.W is a member of the Parker Institute for Cancer Immunotherapy at DFCI. Her work is supported, in part, by the Parker Institute for Cancer Immunotherapy. C.J.W. is also the Lavine Family Chair for Preventative Cancer Therapies at DFCI. The funders had no role in the conduct of the trial or in the analysis of clinical or immunological end points.

Acknowledgement Statement

We are appreciative of S. Hill for input and assistance with tissue processing; A. Afeyan for computational assistance with TCR identification, E. Lin for technical assistance; L. Pomerance for input on immune analyses; B. Igoresceu for input on cell free DNA; S. Pyle for artwork; staff at Almac Sciences for vaccine peptide manufacture; Bristol-Myers Squibb for providing Nivolumab; the DFCI Cell Manipulation Core Facility for sterility and endotoxin testing.

Author Contributions Statement

P.A.K is the principal investigator and directed the overall study. P.A.O. is the IND holder. M.C.S., P.A.K and C.J.W designed and performed experimental and data analysis together with J.A.F., B.S., A.V., R.L, C.F., C.R.T, K.T., S.C., C.S., K.X., P.J., A.C. H.E.S., V.C., W.L., T.J., M.R.Y., K.J.L., S.L., A.S., G.O., and D.B.K; C.F., M.Y.R., C.C., D.B.K., and P.A.K. analyzed sequencing data and selected neoantigen targets; S.C., N.T., and J.M.S. designed and performed statistical analyses; S.S., M.H, O.O., and H.G. coordinated clinical research; R.P., E.H.S, C.K. and U.A.M. were co-investigators on the clinical trial and provided patient samples; M.C.S., R.L., C.S., K.X., P.J., A.C., R.P., and V.A. performed cfDNA analyses; J.A.F., B.S., C.R.T., A.S., A.K., G.G. and J.M.S. performed computational analysis; M.C.S, K.T., H.E.S., and G.O performed TCR/organoid reactivity assays. M.C.S, P.A.K. and C.J.W. wrote the manuscript; all authors discussed and interpreted results and edited the manuscript.

Competing Interests Statement

M.C.S, J.A.F., B.S., A.V., R.L, C.F., C.R.T, K.T., A.K., S.C., C.S., K.X., P.J., A.C. H.E.S., V.C., W.L., T.J.3rd., M.R.Y., A.S., S.S., M.H., O.O., H.G., C.C., S.L., N.T., E.H.S. C.K., R.P., G.O., and J.S.M have nothing to declare. J.K.L. holds equity in Standard BioTools Inc. and is on the scientific advisory board for MBQ Pharma Inc. N.H. holds equity in and advises Repertoire

Immune Medicines, CytoReason, and Danger Bio/Related Sciences, owns equity and has licensed patents to BioNtech, and receives research funding from Bristol Myers Squibb, Moderna, ResolveM/JJDC, Takeda, and Calico Life Sciences. U.A.M. declares participation in scientific advisory boards: NextCure, Abbvie, Immunogen, Profound Bio, Eisai, the Ovarian Cancer Research Alliance, Tango Therapeutics, Novartis, GSK, Daiichi Sankyo, DayOne Bio, and Whitehawk Therapeutics; UAM also reports participation in a data safety-monitoring board: Mural Oncology, Macrogenics, Daiichi Sankyo, Astrazseneca and Symphogen, all unrelated to this work. V.A.A. is a co-inventor of the MAESTRO MRD test which has been licensed to Exact Sciences and receives research funding from Exact Sciences which was not involved in this study. V.A.A. is also a co-founder and advisor to Amplifyer Bio. G.G. receives research funds from IBM, Pharmacyclics/Abbvie, Bayer, Genentech, Calico, Ultima Genomics, Inocras, Google, Kite, AstraZeneca and Novartis and is also an inventor on patent applications filed by the Broad Institute including those related to MSMuTect, MSMutSig, POLYSOLVER, SignatureAnalyzer-GPU, MSEye, MinimuMM-seq, DLBclass, HapASeg, Tonly2, MSIDetect, TuFEst, and ABSOLUTE2. A full list of G.G.'s publicly available patent applications can be requested from the Broad's legal team at patents@broadinstitute.org. G.G is a founder, consultant, and holds privately held equity in Scorpion Therapeutics; he is also a founder of, and holds privately held equity in Predicta Biosciences; and a consultant and holds privately held equity in Antares Therapeutics. D.B.K. owns equity in Affimed N.V., Agenus, Armata Pharmaceuticals, Breakbio, BioMarin Pharmaceuticals, Celldex Therapeutics, Editas Medicine, Immunitybio, Lexicon Pharmaceuticals, Moderna, PDS Biotechnology, Prime Medicine, Sana biotechnologies and Viking Therapeutics. D.B.K. is a scientific advisor for Immunitrack, a wholly owned subsidiary of Eli Lilly and Company and

Breakbio. P.A.O. has received research funding from and/or has advised Agenus, Arcturus, Amgen, Armo BioSciences, Array, AstraZeneca/MedImmune, Bristol-Meyers Squibb, Celldex, CytomX, Evaxion, Immunetune, Imunon, LGChem, Merck, Neon Therapeutics (now BioNTechUS), Novartis, Pharmajet, Phio, Pfizer, Oncorus, Roche/Genentech, Servier, and Xencor. P.A.K. has received grants or contracts from Novartis, AstraZeneca, Pfizer, Eli Lilly, Bayer, Merck, GlaxoSmithKline, Tesaro, and Merck KGaA and has received consulting fees for serving on advisory boards from AstraZeneca, Bayer, GlaxoSmithKline, Alkermes, Kadmon, Bristol Myers Squibb, IMV, Repare, Artios, Mersana, Novartis, Cardiff Oncology, Schrodinger, Inc., Mural Oncology, Scorpion, and Nimbus. C.J.W. is an equity holder of BioNtech, Inc., and is a SAB member of Repertoire, Aethon Therapeutics, Nature's Toolbox and Adventris.

TABLES

Table 1: Baseline characteristics of patients receiving NeoVax:

		Overall (N=10)
Sex	Female	10 (100%)
Age	Mean (SD)	56.3 (6.31)
	Median [Min, Max]	56.4 [47.6, 69.3]
Race	White	9 (90%)
	More Than One Race	1 (10%)
Ethnicity	Hispanic or Latino	2 (20%)
	Non-Hispanic	8 (80%)
Cohort	A	1 (10%)
	B	9 (90%)
PFI	6-12 months	3 (30%)
	>12 months	6 (60%)
	N/A	1 (10%)
Prior PARPi	Yes	7 (70%)
	No	3 (30%)
Histology	Serous	9 (90%)
	Endometroid	1 (10%)
***TP53* Mutation**	Yes	10 (100%)
	No	0 (0%)

Table 2: Treatment related Adverse Events (Grades 1-5), occurring in ≥10% of subjects

AEs related to NeoVax: # of patients (%)	Grade 1	Grade 2	Grade 3	Total
Neutrophil count decreased	2 (20)	2 (20)	1(10)	5 (50)
Allergic reaction	0 (0)	0 (0)	1(10)	1 (10)
Injection site reaction	6 (60)	1 (10)	0(0)	7 (70)
Myalgia	4 (40)	1 (10)	0 (0)	5 (50)
Fatigue	3 (30)	1 (10)	0 (0)	4 (40)
Fever	1 (10)	1 (10)	0 (0)	2 (20)
Alanine aminotransferase increased	0 (0)	1 (10)	0 (0)	1 (10)
Anemia	0 (0)	1 (10)	0 (0)	1 (10)
Lipase increased	0 (0)	1 (10)	0 (0)	1 (10)
Serum amylase increased	0 (0)	1 (10)	0 (0)	1 (10)
Chills	5 (50)	0 (0)	0 (0)	5 (50)
Headache	5 (50)	0 (0)	0 (0)	5 (50)
Pain	3 (30)	0 (0)	0 (0)	3 (30)
Arthralgia	1 (10)	0 (0)	0 (0)	1 (10)
Dysgeusia	1 (10)	0 (0)	0 (0)	1 (10)
Erythema multiforme	1 (10)	0 (0)	0 (0)	1 (10)
Flu like symptoms	1 (10)	0 (0)	0 (0)	1 (10)
Nasal congestion	1 (10)	0 (0)	0 (0)	1 (10)
Platelet count decreased	1 (10)	0 (0)	0 (0)	1 (10)
Pruritus	1 (10)	0(0)	0 (0)	1 (10)
Rash maculo-papular	1 (10)	0 (0)	0 (0)	1 (10)
Skin induration	1(10)	0 (0)	0 (0)	1 (10)
Voice alteration	1(10)	0 (0)	0 (0)	1 (10)
AEs related to Nivolumab: # of patients (%)	**Grade 1**	**Grade 2**	**Grade 3**	**Total**
Diarrhea	0 (0)	1 (10)	1 (10)	2 (20)
Abdominal pain	0 (0)	0 (0)	1 (10)	1 (10)
Fatigue	2 (20)	1 (10)	0 (0)	3 (30)
Headache	1 (10)	1 (10)	0 (0)	2 (20)
Hypothyroidism	1 (10)	1 (10)	0 (0)	2 (20)
Pain	1 (10)	1 (10)	0 (0)	2 (20)
Colitis	0 (0)	1 (10)	0 (0)	1 (10)
Insomnia	0 (0)	1 (10)	0 (0)	1 (10)
Pruritus	3 (30)	0 (0)	0 (0)	3 (30)
Serum amylase increased	2 (20)	0 (0)	0 (0)	2 (20)
Back pain	1 (10)	0 (0)	0 (0)	1 (10)
Blurred vision	1 (10)	0 (0)	0 (0)	1 (10)
Dry mouth	1 (10)	0 (0)	0 (0)	1 (10)

Edema limbs	1 (10)	0 (0)	0 (0)	1 (10)
Hyperthyroidism	1 (10)	0 (0)	0 (0)	1 (10)
Hypoglycemia	1 (10)	0 (0)	0 (0)	1 (10)
Lipase increased	1 (10)	0 (0)	0 (0)	1 (10)
Mucositis oral	1 (10)	0 (0)	0 (0)	1 (10)
Vomiting	1 (10)	0 (0)	0 (0)	1 (10)

569

Figures

Figure 1: Vaccine generation and clinical courses. a. Trial schema including treatment and sample collection. Time periods for analysis of cfDNA in panel **f** are shown (bottom). **b.** Consort diagram of patients who signed prescreening consent, treatment consent and received vaccine (total and by cohort); reasons for withdrawal are indicated by cohort (parentheses). **c**. Summary of mutation characteristics per patient. Personal HLA binding neoantigen epitopes were predicted via HLAthena[14] or NetMHCpan[15], and the best epitope per mutation was defined by HLA binding strength: strong (rank < 0.5 by either algorithm), weak (rank > 0.5 and < 2.0) or very weak (rank > 2.0) (Top). Mutations were classified as derived from single nucleotide variants (SNV) or insertions/deletions (INDEL). **d.** Summary of vaccine target mutations for each patient, including HLA binding strength (top) and mutation type (bottom). **e.** Swimmers plot depicting the clinical outcomes for 10 patients treated with NeoVax plus nivolumab. Platinum free interval (PFI) and maintenance therapy prior to trial enrollment are indicated, as well as SOC maintenance therapy during the course of vaccination (left). “CA125 rising” reflects the first date that CA125 was > ULN or > 2x from nadir. **f.** Detection of SNV vaccine target mutations by cell free (cf)DNA analysis at vaccine priming (D1 and/or D15) or during the duration of the clinical trial.

Figure 2: Clinical benefit defined by serum biomarkers and associated with peripheral immune responses. a-c. For each patient, serum CA125 (closed squares; left y axis) and cfDNA mean tumor variant allele frequency (VAF) (open circles; right y axis; plotted as %) are plotted vs. time relative to vaccine day 0 (x axis). Mean cfDNA VAFs calculated from 150-900 coding and non-coding allele frequencies generated from WGS. Treatments are indicated above each graph and described in the figure legend key. Patients were assigned to one of three groups based on biomarker trends: (**a**) progression, (**b**) transient disease control, and (**c**) prolonged disease control. **d.** Heatmaps (left) represent the relative IFN-γ ELISpot count (normalized by patient) of serial post-vaccination PBMC re-stimulated *ex vivo* with Immunizing peptide (IMP) pools (middle); the maximum ELISpot count per patient is indicated and pools with responses passing response threshold are indicated by an asterisk (> 30 SFU/10^6, >3x over DMSO control, $P < 0.05$ by Distribution Free Resampling (DFR(EQ))[17]; See **Extended Data Fig. 3**). (Right) Fraction of IMPs per vaccine pool inducing T cell responses in each patient as assessed by deconvolution of vaccine peptide pools by *in vitro* IFN-γ ELISpot (See **Extended Data Fig. 4**). **e-i**. Comparison of progression (red; n = 4) vs. transient response and prolonged disease controllers (green; n=6 (**e-h**) and n = 5 (**i**)), with regards to total number of mutations targeted (**e**), fraction of target mutations with immune response (**f**), total number of mutations with induced immune response (**g**), tumor missense mutation count (**h**) and first platinum free interval (**i**). Individual patient values are graphed and box plots represent median +/- 1 quartile and error bars represent the minimum and maximum values; *P* values reflect two-tailed, Mann-Whitney test.

Figure 3: Evaluation of tumor microenvironment and TIL specificities from tumor biopsies.

a. Schema of tumor sample collection and processing in 7 patients. **b**. Cell populations identified by scRNAseq. Time point, biopsy type and clinical group are indicated. See also **Extended Data Fig 5**. **c.** Fraction of the indicated cell types in controllers (n = 6 biopsies) vs. progressors (n = biopsies) **d.** Fraction of the indicated T cell fractions in controllers vs. progressors **e**. TIL TCR Shannon Diversity for progressor and transient controller T cell clonotypes. For **c-e,** patient specific symbols are as indicated in **a**, box plots represent median +/- 1 quartile and whiskers extend to the minimum and maximum values, and, *P* values reflect two tailed Mann-Whitney tests. **f**. P108 Biopsy B2 (post-vax) PDO line validation: Top, PDO bright field images; middle, graphs comparing *TP53* (red), vaccine (orange), and non-vaccine (black) missense mutation variants in RNAseq from the B1 tumor biopsy (x axis) and the PDO line (y axis) (one sequencing sample, each); bottom, treatment timeline. **g**. Validation of P113 Pre-Vax B1 and Post-Vax B2 PDO, as in (**f**). **h**. Summary of CD137 expression screening of TCR reactivity against the indicated targets for 14 T_{EX} (left) and 9 T_{EM} (right) expanded TIL clones from P108. Reactivity defined as > 2 standard deviations above all controls (see also **Methods**, **Supplementary Table 4**, **Extended Data Fig 6a-b**); "borderline" indicates weak reactivity resulting in CD137 expression of < 10% or < 3x that induced by an irrelevant control TCR. Representative of 2 independent experiments. **d**. Summary of TCR reactivity screening for P113 T_{EX} (left) and T_{EM} (right) TIL clones as in (**b**) (see also **Supplementary Table 4**, **Extended Data Fig 7a, c-d**); **e**. Example of CD137 upregulation for vaccine reactive T_{EX} TCR 5 (left) vs. the indicated targets, and as well as for other tested TIL clonotypes vs. the indicated targets (heatmap, right). **d-e** representative of 2 independent experiments (B1 PDO) and 3 independent experiments (B2 PDO, vaccine pools). **f.** Avidity plots for four vaccine reactive TCRs from P113 TIL, for the DPP3 p.L458R epitope T<u>R</u>RDTVLL, as well as the wildtype sequence; Healthy donor T cells transduced with the indicated TCRs, were incubated with P113 autologous EBV-LCL pulsed with WT or mutant DPP3 peptide at the indicated concentrations, and % CD137 expression is graphed. Representative of 3 independent experiments. **g**. DPP3 p.L458R specific TIL as a fraction of non-naïve TIL (T_{EX}, T_{PE}, T_{Prol}, T_{EM}) in P113 tumor biopsy scRNAseq. **h**. Fraction peripheral blood *TCRB* clonotypes matching the indicated vaccine specific TCR clonotypes

(TCR19 beta chain was not detected) are graphed from W1 (pre-vaccine), W14 (after boost 1), and W 22 (after boost 2 and nivolumab). **i.** Proportion of DPP3 p.L458R specific TIL belonging to the indicated clusters.

Figure 4: Mechanisms of immune evasion associated with progression.

a. Heatmaps representing the average expression of Hallmark IFNγ response geneset genes from tumor cells (middle) and T cells (right) from post-vax P113 B2 and B3, relative to pre-vax B1. Genes are ordered (top to bottom) by the most significant differential expression in tumor cells (Wilcoxan rank sum test with Bonferroni correction, calculated with FindMarkers in Seurat); significance is summarized on the far left [-log10(p-Adj + $1e^{-300}$]). **b**. Bulk RNAseq reads from pre-vax B1 and post-vax B2 organoids across the JAK1 locus (top), and phospho-STAT1 intracellular staining of pre-vax B1 and post-vax B2 PDO with or without 45 minutes IFNγ stimulation (bottom; representative of > 3 independent experiments). **c**. HLA-A/B/C expression by flow cytometry, with and without 24h IFNγ treatment for P113 pre-vax (B1) and post-vax (B2) PDO. Representative of > 3 experiments. **d**. Fold CD137 induction for T cells expressing DPP3 reactive TCRs or controls, following incubation with post-vax (B2) transduced with empty vector (GFP) or vector encoding *JAK1* cDNA (JAK1) and pre-treated or not with IFNγ. Analysis was performed in triplicate and values are normalized to mean percent $CD137^{+}$ after incubation with GFP-PDO without IFNγ (bars show mean + S.D.; see also **Extended Data Fig. 8**; representative of 2 independent experiments). **e**. ABSOLUTE copy number across chromosome 6 for P111 and P117 (left). (Right) Graphs depict predicted weak (HLAthena rank < 2.0) and strong (HLAthena rank < 0.5) epitope-HLA binding pairs for short epitopes within vaccine synthetic long-peptides, taking into account germline HLA alleles (“All”), and those HLA alleles retained in the tumor at biopsy B1, prior to vaccination (“Retained”; see **Extended Data Fig. 10**). **f.** cfDNA VAF of vaccine target (blue; n = 15 [P106], 9 [P108] or 8 [P113]) and non-target (pink; n = 36 [P106], 26 [P108], or 41 [P113]) missense mutations at the indicated time points (left; mean +/- S.E.), and normalized biopsy B1 vs. progression biopsy WES VAF for vaccine target genes (right). To account for variable tumor fraction, vaccine target VAFs are normalized to the mean VAF of truncal non-target mutations. **g**. Summary response and resistance mechanisms. From outer circle to inner circle, the following are indicated: biomarker

group (progression, transient control, prolonged control), patient ID, putative resistance mechanism and number of vaccine-induced immune responses.

Main Text References

1. Zhang, L., et al. Intratumoral T cells, recurrence, and survival in epithelial ovarian cancer. N Engl J Med 348, 203-213 (2003).
2. Sato, E., et al. Intraepithelial CD8+ tumor-infiltrating lymphocytes and a high CD8+/regulatory T cell ratio are associated with favorable prognosis in ovarian cancer. Proc Natl Acad Sci U S A 102, 18538-18543 (2005).
3. Varga, A., et al. Pembrolizumab in patients with programmed death ligand 1-positive advanced ovarian cancer: Analysis of KEYNOTE-028. Gynecol Oncol 152, 243-250 (2019).
4. Hamanishi, J., et al. Safety and Antitumor Activity of Anti-PD-1 Antibody, Nivolumab, in Patients With Platinum-Resistant Ovarian Cancer. J Clin Oncol 33, 4015-4022 (2015).
5. Colombo, N., et al. Pembrolizumab plus weekly paclitaxel in platinum-resistant recurrent ovarian cancer (ENGOT-ov65/KEYNOTE-B96): a multicentre, randomised, double-blind, phase 3 study. Lancet 407, 1525-1537 (2026).
6. Cancer Genome Atlas Research, N. Integrated genomic analyses of ovarian carcinoma. Nature 474, 609-615 (2011).
7. Liu, M., et al. Improved T-cell Immunity Following Neoadjuvant Chemotherapy in Ovarian Cancer. Clin Cancer Res 28, 3356-3366 (2022).
8. Kandalaft, L.E., Dangaj Laniti, D. & Coukos, G. Immunobiology of high-grade serous ovarian cancer: lessons for clinical translation. Nat Rev Cancer 22, 640-656 (2022).
9. Vazquez-Garcia, I., et al. Ovarian cancer mutational processes drive site-specific immune evasion. Nature 612, 778-786 (2022).
10. Hornburg, M., et al. Single-cell dissection of cellular components and interactions shaping the tumor immune phenotypes in ovarian cancer. Cancer Cell 39, 928-944 e926 (2021).
11. Keskin, D.B., et al. Neoantigen vaccine generates intratumoral T cell responses in phase Ib glioblastoma trial. Nature 565, 234-239 (2019).
12. Braun, D.A., et al. A neoantigen vaccine generates antitumour immunity in renal cell carcinoma. Nature 639, 474-482 (2025).
13. Rojas, L.A., et al. Personalized RNA neoantigen vaccines stimulate T cells in pancreatic cancer. Nature 618, 144-150 (2023).
14. Sarkizova, S., et al. A large peptidome dataset improves HLA class I epitope prediction across most of the human population. Nat Biotechnol 38, 199-209 (2020).
15. Jurtz, V., et al. NetMHCpan-4.0: Improved Peptide-MHC Class I Interaction Predictions Integrating Eluted Ligand and Peptide Binding Affinity Data. J Immunol 199, 3360-3368 (2017).
16. Parsons, H.A., et al. Sensitive Detection of Minimal Residual Disease in Patients Treated for Early-Stage Breast Cancer. Clin Cancer Res 26, 2556-2564 (2020).
17. Moodie, Z., Huang, Y., Gu, L., Hural, J. & Self, S.G. Statistical positivity criteria for the analysis of ELISpot assay data in HIV-1 vaccine trials. J Immunol Methods 315, 121-132 (2006).
18. Oliveira, G., et al. Phenotype, specificity and avidity of antitumour CD8(+) T cells in melanoma. Nature 596, 119-125 (2021).
19. Caushi, J.X., et al. Transcriptional programs of neoantigen-specific TIL in anti-PD-1-treated lung cancers. Nature 596, 126-132 (2021).
20. Anadon, C.M., et al. Ovarian cancer immunogenicity is governed by a narrow subset of progenitor tissue-resident memory T cells. Cancer Cell 40, 545-557 e513 (2022).

21. Martinez-Jimenez, F., et al. Genetic immune escape landscape in primary and metastatic cancer. Nat Genet 55, 820-831 (2023).
22. Filip, I., et al. Pervasiveness of HLA allele-specific expression loss across tumor types. Genome Med 15, 8 (2023).
23. Takaya, H., Nakai, H., Takamatsu, S., Mandai, M. & Matsumura, N. Homologous recombination deficiency status-based classification of high-grade serous ovarian carcinoma. Sci Rep 10, 2757 (2020).
24. Knijnenburg, T.A., et al. Genomic and Molecular Landscape of DNA Damage Repair Deficiency across The Cancer Genome Atlas. Cell Rep 23, 239-254 e236 (2018).
25. Center, B.I.T.G.D.A. Firehose (stddata__2016_01_28). (Broad Institute of MIT and Harvard, 2016).
26. Sethna, Z., et al. RNA neoantigen vaccines prime long-lived CD8(+) T cells in pancreatic cancer. Nature 639, 1042-1051 (2025).
27. Huber, F. & Bassani-Sternberg, M. Defects in antigen processing and presentation: mechanisms, immune evasion and implications for cancer vaccine development. Nat Rev Immunol (2025).
28. Huber, F., et al. A comprehensive proteogenomic pipeline for neoantigen discovery to advance personalized cancer immunotherapy. Nat Biotechnol 43, 1360-1372 (2025).

METHODS

Study Design

This phase I study (https://clinicaltrials.gov/study/NCT04024878; Registered 7/16/2019) was conducted at the Dana-Farber Cancer Institute. Key eligibility criteria included: age ≥ 18 years, histologically confirmed epithelial ovarian, primary peritoneal or fallopian tube cancer (EOC), Eastern Cooperative Oncology Group (ECOG) performance status ≤ 2, candidacy for platinum-based chemotherapy, and disease that was either amenable to biopsy, or recently biopsied. Cohort A required newly diagnosed, untreated Stage IIIC or IV EOC; Cohort B required platinum sensitive first recurrence of EOC, with platinum sensitivity defined as disease progression > 6 months after the last dose of first line platinum-based chemotherapy. All treated patients had *TP53* mutant tumors with high grade serous (n=9) or endometroid (n=1; P122) histology. The study excluded mucinous or low grade histologies, prior immunotherapy, known central nervous system metastases, or prior or active autoimmune disease.

The study was designed with a two-stage consent process. Following initial "pre-screening" informed consent, patients underwent tumor biopsy (B1; surgical or core), followed by tumor DNA and RNA sequencing, clinical HLA typing and the initiation of SOC chemotherapy. If tissue sampling and sequencing was adequate for vaccine design and patients did not progress on SOC platinum chemotherapy, patients were offered "treatment" consent. The primary objective of the study was to evaluate the safety and feasibility of administering NeoVax with nivolumab in patients with epithelial ovarian cancer. The protocol, amendment summaries, deviations, and summaries of primary, secondary and exploratory endpoints are available in **Supplementary Information**.

Ethical approval and consent

The study was conducted in accordance with the Declaration of Helsinki and with approval by the Dana-Farber/Harvard Cancer Center (DFHCC) Institutional Review Board. Written informed consent was obtained for all patients.

Patient samples

Peripheral blood samples were obtained for HLA typing and for germline DNA sequencing. Clinical HLA class I and II typing was performed by the BWH Tissue Typing laboratory (**Supplementary Table 4**). For immune monitoring of peripheral blood mononuclear cells (PBMCs), leukaphereses were performed prior to vaccination (within 1 week), at week 14 (+/- 1 week; after boost 1) and at week 22 (+/- 1 week; after boost 2). Peripheral blood samples (K2-EDTA tubes) were collected serially. PBMCs were isolated by Ficoll (GE Healthcare) density centrifugation and cryopreserved. Plasma pooled from peripheral blood draws was frozen for cfDNA analysis. Tumor biopsies were collected in DMEM media. Viable tumor cell suspensions were prepared by mincing with a scalpel, then dissociating with PBS containing collagenase (0.4mg/mL), hyaluronidase (0.4mg/mL) and DNase, for 20-60 min at 37 degrees while rocking; cells were then washed in PBS, counted and cryopreserved in 90% heat inactivated FCS/10% DMSO.

Personalized neoantigen vaccine generation and treatment

The workflow of personalized cancer vaccine generation included whole exome sequencing (WES) of tumor tissue and peripheral blood, RNA-sequencing of tumor, somatic mutation

calling, identification and selection of target neoantigens, and peptide synthesis similar to our previously completed trials[12,29], with notable points detailed below. Briefly, for WES of tumor and normal blood to identify neoantigens, FFPE tumor scrolls and a peripheral blood sample were processed for nucleic acid extraction and sequencing at the Broad Institute Clinical Research Sequencing Platform, LLC (CRSP), a CLIA licensed (#22D2055652) and CAP accredited (#8707596) laboratory for standard Somatic WES. Libraries were sequenced on paired 76 cycle runs on Illumina HiSeq or NovaSeq instruments with two 8 cycle index reads, to a goal depth of > 150x mean target coverage. Tumor tissue RNA-sequencing (FFPE scrolls) was performed to confirm putative neoantigen expression, at the non-CLIA/CAP Broad Institute Genomics Platform. RNAseq libraries were sequenced with 76bp paired-end with an eight-base index barcode read with Illumina HiSeq or NovaSeq S2 instruments. Alignment was completed using the STAR alignment algorithm against human reference hg19.

A cloud-based Cancer Genome Analysis WES Characterization Pipeline was used to identify somatic mutations. Mutations were categorized as “green” (high-quality read support in WES and RNA-seq), “yellow” (high quality in WES; not identified in RNA-seq), or “red” (likely artifact). Green, and then yellow, mutations were prioritized. Antigen prediction was performed using HLAthena[14] and NetMHCpan version 4.0 (P106 - 113) and NetMHC pan 4.1 (P114 – 122) [15] (eluted ligand rank). NetMHC prediction scores were ranked using HLAthena's ranking models. Antigens were then ranked favoring agreement between the two prediction scores.

An Epitope Selection Board selected up to 20 short epitopes based on mutation quality, antigen rank, cancer driver status (favoring driver over passenger mutations), clonality (favoring clonal over subclonal mutations), and whether the somatic alteration was a frameshift indel capable

of producing a novel open reading frame. The driver genes list for this cohort was based on known cancer genes and significantly mutated genes in the Cancer Genome Atlas – Ovarian cohort (TCGA-OV)[30] and PanCancer lists from the TumorPortal[31] (http://www.tumorportal.org/). For the selected short epitopes, the ESB designed synthetic long peptides (SLPs; 15 – 33 amino acids in length) containing the short epitope, with a length and sequence intended to maximize synthesizability and solubility.

GMP peptides were synthesized by standard solid phase synthetic peptide chemistry and purified by reverse-phase high-performance liquid chromatography (RP-HPLC; Almac Sciences (UK)). Each peptide was assessed for appearance (visual), purity (RP-HPLC), identity (mass spectrometry), and quantity. Peptide pools were sterile-filtered and tested for sterility and endotoxin prior to vaccination.

NeoVax consisted of up to 20 neoantigen containing synthetic long peptides (SLPs) split into four personalized vaccine pools, each containing up to 5 SLPs (300µg per peptide) in 0.5ml, admixed with 0.25ml polyinosinic polycytidylic acid polylysine carboxymethylcellulose (poly ICLC; Hiltonol; 450µg). Vaccine priming doses were administered into the extremities on days 1, 4 and 8 (+/- 1 day), and 15 and 22 (+/- 3 days); Booster vaccinations were given in weeks 12 and 20 (days 78 and 134, +/- 7 days). Individual pools were injected into the same anatomical site throughout treatment. Starting at week 14 (day 92 +/- 3 days), Nivolumab was administered every 2 weeks at 240mg flat dose for up to 2 years, or until progression or intolerable toxicity. Amendments allowed the administration of standard of care maintenance therapies (e.g. PARPi, bevacizumab) and nivolumab 480mg every 4 weeks after the completion of all vaccine booster doses.

Clinical assessments and outcomes

Clinical outcome and safety data were reported until the clinical data cutoff of December 1, 2025. Adverse events, laboratory values, and vital signs were assessed regularly and graded according to the National Cancer Institute Common Terminology Criteria for Adverse Events, version 5.0. Imaging assessments were performed prior to starting vaccination and subsequently every 12 weeks according to Response Evaluation Criteria in Solid Tumors (RECIST), version 1.1. Biomarker groups were delineated as follows: Prolonged controllers were defined as those patients who exhibited (i) stable disease (RECIST) or no evidence of disease and (ii) CA125 < the ULN, throughout the entire course of vaccination. Transient controllers did not meet prolonged controller criteria due to RECIST progression or CA125 levels > ULN; however, after an initial period of increasing CA125 and cfDNA, they exhibited a decrease or change in slope in at least one biomarker for >1 assessed time point, without alternative explanation. Progressors exhibited (i) RECIST progression prior to boosting and either (iia) increases in CA125 and/or cfDNA VAF at all assayed timepoints over the course of vaccination, or (iib) any decreases in CA125 or cfDNA VAF between assayed timepoints were only associated with alternative therapies (e.g. radiation or ablation).

Organoid generation and culture

Organoids were generated and cultured as previously described[32]. PDO lines tested negative for mycoplasma contamination at late passages. For phospho-STAT1 staining, PDO cells were digested to single cells with TrypLE, rested for one-hour in organoid media at 37˚C and then treated or not with IFN-γ (20ng/ml; Peprotech) for 1 hour. Cells were fixed with 2%

paraformaldehyde (10 min, room temperature). After washing, cells were permeabilized (90% ice cold methanol, on ice, 30 min). After washing, cells were stained with Alexa Fluor 647 anti-phospho-STAT1 (BioLegend Cat. 666409) or isotype control (BioLegend Cat. 400130). For HLA flow cytometry, Matrigel encased PDOs were treated or not with IFN-γ (20ng/ml) for 24 hours. Single cells were isolated via TrypLE digestion and stained with Pacific Blue anti-human HLA-A/B/C (Biolegend Cat. 311426) or matched isotype (Biolegend Cat.400235). To rescue *JAK1* expression, the *JAK1* CDS was PCR-amplified from plasmid pDONR223-JAK1 (gift of W. Hahn & D. Root; Addgene plasmid # 23932) and inserted into a pLKO lentiviral-backbone with a P2A-GFP cassette using the NEBuilder® HiFi DNA Assembly kit. Virus was produced as below (**TCR screening**) using Lenti-X 293T cells (Takara Bio Cat. 632180). Sucrose gradient concentrated lentivirus (Lenti-X concentrator; Takara Bio Cat. 631231) was used to transduce single cell suspensions of PDO cells (spinoculation at 2000RPM x 1h with 10ug/mL Polybrene (Millipore)), and transduced cells were subsequently enriched via fluorescence activated cell sorting. Plasmids are available upon request.

Assessment of vaccine immunogenicity by IFNγ ELISpot

PBMCs containing circulating T cells were assessed for immune reactivity to vaccine peptide pools immediately upon thawing and rest (*ex vivo*) and to individual vaccine peptides following *in vitro* stimulation with pools of peptides. All T cell culture and ELISpot methods (including plate development and analysis) were previously described[33,34]. Briefly, to assess *ex vivo* immunogenicity, PBMCs were screened against neoantigen vaccine peptide pools by *ex vivo* IFNγ ELISpot assays. Opaque ELISpot plates with 0.45 mm hydrophobic high protein binding immobilon-p membranes (Millipore) were wetted with 35% ethyl alcohol, washed 3x with

distilled water and coated with anti-IFNγ antibody at 4°C (1-DK1 Mabtech) for final washes with PBS. Cryopreserved PBMC were thawed in complete DMEM media supplemented with 10% human serum and rested overnight. The PBMCs were then plated at 2×10^5 cells per well and stimulated with 10µg of peptide pool. Controls included DMSO, peptide pools derived from HIV or CEF (CMV, EBV, and influenza) (Mabtech), and phytohemagglutinin (PHA, Gibco). PBMC were stimulated in triplicate for 18-24 hours at 37°C. Plates were developed using manufacturer's protocols.

In vitro IFNγ ELISpot assays were used to assess individual peptide immunogenicity[29]. Briefly, PBMCs were plated in 24 well plates at 5×10^6 to 1×10^7 cells per well and stimulated with 10µg/mL of vaccine peptide pools in DMEM media supplemented with 10% human serum and 20 ng/mL of IL-7 (PeproTech). On day 3, cultures were supplemented with 20 U/mL of IL-2 (PeproTech). *In vitro* IFNγ ELISpot assays were performed 10-14 days post-stimulation, after an overnight rest in cytokine-free media. 2×10^5 cells were plated with 10µg of individual vaccine peptides, as well as negative controls, DMSO and 10µg of HIV, and positive controls, CEF peptides and PHA. For all ELISpot analyses, responses were considered positive if the mean spot count was > 6 (LOD: 3x the median DMSO), 3x matched DMSO control and significant by distribution free resampling (DFR(EQ) $P < 0.05$; https://rundfr.fredhutch.org/)[17] without adjustments for multiple comparisons.

scRNA-seq and scTCRseq data generation and analysis

The samples processed for scRNAseq were obtained following tumor digestion and cryopreservation. Upon thawing, dead cells were depleted via the Miltenyi Dead Cell Removal Kit. Tumor cells were washed and resuspended in PBS with UltraPure 0.04% BSA for

downstream 10x analysis. Cells were loaded onto a 10× Genomics Chromium™ instrument (10x Genomics) according to the manufacturer's recommendations. The scRNAseq libraries were processed using Chromium Next GEM Single Cell 5' Kit v2, and the scTCRseq libraries were made using Chromium Single Cell Human TCR Amplification Kit (10x Genomics). cDNA and library quality was confirmed by Bioanalyzer High Sensitivity DNA Kit (Agilent). Sequencing libraries were normalized to 4nM concentration and pooled before sequencing on an Illumina NovaSeq S4 300 cycle platform: Read 1 of 26bp, Read 2 of 90bp, Index 1 of 10bp and Index 2 of 10bp.

Single-cell RNA-seq processing and analyses

Following CellRanger (v 7.1.0) processing, scRNAseq data were read into R v4.2.1 and processed with Seurat v5.1.0[35] where they were filtered to remove mitochondrial genes and debris by eliminating cells with low RNA counts (min.cells = 3 & min.features = 200 and nCount_RNA > 1500 & nFeature_RNA > 750). Additional filtering of low-quality cells was completed with miQC v1.6.0[36] (posterior.cutoff 0.6). Data were subsequently normalized, variable features were identified, and data were scaled prior to running Principal Component Analysis (PCA). Visualization via Uniform Manifold Approximation and Projection (UMAP) revealed data stratification by batch, timepoint, and patient, which led to the use of Harmony v1.2.3[37] to integrate samples. Doublets were removed with scDblFinder v1.12.0[38]. A shared nearest-neighbor graph was constructed that was used to cluster the Seurat object with the Louvain algorithm at low resolution to identify broad cell types. To label the clusters, the top differentially expressed genes were analyzed for each cluster via FindAllMarkers. Additionally, canonical cell lineage markers were assessed for their expression across clusters. Gene set

928 signatures from Oliveira *et al*. 2023[39] were scored with AddModuleScore. Separate tumor and
929 T cell objects were subsetted from the main Seurat object. FindMarkers was used to identify
930 differential gene expression for the tumor or T cell objects over time. The CD4 and CD8 T cell
931 objects each underwent PCA and re-clustering. Cluster resolution was determined using
932 Clustree v0.5.1[40]. T cell subtypes were identified by analyzing the top differentially expressed
933 genes for each cluster found from FindAllMarkers. Additionally, gene set signatures for
934 cytotoxicity, exhaustion, memory, and proliferation from Oliveira *et al*. 2023[39] were scored with
935 AddModuleScore. Comparisons to previous studies[18,41] aided in the annotation of T cell
936 subclusters. Gene set enrichment analysis (GSEA) on the tumor cells per patient was
937 conducted using the Human MSigDB Hallmark Gene Sets[42]. A Wilcoxon rank sum test was
938 executed using presto v1.0.0 to find differentially expressed genes across time points, which
939 was then used with msigdbr v7.5.1 and fgsea v1.24.0[43] to identify enriched and depleted
940 pathways. Plots in R were generated with ggplot2 v3.5.1[44], cowplot v1.1.3, pheatmap 1.0.12,
941 and paletteer v1.6.0. Data analysis utilized tidyr v1.3.1, tidyverse v2.0.0, and dplyr v1.1.4.
942
943 Single-cell TCRseq data were filtered for low-quality and low-confidence reads after CellRanger
944 (v7.1.0) processing. TCRs were labeled as one of six categories based on the number of alpha
945 and beta chains that paired together: (1) 1 alpha 1 beta, (2) 2 alpha 1 beta, (3) 1 alpha 2 beta,
946 (4) 1 or 2 alpha and 0 beta, (5) 0 alpha and 1 or 2 beta, and (6) more than 2 alpha and/or beta
947 chains. TCRs labeled as category 6 were removed from further analysis. Single-cell TCRseq
948 data were merged with the scRNAseq Seurat object based on exact sample barcode matching.
949
950 **Bulk RNAseq analysis**

Gene expression was quantified using RSEM. Genes of interest expressed (>=1 TPM) in at least one patient tumor sample, were plotted.

TCR reconstruction and expression in T cells for vaccine and PDO specificity screening.

TCRs were cloned, expressed in human T cells and screened for specificity of neoantigen peptides using our protocols[45]. Briefly, the full-length *TCRA* and *TCRB* chains with murinized constant domains were synthesized in the *TCRB/TCRA* orientation, separated by Furin SGSG P2A linker (Integrated DNA Technologies). Gene fragments were cloned into a lentiviral vector under the control of the pEF1α promoter using Gibson assembly (New England Biolabs Inc).

Healthy donor T cells enriched from PBMCs using PanT cell selection kit (Miltenyi) were activated with antiCD3/CD28 dynabeads (ThermoFisher Scientifics) in the presence of 5ng/mL of IL-7 and IL-15 (Peprotech) in 96 well plates. On days 2-4, activated cells were transduced with a lentiviral vectors encoding TCRB-TCRA chains. Lentiviral particles were generated by Transit LT-1 (Mirus) transient transfection of Lenti-X 293T cells (Takara) in 96 well plates, using TCR encoding plasmids and packaging plasmids (VSVg and PSPAX2[45]). Lentiviral supernatant was harvested on days 1, 2 and 3, supplemented with Polybrene (10mg/mL; Millipore) and immediately used to transduce activated T cells, including one spinoculation of the virus at 2,000 rpm and 37°C for 2 hours on the second transduction day. Six days after activations, dynabeads were removed and T cells were expanded in G-REX 24 well plates in media enriched with IL-7 and IL-15.

TCR-transduced T cells were used at 14-21 days post-transduction for TCR reactivity tests. Briefly up to 28 TCR-transduced T cell lines were separately stained with up to 4 concentrations

of CellTrace Far Red (FR), CellTrace Violet, and/or CFSE (Life Technology), and pooled. $2.5x10^5$ pooled T cell effectors were incubated with either ~ 5 $x10^4$ PDO cells liberated from Matrigel via TRYPLE digestion or $2.5x10^5$ patient-derived, EBV immortalized B cells (EBV lymphoblastoid cell lines, EBV-LCL). EBV-LCLs were pulsed with 10^8 pg/mL of vaccine peptide pools, or the indicated concentrations of individual neoantigen and wildtype peptides (Almac, Genscript). After an overnight incubation, TCR reactivity was measured via detection of CD137 surface expression on CD8+, TCR transduced (murine TCRB+) T cells using a Fortessa flow cytometer equipped with a high-throughput system acquisition (BD Biosciences). Data were analyzed on Flowjo (v10.8). Criteria for determining TCR reactivity were (must meet all three): Target average % CD137+ > 2 standard deviations higher than (1) Average of untransduced T cells across all targets; (2) Matched background (average of the TCR without target); (3) Average of an irrelevant control TCR across all targets. Borderline reactivity was defined as meeting the above criteria, but with average CD137 < 10% or < 3 fold the irrelevant TCR average across targets

Whole Genome Sequencing (WGS) of tumor and normal samples for cfDNA and SV analysis.

DNA was obtained as above. WGS of tumor DNA (median depth 84x; range: 61x–103x), and normal DNA (median depth 41x; range: 30x–53x) was performed using NovaSeq S4. For cfDNA analysis, patient-specific MRD Tracker panels were designed as previously described from tumor and normal WGS[16,46]. Neoantigen variants identified in the CGA pipeline were expressly included in the MRD Tracker panels.

Structural variants (SVs) were identified using the Manta structural variant caller[47] (v1.6.0). Aligned tumor WGS BAM format data was used as input, with the *GRCh37/hg19* reference genome. Manta was executed with default parameters, and candidate SVs were filtered to retain high-confidence calls passing internal quality filters (i.e., FILTER == PASS in the VCF). Integrative Genomics Viewer (IGV) was used to examine supporting split reads and discordant read pairs at candidate both breakpoints. PCR primers were designed to amplify *chr1* break points and adjacent DNA and sanger sequencing was used to confirm the chr1 structural variant. Primers are provided in the **Supplementary Iinformation.**

Plasma sample processing for cfDNA

cfDNA was extracted from median 4.5 ml (range 0.6 – 78.5 ml) plasma using the QIAsymphony Circulating DNA kit and quantified using the Quant-iT PicoGreen assay on a Hamilton STAR-line liquid handling system. cfDNA libraries were constructed using the Kapa Hyper Prep kit with custom dual index duplex UMI adapters (IDT)[16]. Libraries were quantified via the Quant-iT PicoGreen assay on a Hamilton STAR-line liquid handling system. MRD Tracker assay was performed[16]. Briefly, patient specific probe panels (IDT) and the xGen hybridization and wash kit with xGen Universal blockers (IDT) were used for hybrid capture (HC). For each HC reaction, libraries were pooled up to 8-plex with a library mass equivalent to 25 times DNA mass into library construction for each sample, and 4 pmol of probe panel (IDT) was applied. Following round one of HC, libraries were PCR amplified (16 cycles) and then carried through a second HC using half amounts of human Cot-1 DNA, xGen Universal blockers and probes. Libraries were again PCR amplified (8-10 cycles) before sequencing to a target raw depth of 10,000 x per site, per 20 ng input DNA mass.

MRD data analysis

FASTQs were first aligned, deduplicated, and recalibrated by following the GATK Best Practices “Data pre-processing for variant discovery” workflow. Next, UMIs were extracted using *fgbio*, raw sequencing reads were converted into duplex consensus molecules. Then tumor fractions and tumor VAFs were estimated[16].

Visualization of HLA haplotype loss

cDNA sequences from patient HLA alleles were retrieved from IDP-IMGT/HLA database (https://www.ebi.ac.uk/ipd/imgt/hla/; v3.61) and aligned locally to identify allele specific SNPs. cDNA coordinates were converted to hg19 coordinates and samtools mpileup was used to collect base calls from WES BAM files. SNP VAFs were graphed in prism.

Data Availability

Bulk WES, RNA-seq, WGS and TCR-seq, and single-cell RNA and single-cell TCR-seq data is deposited and available on dbGaP under the accession phs004380.v1.

Code Availability

All code used in the processing and analysis of bulk TCRseq data is available on GitHub at https://github.com/jeremymsimon/. Other code using established tools will be made available within 30 days upon request to the corresponding authors

Complete References

1. Zhang, L.*, et al.* Intratumoral T cells, recurrence, and survival in epithelial ovarian cancer. *N Engl J Med* **348**, 203-213 (2003).
2. Sato, E.*, et al.* Intraepithelial CD8+ tumor-infiltrating lymphocytes and a high CD8+/regulatory T cell ratio are associated with favorable prognosis in ovarian cancer. *Proc Natl Acad Sci U S A* **102**, 18538-18543 (2005).
3. Varga, A.*, et al.* Pembrolizumab in patients with programmed death ligand 1-positive advanced ovarian cancer: Analysis of KEYNOTE-028. *Gynecol Oncol* **152**, 243-250 (2019).
4. Hamanishi, J.*, et al.* Safety and Antitumor Activity of Anti-PD-1 Antibody, Nivolumab, in Patients With Platinum-Resistant Ovarian Cancer. *J Clin Oncol* **33**, 4015-4022 (2015).
5. Colombo, N.*, et al.* Pembrolizumab plus weekly paclitaxel in platinum-resistant recurrent ovarian cancer (ENGOT-ov65/KEYNOTE-B96): a multicentre, randomised, double-blind, phase 3 study. *Lancet* **407**, 1525-1537 (2026).
6. Cancer Genome Atlas Research, N. Integrated genomic analyses of ovarian carcinoma. *Nature* **474**, 609-615 (2011).
7. Liu, M.*, et al.* Improved T-cell Immunity Following Neoadjuvant Chemotherapy in Ovarian Cancer. *Clin Cancer Res* **28**, 3356-3366 (2022).
8. Kandalaft, L.E., Dangaj Laniti, D. & Coukos, G. Immunobiology of high-grade serous ovarian cancer: lessons for clinical translation. *Nat Rev Cancer* **22**, 640-656 (2022).
9. Vazquez-Garcia, I.*, et al.* Ovarian cancer mutational processes drive site-specific immune evasion. *Nature* **612**, 778-786 (2022).
10. Hornburg, M.*, et al.* Single-cell dissection of cellular components and interactions shaping the tumor immune phenotypes in ovarian cancer. *Cancer Cell* **39**, 928-944 e926 (2021).
11. Keskin, D.B.*, et al.* Neoantigen vaccine generates intratumoral T cell responses in phase Ib glioblastoma trial. *Nature* **565**, 234-239 (2019).
12. Braun, D.A.*, et al.* A neoantigen vaccine generates antitumour immunity in renal cell carcinoma. *Nature* **639**, 474-482 (2025).
13. Rojas, L.A.*, et al.* Personalized RNA neoantigen vaccines stimulate T cells in pancreatic cancer. *Nature* **618**, 144-150 (2023).
14. Sarkizova, S.*, et al.* A large peptidome dataset improves HLA class I epitope prediction across most of the human population. *Nat Biotechnol* **38**, 199-209 (2020).
15. Jurtz, V.*, et al.* NetMHCpan-4.0: Improved Peptide-MHC Class I Interaction Predictions Integrating Eluted Ligand and Peptide Binding Affinity Data. *J Immunol* **199**, 3360-3368 (2017).
16. Parsons, H.A.*, et al.* Sensitive Detection of Minimal Residual Disease in Patients Treated for Early-Stage Breast Cancer. *Clin Cancer Res* **26**, 2556-2564 (2020).
17. Moodie, Z., Huang, Y., Gu, L., Hural, J. & Self, S.G. Statistical positivity criteria for the analysis of ELISpot assay data in HIV-1 vaccine trials. *J Immunol Methods* **315**, 121-132 (2006).
18. Oliveira, G.*, et al.* Phenotype, specificity and avidity of antitumour CD8(+) T cells in melanoma. *Nature* **596**, 119-125 (2021).
19. Caushi, J.X.*, et al.* Transcriptional programs of neoantigen-specific TIL in anti-PD-1-treated lung cancers. *Nature* **596**, 126-132 (2021).

20. Anadon, C.M.*, et al.* Ovarian cancer immunogenicity is governed by a narrow subset of progenitor tissue-resident memory T cells. *Cancer Cell* **40**, 545-557 e513 (2022).
21. Martinez-Jimenez, F.*, et al.* Genetic immune escape landscape in primary and metastatic cancer. *Nat Genet* **55**, 820-831 (2023).
22. Filip, I.*, et al.* Pervasiveness of HLA allele-specific expression loss across tumor types. *Genome Med* **15**, 8 (2023).
23. Takaya, H., Nakai, H., Takamatsu, S., Mandai, M. & Matsumura, N. Homologous recombination deficiency status-based classification of high-grade serous ovarian carcinoma. *Sci Rep* **10**, 2757 (2020).
24. Knijnenburg, T.A.*, et al.* Genomic and Molecular Landscape of DNA Damage Repair Deficiency across The Cancer Genome Atlas. *Cell Rep* **23**, 239-254 e236 (2018).
25. Center, B.I.T.G.D.A. Firehose (stddata__2016_01_28). (Broad Institute of MIT and Harvard, 2016).
26. Sethna, Z.*, et al.* RNA neoantigen vaccines prime long-lived CD8(+) T cells in pancreatic cancer. *Nature* **639**, 1042-1051 (2025).
27. Huber, F. & Bassani-Sternberg, M. Defects in antigen processing and presentation: mechanisms, immune evasion and implications for cancer vaccine development. *Nat Rev Immunol* (2025).
28. Huber, F.*, et al.* A comprehensive proteogenomic pipeline for neoantigen discovery to advance personalized cancer immunotherapy. *Nat Biotechnol* **43**, 1360-1372 (2025).
29. Blass, E.*, et al.* A multi-adjuvant personal neoantigen vaccine generates potent immunity in melanoma. *Cell* (2025).
30. Cancer Genome Atlas Research, N. Comprehensive molecular characterization of clear cell renal cell carcinoma. *Nature* **499**, 43-49 (2013).
31. Lawrence, M.S.*, et al.* Discovery and saturation analysis of cancer genes across 21 tumour types. *Nature* **505**, 495-501 (2014).
32. Hill, S.J.*, et al.* Prediction of DNA Repair Inhibitor Response in Short-Term Patient-Derived Ovarian Cancer Organoids. *Cancer Discov* **8**, 1404-1421 (2018).
33. Lee, P.C.*, et al.* Reversal of viral and epigenetic HLA class I repression in Merkel cell carcinoma. *J Clin Invest* **132**(2022).
34. Keskin, D.B.*, et al.* Direct identification of an HPV-16 tumor antigen from cervical cancer biopsy specimens. *Front Immunol* **2**, 75 (2011).
35. Hao, Y.*, et al.* Dictionary learning for integrative, multimodal and scalable single-cell analysis. *Nat Biotechnol* **42**, 293-304 (2024).
36. Hippen, A.A.*, et al.* miQC: An adaptive probabilistic framework for quality control of single-cell RNA-sequencing data. *PLoS Comput Biol* **17**, e1009290 (2021).
37. Korsunsky, I.*, et al.* Fast, sensitive and accurate integration of single-cell data with Harmony. *Nat Methods* **16**, 1289-1296 (2019).
38. Germain, P.L., Lun, A., Garcia Meixide, C., Macnair, W. & Robinson, M.D. Doublet identification in single-cell sequencing data using scDblFinder. *F1000Res* **10**, 979 (2021).
39. Oliveira, G.*, et al.* Preexisting tumor-resident T cells with cytotoxic potential associate with response to neoadjuvant anti-PD-1 in head and neck cancer. *Sci Immunol* **8**, eadf4968 (2023).
40. Zappia, L. & Oshlack, A. Clustering trees: a visualization for evaluating clusterings at multiple resolutions. *Gigascience* **7**(2018).

41. Oliveira, G.*, et al.* Landscape of helper and regulatory antitumour CD4(+) T cells in melanoma. *Nature* **605**, 532-538 (2022).
42. Liberzon, A.*, et al.* The Molecular Signatures Database (MSigDB) hallmark gene set collection. *Cell Syst* **1**, 417-425 (2015).
43. Korotkevich, G.*, et al.* Fast gene set enrichment analysis. *bioRxiv*, 060012 (2021).
44. Wickham, H. ggplot2 : Elegant Graphics for Data Analysis. in *Use R!,* 1 online resource (XVI, 260 pages 232 illustrations, 140 illustrations in color (Springer International Publishing : Imprint: Springer,, Cham, 2016).
45. Afeyan, A.B., Wu, C.J. & Oliveira, G. Rapid parallel reconstruction and specificity screening of hundreds of T cell receptors. *Nat Protoc* (2024).
46. Parsons, H.A.*, et al.* Circulating tumor DNA association with residual cancer burden after neoadjuvant chemotherapy in triple-negative breast cancer in TBCRC 030. *Ann Oncol* **34**, 899-906 (2023).
47. Chen, X.*, et al.* Manta: rapid detection of structural variants and indels for germline and cancer sequencing applications. *Bioinformatics* **32**, 1220-1222 (2016).

Personalized neoantigen-targeting cancer vaccines in ovarian cancer: a phase 1 trial

MacLean C. Sellars[1,2], Jessica A. Frank[1, 2], Bohoon Shim[3], Allison Vanasse[4], Ruolin Liu[5], Cleo Forman[1, 3], Chloe R. Tu[1, 3], Kyohei K. Tabata[1], Antonia Kowelewski[2, 5], Su-Chun Cheng[3,6], Catherine Song[5], Kan Xiong[5], Pia Jain[5], Andjela Crnjac[5], Haley E. Sax[1], Vipheaviny Chea[4], Wesley Lu[4], J. Thomas Janes 3rd [4], Micah Rickles-Young[5], Amit Sud[1,7], Savni Sarolkar[1], Martin Hayes[1], Oriol Olive[1], Haley Greenslade[1], Carrie Cibulskis[5], Nir Hacohen[2, 5, 8], Edward F. Fritsch[1, 5], Shuqiang Li[4, 5], Kenneth J. Livak[4], Nabihah Tayob[3, 6], Elizabeth H. Stover[1, 2], Carolyn Krasner[1, 2], Rebecca Porter[1, 2], Ursula Matulonis[1,2], Gad Getz[5, 9, 10], Giacomo Oliveira[1, 2], Patrick A. Ott[1, 2, 5, 11, 12], Jeremy M. Simon[3, 6], Viktor A. Adalsteinsson[5], Derin B. Keskin[1, 2, 4, 5, 13, 14], Panagiotis A. Konstantinopoulos[1,2,15, *], Catherine J. Wu[1, 2, 5, 12,*]

*These authors contributed equally and are both corresponding authors
Corresponding Authors: Catherine_Wu@dfci.harvard.edu, Panogiotis_Konstantinopoulos@dfci.harvard.edu

Affiliations:
[1] Department of Medical Oncology, Dana-Farber Cancer Institute, Boston, MA, USA
[2] Harvard Medical School, Boston, MA, USA
[3] Department of Data Science, Dana-Farber Cancer Institute, Boston, MA, USA
[4] Translational Immunogenomics Laboratory, Dana-Farber Cancer Institute, Boston, MA, USA
[5] Broad Institute of MIT and Harvard, Cambridge, MA, USA
[6] Department of Biostatistics, Harvard T.H. Chan School of Public Health
[7] Centre for Immuno-Oncology, Nuffield Department of Medicine, University of Oxford, Oxford, UK
[8] Krantz Family Center for Cancer Research, Massachusetts General Hospital, Boston, MA, USA
[9] Department of Pathology, Massachusetts General Hospital, Boston, MA, USA
[10] Department of Pathology, Harvard Medical School, Boston, MA, USA
[11] Center for Immuno-Oncology, Dana-Farber Cancer Institute, Boston, MA, USA
[12] Department of Medicine, Brigham and Women's Hospital, Boston, MA, USA
[13] Section of Computational Biomedicine, Department of Medicine, Boston University School of Medicine
[14] Department of Medical Education and Biomedical Sciences, Methodist University CFVH School of Medicine, Fayetteville, North Carolina, USA
[15] Mellen and Eisenson Family Center for BRCA and Related Genes, Dana-Farber Cancer Institute, Boston, MA, USA

ABSTRACT

Personalized neoantigen-targeting cancer vaccines (PCV) in the adjuvant setting are of increasing interest across malignancies. Herein, we report the results of a first-in-disease phase I clinical trial testing the feasibility and safety of PCV for high-grade epithelial ovarian cancer (HGOC). 'NeoVax' consisted of pools of synthetic long peptides targeting patient-specific neoantigens admixed with the immunostimulant polyICLC, was combined with delayed administration of anti-PD-1 antibody, and was tested in 10 patients (one newly diagnosed patient (Cohort A) and 9 patients at first recurrence (Cohort B)) with platinum-sensitive OC following standard-of-care (SOC) platinum doublet chemotherapy. Nine of 12 evaluable Cohort B patients were vaccinated (75%, 90% CI 47-93%) and 1 of 9 Cohort A patients (11%, 90% CI 0.6 – 43%). No unexpected safety signals were encountered and no patients discontinued treatment due to toxicity. Across patients, >70% selected targets remained detectable by non-invasive cell-free DNA analysis despite a median of 6.5 months from the time of diagnostic biopsy to vaccine administration, during which patients received SOC chemotherapy. Biomarker analysis was suggestive of biologic activity of the vaccine in 6 of 10 patients and this was associated with broader tumor and vaccine-specific immune responses in blood and tumor following vaccination. Resistant tumor clones reflected diverse mechanisms affecting antigen presentation, indicative of immune-selective pressure exerted by vaccination. Overall, the interplay between the repertoire of antigens presented by the tumor and the breadth of induced immunity appeared to dictate clinical efficacy following vaccination. ClinicalTrials.gov Identifier: NCT04024878

INTRODUCTION

Epithelial ovarian cancers, 90% of which are *TP53* mutant, high grade serous type, were among the first malignancies for which the frequency of CD8 tumor infiltrating lymphocytes (TIL) and their ratio to regulatory T cells (Treg) were associated with overall survival[1,2]. However, OC has largely not benefited from modern cancer immunotherapy. Anti PD-(L)1 monotherapy induces objective responses in <10% of patients with ovarian cancer[3,4] and the addition of immune checkpoint blockade (ICB) to standard cytotoxic therapy has only recently received FDA approval[5], after multiple negative trials. Underlying reasons include tumor heterogeneity, low tumor mutation burden (TMB)[6], systemic immune suppression[7], and an immunosuppressive microenvironment, characterized by suppressive myeloid populations[8], Tregs[2,9] and stromal cells[8]. Furthermore, most OC tumors exhibit immune desert or immune excluded immunopathology[10], likely reflecting poor priming of endogenous immune responses.

The rate of HGOC missense mutations arising from single nucleotide variants (SNVs) and short insertions and deletions (INDELs) is similar to other low TMB malignancies in which PCVs have generated vaccine-specific immunity[11-13]. We hypothesized that PCVs in the adjuvant setting following SOC therapy would directly address tumor heterogeneity and overcome deficiencies in immune priming, allowing anti-tumor T cell responses to be initiated, amplified, and diversified. Moreover, PCV administration after chemotherapy (and in select cases, surgery) at a time of low tumor burden, could potentially provide consolidating therapy and prevent recurrence. We thus conducted an phase 1 study integrating PCV into SOC therapy for platinum-sensitive HGOC.

RESULTS

Integrating a PCV with standard-of-care treatment for ovarian cancer

The study enrolled patients with newly diagnosed disease (cohort A), or with first platinum-sensitive recurrence (cohort B) (NCT04024878). Adjuvant NeoVax was administered as 5 priming doses over 3 weeks followed by booster doses at 12 and 20 weeks, with ICB (nivolumab) starting at week 14 (**Fig. 1a, Methods**). All patients underwent a tissue biopsy prior to starting SOC chemotherapy; newly diagnosed patients received interval cytoreductive surgery after 3 cycles. Feasibility and safety were the primary endpoints; for feasibility, <45% of prescreening patients achieving vaccination was defined as unacceptable (see **Supplementary Information** for full accounting of pre-defined endpoints). From November 20, 2020 to September 7, 2023, twenty-two patients consented to prescreening (**Fig 1b**); of these, 1 withdrew prior to prescreening biopsy and 9 subjects withdrew from the study before treatment consent (inadequate tissue from core needle biopsies [4], progression on SOC therapy [2], preference [2], and impaired performance status [1]). In total, 12 patients consented to treatment, and PCVs were designed and successfully synthesized for 11 patients (**Methods, Extended Data Fig. 1**); one patient withdrew consent prior to vaccine manufacture and one prior to treatment. In sum, nine of 12 evaluable Cohort B patients were successfully vaccinated (75%, 90% CI 47-93%) and one of 9 Cohort A patients (11%, 90% CI 0.6 – 43%) (**Fig 1b**).

Amongst the 10 vaccinated patients (**Fig. 1b**), their tumors harbored a median of 103 missense mutations (SNV and INDELs; range 51-150) (**Fig. 1c-top, Supplementary Table 1**), corresponding to a median TMB of 2.8 (range 1.4-4.1). Of these mutations, a median of 86.5 (range 45-127) encoded neoepitopes predicted to bind at least weakly (rank<2.0 by either class

I epitope prediction tools HLAthena[14] or NetMHCpanv4.0[15]) to the personal study subject HLA alleles **(Supplementary Table 2)**. Vaccines targeted a median of 14 mutations (range 7-15), consisting of a median of 15 peptides (range 8–18), 17-32 amino acids long (median: 23), that were allocated to 1 of 4 peptide pools (A-D) per patient **(Fig. 1d, Supplementary Table 3),** and administered subcutaneously/intradermally (sc/id) at each of 4 injection sites.

Median follow up after vaccination initiation was 6.3 months (range 3.9-21.3) at the time of the data cutoff (December 31, 2025). The median platinum-free interval (PFI) prior to sample collection for the 9 patients with recurrent disease was 19.7 months (range 7.9-51.5). Six patients entered into the clinical trial following progression through first-line maintenance therapy (PARP inhibitor [5], bevacizumab [1] [**Table 1, Fig. 1e**]); two others previously completed first-line maintenance PARPi therapy without progression. Four patients exhibited rising CA125 prior to starting vaccination (P106, P108, P114, P117), suggesting emergence of platinum refractory/resistant disease; three others exhibited signs of recurrence between priming (days 1-21) and the first booster dose at day 78 (P113 by imaging; P116 by rising CA125; P111 by both). Per protocol, treatment was allowed post-progression, if deemed that patients were deriving clinical benefit, progression was not rapid, treatment was tolerated, and continued treatment did not delay intervention to prevent serious complications of disease.

The study regimen was well-tolerated, without unexpected treatment-related adverse events (AEs, **Table 2**). The most common NeoVax-associated AEs were injection site reactions (70%), myalgias (50%), chills (50%) and neutropenia (50%); two grade 3 AEs occurred in one patient each (allergic reaction, neutropenia). In one patient (P111), grade 3 abdominal pain and

diarrhea were associated with Nivolumab. The primary safety endpoint was to report the percentage of patients who complete vaccine therapy without discontinuation due to toxicity. Nine of 10 vaccinated patients received all planned vaccine doses. P111's G3 ICB-associated diarrhea occurred in the context of progression on post-progression Nivolumab treatment, and was not considered the primary factor in discontinuing therapy (**Supplementary Information**). Thus, all evaluable, treatment-consented patients completed NeoVax and Nivolumab without discontinuation for toxicity (Cohort A: 1 of 1 [90% CI: 5-100%], Cohort: B 8 of 8 [90% CI: 69-100%]).

In the intervening months between the vaccine design biopsy (B1), and vaccine priming (median of 6.5 months; range 6.0-7.6), patients received SOC chemotherapy +/- surgery. As an *ad hoc* analysis, we interrogated the extent to which somatic mutations encoding neoantigens were still present at the start of vaccination via bespoke cell-free DNA (cfDNA) analysis ('MRD Tracker'[16], **Methods**). We detected > 50% of vaccine target SNV mutations for 7 of 10 subjects at priming (D1 or D15), and for an 8th, prior to the last NeoVax boost (D140). In aggregate, 56.5% and 73.1% of target SNV mutations were detected at priming and by the last boost, respectively (**Fig 1f**), indicating that vaccines remained relevant to tumor mutations present at the time of vaccine administration, despite intervening treatment.

Patterns of tumor biomarker and vaccine immune responses following NeoVax plus nivolumab

Progression-free survival (PFS) after vaccination was highly variable (median 3.3 months, range 1-NR). We used blood-based CA125 and cfDNA-based assays to indirectly track tumor

burden across organ sites over time. Nine of 10 patient tumors expressed plasma CA125 (all except P113); all subjects were analyzable with bespoke MRD Tracker assays, using a median of 900 (range 160-950) coding and non-coding SNV mutations, to assess average tumor variant allele frequencies (VAFs) and limits of detection by time point (**Fig 2a-c**; **Extended Data Fig 2**).

We observed three patterns of tumor-burden response (see **Methods**). First, four patients were "progressors" (P111, P113, P114, P117), exhibiting progression by RECIST criteria prior to vaccine boosting *and* steep and unabated rises in CA125 and/or cfDNA VAF following vaccination. In the case of P114, an early stabilization of cfDNA was attributed to palliative radiation of a residual, symptomatic vaginal cuff lesion in week 5, followed by rising biomarkers (**Fig. 2a)**.

A second group also exhibited early rising CA125 and cfDNA (P106 and P108 prior to starting priming; P116 prior to first boost), but in contrast to the trend for progressors, both measures concordantly leveled-off or decreased around the first booster dose (D78+/-7), before eventually rising again (**Fig. 2b**), suggesting "transient control" of disease. For P106 and P108, the timing of biomarker-measured control before the start of nivolumab (D92+/-7)) was consistent with an effect from vaccination. For P116, the CA125 and cfDNA declines occurred following nivolumab administration and while on SOC PARPi maintenance therapy.

Finally, three patients exhibited prolonged disease control (P118, P119, P122), in which CA125 remained consistently low following vaccination (**Fig. 2c**). P118 exhibited a partial response to

SOC chemotherapy, with normalization of CA125, but residual disease by imaging; P119 and P122 were in complete response (CR) following SOC chemotherapy. Strikingly, despite persistently low CA125 levels, all three patients exhibited dynamic cfDNA changes between D15 and D300, suggesting episodes of tumor growth and regression, with vaccination and nivolumab as the only interventions. For P122, cfDNA levels peaked at D140 and then decreased to below the limit of detection (D274), with the patient remaining disease free through to data cut off (Day 650) (**Fig. 1e, Fig. 2c; Extended Data Fig. 2)**.

Overall, these *ad hoc* serologic tumor burden analyses reveal dynamic changes in serum biomarkers for 6 of 10 patients, which may be consistent with on target immunologic activity from combined NeoVax with nivolumab.

Peripheral immune responses following NeoVax

To define the extent to which NeoVax followed by nivolumab elicited circulating vaccine peptide-specific T cell responses and whether these differed amongst the biomarker subgroups, we performed exploratory *ex vivo* IFN-γ ELISpot assays on pre- and serially collected post-vaccine PBMC, using treatment pools of full-length 17-32-mer immunizing peptides. In 8 of 10 patients, we detected *ex vivo* IFN-γ reactivity[17] to at least one vaccine pool, most commonly peaking after the week 12 boost (**Fig. 2d, Extended Data Fig. 3a**). To define the immunogenicity of individual peptides, we further tested each immunizing peptide for its ability to stimulate IFNγ reactivity using post-boost PBMCs (after first ['week 14', W14] or second boost ['week 22', W22]) that were expanded *in vitro* against vaccine peptide pools. Overall, 85 of 144 (59.0%) peptides were immunogenic (**Extended Data Fig. 4)**. A median of 7 peptides (range 4-15), from

a median of 7 mutations (range 4-13) were immunogenic, per patient. Of note, the vaccines of the 6 patients with transient or prolonged disease control induced immune responses to a larger number of vaccine target mutations than for progressors (mean 9.3 vs. 5.5 mutations; $P = 0.029$) (**Fig. 2e**); there was also a trend towards an increased number of targeted mutations for transient and prolonged controllers (mean 14.3 vs. 10.5 mutations; $P = 0.132$; **Fig. 2f**). No differences were found between the serum biomarker-defined groups in relation to immunogenicity rate, missense mutation burden, PFI (**Fig. 2g-i**), or frequency of recurrence on active PARPi treatment prior to prescreening consent ($P = 0.77$ [Chi Square]).

To identify vaccine- and nivolumab-induced TCR clonotypes, we assessed peripheral TCRβ chain dynamics in $CD3^+$ PBMC across the vaccination course for all subjects (**Methods**; **Extended Data Fig. 3b-c**). A median of 82.5 (range 7-150) NeoVax-, and 96.5 (range 18-650) post-nivolumab-expanded clonotypes **(**Fisher's exact test $P < 0.05$; **Extended Data Fig. 3b)** were detected. In two transient controllers (P108, P116) for whom TCRβ clonotypes at a later timepoint (~ W40) could be assessed, post-NeoVax- and post-nivolumab-expanded clonotypes were long-lived, comprising a similar frequency of the TCR repertoire at W40 as at W14 and W22 (**Extended Data Fig. 3c**), consistent with T cell memory responses.

Identification of immune populations in NeoVax patient biopsies

We collected and processed fresh tumor biopsies from 6 of 10 patients for single cell (sc) RNA- and TCR- sequencing (**Fig. 3a**). These included biospecimens collected at individual time points (B1, B2, and B3) for three disease progressors (P117, P111, P114), and paired pre- and post-vaccine time points for one progressor (P113) and two transient controllers (P108, P116).

To increase resolution of cell type identification, a pre-vaccine sample was included for one additional patient who did not proceed with vaccination due to progression (P112). We obtained 25,103 high-quality single-cell transcriptomes (median 7,371 UMI/cell, 3,045 genes/cell). By unsupervised clustering, we identified 16 clusters comprised of diverse immune and non-immune cells (e.g. tumor, fibroblasts) **(Fig. 3b, Extended Data Fig. 5a**). Progressors exhibited a trend towards higher intratumoral fractions of monocyte/macrophages (**Fig. 3b-c**), which expressed inhibitory receptors (e.g. *VSIR*, *TNFRSF14*, *LGALS9*, *SIRPA*; **Supplementary Fig. 1a**), consistent with a suppressive role. In contrast, higher fractions of T/NK and B cell populations were detected in transient controllers than in progressors (**Fig. 3b-c**).

To better understand the interaction between the intratumoral T cell compartment and treatment with NeoVax with nivolumab, we re-clustered T cell populations (**Extended Data Fig. 5b-c, Supplementary Fig. 1b**). Progressor tumor biopsies contained higher fractions of exhausted T cells (CD4.TTE, CD8.TTE) and Tregs (CD4.TReg, CD4.NR4A1.TReg), as well as a trend towards lower CD8:CD4 ratio **(Fig. 3d**). We observed a higher Shannon diversity index amongst T cell clonotypes in transient controller biopsies (**Fig 3e**; two tailed Mann Whitney test, P = 0.004). Progressor patient P113 uniquely displayed relatively larger numbers of TIL with expanded clonotypes, the majority of which represented T_{EX} phenotypes (**Extended Data Fig 5d-e**). While limited by the number of paired pre- and post-vaccine biopsies, we noted a trend toward higher Treg fractions amongst progressor patients, and increased intratumoral T cell clonotype diversity amongst transient controllers.

Assessment of TIL tumor and vaccine target reactivity following NeoVax

To discern the extent to which TIL might recognize tumor and vaccine target antigens, we analyzed the T cell responses of P108 (transient controller) and P113 (progressor), whose tumors had been profiled at single cell resolution over time and from which patient-derived organoids (PDO) had been generated. The source cells for P108 PDO (O108-B2; **Fig. 3f**) were obtained on D126, ~1 month after booster 1 and the initiation of nivolumab; we were unable to generate a PDO from pre-treatment cells (B1). For P108, 45 of 83 mutations were detected at the RNA level from the B1 biopsy, including 13 of 14 vaccine target mutations. All O108-B2 *TP53* reads mapped to the parental tumor's *TP53* mutation, reflecting pure tumor origin. However, only 13 of 83 somatic missense variants, and only 3 of 14 vaccine target mutations were expressed, consistent with either lost target antigen expression in the subclone represented in the biopsied recurrence or subclone selection during organoid generation. We observed less clonal evolution in the tumors from P113, from which we propagated PDO lines from 2 independent biopsies (**Fig 3g**): (i) the "pre-Vax" B1 biopsy procured prior to SOC chemotherapy from a left upper quadrant abdominal wall mass (O113-B1); and (ii) the "post-Vax" B2 biopsy, procured on D95, 17 days after booster 1 and 4 days after nivolumab initiation, from an abdominal wall lesion at the same site as B1 (O113-B2). All *TP53* RNAseq reads from the O113 lines represented the tumor variant allele, and >50% of B1 missense mutations were expressed (including 4 and 5 of 9 vaccine target mutations for O113-B1 and -B2, respectively); 58.4% (59 of 101) of the B1 mutations were expressed in the parental tumor RNA.

Expanded TIL clonotypes with an exhausted phenotype (T_{EX}) in solid tumors have been reported to be enriched for tumor-reactive cells[18,19], including a small series of TIL TCRs in ovarian cancer[20], whereas expanded effector memory (T_{EM}) TIL clonotypes are enriched for viral

specificity[18]. To confirm this in OC and in the PCV setting, we evaluated 14 expanded T_{EX} clonotypes (having ≥ 3 cells through the entire data set, majority from the CD8.TTE cluster) and 9 expanded T_{EM} clonotypes identified from the B1 and B2 biopsies of P108 (**Extended Data Fig 5e**; **Supplementary Table 4**). Thirteen of 14 T_{EX} clonotypes were present in the post-vaccine B2 biopsies and 11 of 14 were more highly represented in the post- vs. pre-vaccine biopsies, consistent with post-vaccine/nivolumab expansion. Cloning and specificity testing of individual clonotypes revealed that 9 (5 strong, 4 borderline) of 14 expanded T_{EX} clonotypes (but only 1 (borderline) of 9 T_{EM} TCRs) exhibited CD137 upregulation after co-culture with O108-B2 PDO (**Fig. 3h; Extended Data Fig. 6a-b**). Five of 9 T_{EM} TCRs exhibited reactivity against autologous EBV-immortalized lymphoblastoid cell lines (LCL). These data confirmed that the T_{EX} and T_{EM} TIL are enriched for tumor and viral reactivity, respectively[18]. We did not identify NeoVax-specific clonotypes amongst tested P108 TIL. As O108-B2 lacked expression of the majority of vaccine target antigens, we interpreted the presence of TIL tumor-reactivity in the absence of vaccine reactivity as potentially consistent with epitope spreading of T cell responses to non-vaccine target antigens.

Analogous evaluation of P113 revealed a strikingly different pattern of TIL reactivity. P113 biopsies B1, B2 and B3 captured more T cells than for P108, including a higher proportion of T_{EX} cells, and a larger number of expanded clonotypes (**Extended Data Fig. 5d-e**). We cloned and tested TCRs from 22 expanded T_{EX} clonotypes (in this case, each representing > 10 cells), including the top 6 expanded exhausted TCRs in each biopsy (**Extended Data Fig. 5e**; **Supplementary Table 4**). TCRs from 20 of 22 T_{EX} cells reacted strongly to Pre-Vax O113-B1, with the level of CD137 upregulation generally increased by PDO pretreatment with IFNγ (**Fig 3i, Extended Data Fig. 6a**

& c, Supplementary Table 4); 19 recognized Post-Vax O113-B2, but generally with lower levels of CD137 upregulation when compared to co-incubation with O113-B1 (**Fig. 3j**). Of the 3 expanded T_{EM} clonotypes (≥6 cells) tested, 2 recognized autologous EBV-LCL, again consistent with enrichment of viral antigen specificity in the T_{EM} compartment; 1 of these, exhibited reactivity to both B1 and B2 PDO. Overall, the majority of expanded T_{EX} TIL recognized autologous PDO, with the highest reactivity against the Pre-Vax PDO.

Pulsing of P113 autologous EBV-LCLs with vaccine peptide pools prior to co-incubation with cloned TIL-TCRs, revealed 4 T_{EX} TCRs (5, 6, 19 and 20), which recognized vaccine pool C. All four were reactive against the same DPP3 p.L658R epitope, LT**R**RDTVLL (**Fig 3j; Extended Data Fig 6e-f**). TCR6 had the highest avidity, followed by TCR20, TCR5 and TCR19 (**Fig 3k**). Only TCRs 5, 19, and 20 were present in B1, where they comprised ~15% of T_{EX} cells, and 12.5% of antigen-experienced, non-T_{Naive} T cells overall, with TCR5 dominating (**Extended Data Fig 5g**; **Fig 3l**), consistent with a pre-existing immune response. However, in the post-Vax recurrent tumor at B2, all 4 clonotypes were present (TCR 6 was newly detected), with over 80% of the DPP3 p.L658R specific TIL now represented by the two TCRs with highest avidity (6 and 20). The fraction of DPP3 p.L658R-specific, antigen experienced, non-T_{naive} TIL remained relatively stable across the vaccine booster doses, but was dominated by further expansion of the highest avidity TCR6 (**Fig 3l**). This shift was mirrored in the peripheral blood, where we detected circulating TCRβ chains matching TCR 5, 6 and 20 at W14 (after boost 1), with further increased fraction by W22 (**Fig 3m**). Although the distribution of DPP3 p.L658R-specific TIL with non-naïve, T_{TE}, T_{PE}, T_{Prol} and T_{EM} phenotypes was similar between B1 and B2, there was a shift towards $T_{PE,}$ T_{Prol}, and even T_{EM} phenotypes at B3, following booster dose 2 and ~ 6 weeks of nivolumab treatment (**Fig 3n**).

Altogether, these observations support the expansion of vaccine-reactive clonotypes in P113, especially a new high avidity clonotype, following vaccine boost and nivolumab, both in tumor and peripheral blood.

Mechanisms of tumor escape across study subjects

To dissect the potential immune selective pressure imposed by NeoVax with nivolumab, we first assessed if vaccination was linked to changes in tumor transcriptional programs. Bulk tumor RNAseq from B1 pre-vax biopsies revealed relatively similar class I and class II antigen presentation-related gene expression across tumors, with only progressor P117's tumor exhibiting a trend towards lower expression than other tumors (**Supplementary Fig. 2a)**. We next used GSEA analysis of pre- and post-vaccination biopsy scRNA-seq to assess tumor cell transcriptional programs. While this did not reveal any clear mechanisms of immune escape for post-vaccine tumor cells from P108 or P116, P113 post-vaccine and nivolumab (B2 and B3) tumor cells (but not T cells) exhibited significantly down-regulated gene sets related to TNFα, IFNα and IFNγ signaling compared to pre-vaccine (B1) (**Supplementary Fig. 2b; Fig. 4a**). Of note, O113-B2 genomic DNA harbored a chromosome 1 inversion structural variant (SV) at p31.3, affecting the 3rd intron of *JAK1* and an intergenic region ~1.6Mb away (*chr1:64,882,954::chr1:63,277,187* (hg19); **Extended Data Fig. 7a-d).** This breakpoint was not observed in genomic DNA from pre-vaccine B1 whole genome sequencing, nor detectable via PCR from B1-derived PDOs (**Extended Data Fig. 7c-d**), consistent with a treatment emergent SV. RNAseq from only the post-vaccine PDO showed a loss of poly-adenylated RNA derived from *JAK1* exons 4-25 (**Fig. 4b**). As expected, *JAK1* interruption in post-vaccination PDO was associated with abrogation of STAT1 phosphorylation and HLA-I upregulation following IFNγ stimulation compared to pre-vaccination

organoid (**Fig. 4b-c**); it was not associated with resistance to carboplatin and doxorubicin, the SOC chemotherapies received prior to vaccination (**Extended Data Fig. 7e**). Strikingly, re-introduction of *JAK1* cDNA into O113-B2 rescued STAT1 phosphorylation, HLA-I expression and DPP3 p.L558R vaccine-specific TIL TCR recognition (**Fig. 4d, Extended Data Fig. 7f-k)**. Thus, a *JAK1* SV mediating reduced antigen presentation was associated with escape from combined NeoVax with nivolumab therapy in P113.

We asked if there might have been pre-existing mechanisms of immune escape in any of our patients. Loss of heterozygosity (LOH) in the HLA loci on chromosome 6 (chr6) has been previously associated with immune escape[21] and has been reported at least 15% of OC tumors at the time of diagnosis[9,21]. We detected regions of chr6 LOH in tumor cells from B1 biopsies of 3 of 10 vaccinated patients, including 2 of 4 progressors (P111, P117; **Fig 4e** and **Extended Data Fig 8a**); WES data from 6 unvaccinated, prescreening consent patients, revealed 2 further cases of chr6 LOH in the HLA locus, (total 5 of 16 [31%]; **Extended Data Fig 8b**). For P111 and P117, such LOH was associated with loss of an entire haplotype covering HLA-A, B and C (**Extended Data Fig 9)**. Thus, the HLA alleles for a substantial fraction of the best predicted epitopes (by *HLAthena*) for vaccine mutations were lost (3 of 7 for P111; 6 of 16 for P117) and for mutations for which we could measure a peripheral immune response (2 of 4 for P111; 3 of 8 for P117). Taking into account all possible strong and weak binders, >45% of predicted epitopes contained in the immunizing peptides lost their predicted HLA binding allele (**Fig 4e**). Likewise, for the prolonged controller P118, the HLA alleles for the best epitope were lost for 10 of 14 target mutations and 10 of 13 immune response mutations. No new HLA LOH was evident by WES at progression in the 3 patients with a recurrence biopsy (P106, P108, P113), though tumor fraction

of < 20% in the samples tested for P108 and P106, limited sensitivity for LOH analysis. Altogether, across these three patients with chr6 LOH, the HLA alleles for the best predicted vaccine targets were lost for 19 of 36 mutations, constituting substantial baseline compromise of potential vaccine target epitope presentation in tumors. The difference in clinical outcome for P118 vs. P111 and P117, may be related to productive immune responses against an antigen(s) presented by retained HLA alleles, or potentially, other factors.

To better understand the importance of these observations in OC, we asked how allele specific HLA-loss intersects with important clinical ovarian cancer biomarkers: (i) homologous recombination deficiency (HRD) or HR proficiency, which defines the use of PARP inhibitors; and (ii) *CCNE1* amplification, which is enriched in HRP tumors[6], portends worse prognosis, and is an emerging target. Analysis of a TCGA ovarian cohort (n = 160) with paired RNA and WES data revealed a ~31% rate of loss of HLA diversity (25.6% rate of HLA-LOH, 5.6% as loss allele specific expression (ASE) at the RNA level, without detected LOH [data retrieved from Filip et al.[22]]). As high levels of genomic LOH are a defining characteristic of HRD status[23,24], we hypothesized that HLA LOH might be more frequently associated with HRD than HRP tumors. Indeed, across all TCGA tumors, HRD status[24] associated with increased HLA-LOH but not transcriptionally detected loss of HLA ASE. Within OC, however, there were similar levels of HLA-LOH, as well as -ASE, in both HRD and HRP tumors (**Extended Data Fig. 8c**). Similarly, we found no difference in the rate of HLA-LOH or -ASE loss[22] in *CCNE1* amplified vs. non-amplified tumors[25] (**Extended Data Fig. 8d**). These data highlight the broad importance, across biomarker subgroups, of considering HLA allele retention and expression for antigen-directed therapies in high grade OC.

Finally, we asked if there was evidence of immune selective pressure against vaccine target mutations in either recurrence biopsies or by cfDNA, independent of HLA LOH. We were able to generate WES data from recurrence biopsies for P106, P108 and P113; of note, we did not identify any mutations in genes which would be expected to contribute to immune escape (e.g. *TAP1/2*, *B2M*, *JAK/STAT*, etc). For transient controllers P106 and P108, we found 3 of 15 and 6 of 14 vaccine target mutations, respectively, that were lost in the recurrence biopsies (**Fig 4f**). This included the loss of one truncal mutation for P108 (Cancer Cell Fraction (CCF) = 1; *POLQ2* [p.R708G]) and 3 mutations with CCF > 0.5 (*FDFT1* [p.T275S]; *URB1* [p.A1107T]; *ACTR10* [p.A229G]); of note the *URB1* SNV was detected in cfDNA at priming, indicating that it was not lost during SOC chemotherapy prior to vaccination. For P108 we also noted decreased RNA expression of three vaccine target genes *TTC3, FLNA*, and *SRSF3* in B2 vs. B1 biopsy tumor cells by scRNAseq, consistent with transcriptional down-regulation of some vaccine targets, though we could not determine mutant allele expression (**Supplementary Fig. 2**). For P106, two mutations lost at recurrence were truncal (*ARHGAP27* [p.A509G] and *PLCB2* [p.E741Q]) and the third had CCF > 0.5 (*PPP1R12A* [p.R682T]). In contrast, P113, for whom *JAK1* loss globally decreased antigen presentation (**Fig. 3j, 4c-d**), only 1 of 9 vaccine target mutations was lost at recurrence (**Fig 4g**) and no vaccine target mutation genes exhibited decreased RNA expression (**Supplementary Fig. 2**).

To corroborate these results, we asked if we might see differences in cfDNA VAFs of vaccine target SNVs vs. non-target, missense SNVs. Although the small sample size limited our power to identify significant differences, for P106 and P108, we observed a trend towards lower mean VAFs for vaccine target mutations vs. non-target mutations at post-priming timepoints (**Fig 4f**). In

contrast for P113, vaccine target and non-target SNV mutation cfDNA VAFs were similar at all timepoints. In other patients, cfDNA VAFs did not clearly differ between target and non-target mutations (**Extended Data Fig 10**). Taken together, these data suggest differential selective pressure on vaccine target vs. non-target mutations in patients P106 and P108.

DISCUSSION

We report a first-in-disease clinical trial in the low TMB setting of High Grade OC of synthetic long peptide neoantigen vaccination combined with nivolumab as maintenance therapy following SOC chemotherapy +/- cytoreductive surgery. Consistent with efforts in other low TMB diseases[11-13,26], we generated personalized genomics-guided vaccines that induced robust immune responses in all patients.

Non-invasive tumor monitoring utilizing blood serum/plasma biomarkers enabled us to demonstrate vaccine targeting and activity. We confirmed that personalized approaches can be integrated around prolonged SOC treatments via cfDNA-based detection of the majority of vaccine target mutations (designed using pre-treatment biopsies) even after ~6 months of SOC therapy. Further, we demonstrated dynamic cfDNA changes in six of 10 patients, supported by CA125 dynamics, consistent with waves of on-target immune activity; in P122, cfDNA rose during the initial vaccine course, peaking at the time of the final NeoVax booster, before declining to below the LOD, with the patient remaining disease-free through data cut off (>12 months), potentially reflecting immune-mediated disease clearance. Importantly, observed biomarker responses were associated with broader immune responses highlighting the importance of a multi-targeted vaccine, presumably to better address tumor heterogeneity and/or maximize the likelihood of inducing effective on-tumor responses. These data also highlight the utility of cfDNA in adjuvant vaccination trials – allowing both an understanding of vaccine relevance to residual disease, and serving as a biomarker for response. With primary tissue often difficult to access, cfDNA will be a critical biomarker for future studies.

We identified several potential resistance mechanisms (either pre-existing or treatment-emergent) that point to the impact of immune selective pressure. Our analyses highlighted previously identified mechanisms of immune resistance in OC, including elevated T_{reg} fractions[2] and immunosuppressive macrophage/monocyte[10] populations in progression patients. However, the most robust link to therapy resistance in our study was loss of antigen presentation in tumors: two of four primary progressor patients exhibited loss of HLA haplotype heterozygosity prior to vaccination, likely rendering more than half of vaccine antigens off target, and a third subject's tumor revealed treatment-emergent deficiency in interferon signaling, severely abrogating antigen presentation. We further identified evidence of immune editing or suppression by cfDNA and WES in 2 of 3 transient controllers, though we cannot exclude clonal evolution during SOC chemotherapy. Combined with our observation that broader immune response induction correlates with clinical benefit, a common theme emerges around the balance of induced immune responses and the capacity of tumor cells to present immunogenic antigens. Considering that ~31% of tumors analyzed in both our cohort and TCGA ovarian tumors exhibit allele specific HLA loss due to either genomic deletion or transcriptional repression, our work strongly supports recent calls to take into account HLA LOH and mechanisms of antigen presentation loss in vaccine design[27], for example by integrating this information into antigen selection workflows[28].

Finally, our work highlights the importance of choosing an optimal setting for PCV trials. High tumor burden carries with it increased extent of tumor heterogeneity, the fuel for clonal evolution and therapeutic resistance. In this vein, 5 of 10 enrolled patients exhibited progressing tumors at the time of vaccination, largely associated with recurrence on PARP inhibitor at trial

enrollment. We speculate that actively growing tumors, with an established immunosuppressive microenvironment and greater heterogeneity, pose substantial barriers to immune control in a disease that is minimally responsive to PD-1 blockade alone. We assert that introducing PCVs with first line treatment, at times of truly minimal residual disease may be more beneficial. Our work thus argues for (i) early vaccine approaches to target low volume disease, (ii) improved vaccine antigen selection to obtain broad and balanced responses, and (iii) targeting of antigens that tumors retain the HLA machinery to present.

We acknowledge limitations to our study. We experienced accrual challenges to cohort A, due to limited tissue from core needle biopsies and the changing regulatory environment for 1L maintenance; both issues are easily addressed for future studies. Our cohort was small and heterogenous with regards to the degree of platinum sensitivity, limiting our ability draw strong conclusions about clinical efficacy. We have utilized several orthogonal analysis platforms to define clinical benefit and identify resistance mechanisms that point to immunologic efficacy. Nonetheless, deep characterization of resistance mechanisms and cfDNA analysis in future trials will assuredly provide clearer insights into how best to establish vaccine efficacy in difficult-to-treat tumors like HGOC.

Funding Statement

This work was supported by NCI Dana Farber / Harvard Cancer Center Ovarian Cancer SPORE (P50-CA240243-05; to U.A.M, P.A.K, C.J.W), the Mark Foundation Endeavor Award (to C.J.W), NIH/NCI award 5R01CA276865 (to C.J.W.), Breast Cancer Research Fund award (to U.A.M and P.A.K), Friends of Dana Farber (to M.C.S and R.J.P.), the Fund in Memory of Patty Klein, the Feldmann Ovarian Cancer Research Fund, and the Blavatnik Family Foundation. M.C.S. received support from the Lubin Family Foundation, the Dana Farber NIH Medical Oncology training grant (NIH T32CA009172**)** and the Ovarian Cancer Research Association**.** A.S. was supported by a Wellcome Trust Early Career Award (227000/Z/23/Z). S.L is supported by the NCI Research Specialist Award (R50CA251956). E.H.S is supported in part by NCI K08CA237871. G.O. received support from the Claudia Adams Barr Program for Innovative Cancer Research and an American Cancer Society Institutional Research Grant. D.B.K. is supported by U54-CA272688, R01-HL157174, R01-CA285308, R01-CA279391, R01-NS140967 and Alex's Lemonade Stand. P.A.O. is supported in part by NCI-1R01CA229261, the Francis and Adele Kittredge Family Immuno-Oncology and Melanoma Research Fund, the Fisher Family Fund, The Morgan Family Fund for Melanoma Research, the Susana and Bruce Hampton Research Fund and the Faircloth Family Research Fund. C.J.W is a member of the Parker Institute for Cancer Immunotherapy at DFCI. Her work is supported, in part, by the Parker Institute for Cancer Immunotherapy. C.J.W. is also the Lavine Family Chair for Preventative Cancer Therapies at DFCI. The funders had no role in the conduct of the trial or in the analysis of clinical or immunological end points.

Acknowledgement Statement

We are appreciative of S. Hill for input and assistance with tissue processing; A. Afeyan for computational assistance with TCR identification, E. Lin for technical assistance; L. Pomerance for input on immune analyses; B. Igoresceu for input on cell free DNA; S. Pyle for artwork; staff at Almac Sciences for vaccine peptide manufacture; Bristol-Myers Squibb for providing Nivolumab; the DFCI Cell Manipulation Core Facility for sterility and endotoxin testing.

Author Contributions Statement

P.A.K is the principal investigator and directed the overall study. P.A.O. is the IND holder. M.C.S., P.A.K and C.J.W designed and performed experimental and data analysis together with J.A.F., B.S., A.V., R.L, C.F., C.R.T, K.T., S.C., C.S., K.X., P.J., A.C. H.E.S., V.C., W.L., T.J., M.R.Y., K.J.L., S.L., A.S., G.O., and D.B.K; C.F., M.Y.R., C.C., D.B.K., and P.A.K. analyzed sequencing data and selected neoantigen targets; S.C., N.T., and J.M.S. designed and performed statistical analyses; S.S., M.H, O.O., and H.G. coordinated clinical research; R.P., E.H.S, C.K. and U.A.M. were co-investigators on the clinical trial and provided patient samples; M.C.S., R.L., C.S., K.X., P.J., A.C., R.P., and V.A. performed cfDNA analyses; J.A.F., B.S., C.R.T., A.S., A.K., G.G. and J.M.S. performed computational analysis; M.C.S, K.T., H.E.S., and G.O performed TCR/organoid reactivity assays. M.C.S, P.A.K. and C.J.W. wrote the manuscript; all authors discussed and interpreted results and edited the manuscript.

Competing Interests Statement

M.C.S, J.A.F., B.S., A.V., R.L, C.F., C.R.T, K.T., A.K., S.C., C.S., K.X., P.J., A.C. H.E.S., V.C., W.L., T.J.3rd., M.R.Y., A.S., S.S., M.H., O.O., H.G., C.C., S.L., N.T., E.H.S. C.K., R.P., G.O., and J.S.M have nothing to declare. J.K.L. holds equity in Standard BioTools Inc. and is on the scientific advisory board for MBQ Pharma Inc. N.H. holds equity in and advises Repertoire

Immune Medicines, CytoReason, and Danger Bio/Related Sciences, owns equity and has licensed patents to BioNtech, and receives research funding from Bristol Myers Squibb, Moderna, ResolveM/JJDC, Takeda, and Calico Life Sciences. U.A.M. declares participation in scientific advisory boards: NextCure, Abbvie, Immunogen, Profound Bio, Eisai, the Ovarian Cancer Research Alliance, Tango Therapeutics, Novartis, GSK, Daiichi Sankyo, DayOne Bio, and Whitehawk Therapeutics; UAM also reports participation in a data safety-monitoring board: Mural Oncology, Macrogenics, Daiichi Sankyo, Astrazseneca and Symphogen, all unrelated to this work. V.A.A. is a co-inventor of the MAESTRO MRD test which has been licensed to Exact Sciences and receives research funding from Exact Sciences which was not involved in this study. V.A.A. is also a co-founder and advisor to Amplifyer Bio. G.G. receives research funds from IBM, Pharmacyclics/Abbvie, Bayer, Genentech, Calico, Ultima Genomics, Inocras, Google, Kite, AstraZeneca and Novartis and is also an inventor on patent applications filed by the Broad Institute including those related to MSMuTect, MSMutSig, POLYSOLVER, SignatureAnalyzer-GPU, MSEye, MinimuMM-seq, DLBclass, HapASeg, Tonly2, MSIDetect, TuFEst, and ABSOLUTE2. A full list of G.G.'s publicly available patent applications can be requested from the Broad's legal team at patents@broadinstitute.org. G.G is a founder, consultant, and holds privately held equity in Scorpion Therapeutics; he is also a founder of, and holds privately held equity in Predicta Biosciences; and a consultant and holds privately held equity in Antares Therapeutics. D.B.K. owns equity in Affimed N.V., Agenus, Armata Pharmaceuticals, Breakbio, BioMarin Pharmaceuticals, Celldex Therapeutics, Editas Medicine, Immunitybio, Lexicon Pharmaceuticals, Moderna, PDS Biotechnology, Prime Medicine, Sana biotechnologies and Viking Therapeutics. D.B.K. is a scientific advisor for Immunitrack, a wholly owned subsidiary of Eli Lilly and Company and

Breakbio. P.A.O. has received research funding from and/or has advised Agenus, Arcturus, Amgen, Armo BioSciences, Array, AstraZeneca/MedImmune, Bristol-Meyers Squibb, Celldex, CytomX, Evaxion, Immunetune, Imunon, LGChem, Merck, Neon Therapeutics (now BioNTechUS), Novartis, Pharmajet, Phio, Pfizer, Oncorus, Roche/Genentech, Servier, and Xencor. P.A.K. has received grants or contracts from Novartis, AstraZeneca, Pfizer, Eli Lilly, Bayer, Merck, GlaxoSmithKline, Tesaro, and Merck KGaA and has received consulting fees for serving on advisory boards from AstraZeneca, Bayer, GlaxoSmithKline, Alkermes, Kadmon, Bristol Myers Squibb, IMV, Repare, Artios, Mersana, Novartis, Cardiff Oncology, Schrodinger, Inc., Mural Oncology, Scorpion, and Nimbus. C.J.W. is an equity holder of BioNtech, Inc,, and is a SAB member of Repertoire, Aethon Therapeutics, Nature's Toolbox and Adventris.

TABLES

Table 1: Baseline characteristics of patients receiving NeoVax:

		Overall (N=10)
Sex	Female	10 (100%)
Age	Mean (SD)	56.3 (6.31)
	Median [Min, Max]	56.4 [47.6, 69.3]
Race	White	9 (90%)
	More Than One Race	1 (10%)
Ethnicity	Hispanic or Latino	2 (20%)
	Non-Hispanic	8 (80%)
Cohort	A	1 (10%)
	B	9 (90%)
PFI	6-12 months	3 (30%)
	>12 months	6 (60%)
	N/A	1 (10%)
Prior PARPi	Yes	7 (70%)
	No	3 (30%)
Histology	Serous	9 (90%)
	Endometroid	1 (10%)
***TP53* Mutation**	Yes	10 (100%)
	No	0 (0%)

Table 2: Treatment related Adverse Events (Grades 1-5), occurring in ≥10% of subjects

AEs related to NeoVax: # of patients (%)	Grade 1	Grade 2	Grade 3	Total
Neutrophil count decreased	2 (20)	2 (20)	1(10)	5 (50)
Allergic reaction	0 (0)	0 (0)	1(10)	1 (10)
Injection site reaction	6 (60)	1 (10)	0(0)	7 (70)
Myalgia	4 (40)	1 (10)	0 (0)	5 (50)
Fatigue	3 (30)	1 (10)	0 (0)	4 (40)
Fever	1 (10)	1 (10)	0 (0)	2 (20)
Alanine aminotransferase increased	0 (0)	1 (10)	0 (0)	1 (10)
Anemia	0 (0)	1 (10)	0 (0)	1 (10)
Lipase increased	0 (0)	1 (10)	0 (0)	1 (10)
Serum amylase increased	0 (0)	1 (10)	0 (0)	1 (10)
Chills	5 (50)	0 (0)	0 (0)	5 (50)
Headache	5 (50)	0 (0)	0 (0)	5 (50)
Pain	3 (30)	0 (0)	0 (0)	3 (30)
Arthralgia	1 (10)	0 (0)	0 (0)	1 (10)
Dysgeusia	1 (10)	0 (0)	0 (0)	1 (10)
Erythema multiforme	1 (10)	0 (0)	0 (0)	1 (10)
Flu like symptoms	1 (10)	0 (0)	0 (0)	1 (10)
Nasal congestion	1 (10)	0 (0)	0 (0)	1 (10)
Platelet count decreased	1 (10)	0 (0)	0 (0)	1 (10)
Pruritus	1 (10)	0(0)	0 (0)	1 (10)
Rash maculo-papular	1 (10)	0 (0)	0 (0)	1 (10)
Skin induration	1(10)	0 (0)	0 (0)	1 (10)
Voice alteration	1(10)	0 (0)	0 (0)	1 (10)
AEs related to Nivolumab: # of patients (%)	**Grade 1**	**Grade 2**	**Grade 3**	**Total**
Diarrhea	0 (0)	1 (10)	1 (10)	2 (20)
Abdominal pain	0 (0)	0 (0)	1 (10)	1 (10)
Fatigue	2 (20)	1 (10)	0 (0)	3 (30)
Headache	1 (10)	1 (10)	0 (0)	2 (20)
Hypothyroidism	1 (10)	1 (10)	0 (0)	2 (20)
Pain	1 (10)	1 (10)	0 (0)	2 (20)
Colitis	0 (0)	1 (10)	0 (0)	1 (10)
Insomnia	0 (0)	1 (10)	0 (0)	1 (10)
Pruritus	3 (30)	0 (0)	0 (0)	3 (30)
Serum amylase increased	2 (20)	0 (0)	0 (0)	2 (20)
Back pain	1 (10)	0 (0)	0 (0)	1 (10)
Blurred vision	1 (10)	0 (0)	0 (0)	1 (10)
Dry mouth	1 (10)	0 (0)	0 (0)	1 (10)

Edema limbs	1 (10)	0 (0)	0 (0)	1 (10)
Hyperthyroidism	1 (10)	0 (0)	0 (0)	1 (10)
Hypoglycemia	1 (10)	0 (0)	0 (0)	1 (10)
Lipase increased	1 (10)	0 (0)	0 (0)	1 (10)
Mucositis oral	1 (10)	0 (0)	0 (0)	1 (10)
Vomiting	1 (10)	0 (0)	0 (0)	1 (10)

569

Figures

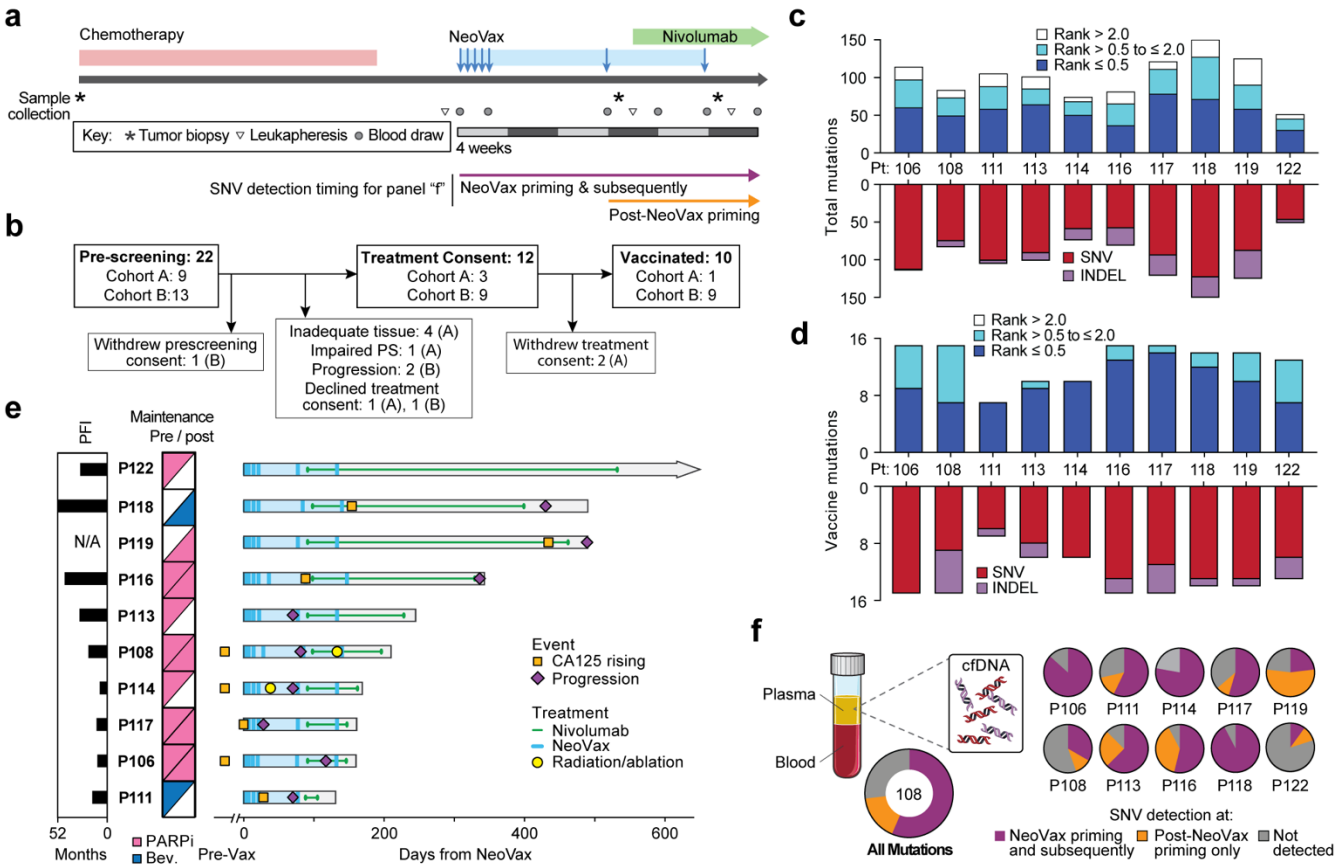


Figure 1: Vaccine generation and clinical courses. a. Trial schema including treatment and sample collection. Time periods for analysis of cfDNA in panel **f** are shown (bottom). **b.** Consort diagram of patients who signed prescreening consent, treatment consent and received vaccine (total and by cohort); reasons for withdrawal are indicated by cohort (parentheses). **c**. Summary of mutation characteristics per patient. Personal HLA binding neoantigen epitopes were predicted via HLAthena[14] or NetMHCpan[15], and the best epitope per mutation was defined by HLA binding strength: strong (rank < 0.5 by either algorithm), weak (rank > 0.5 and < 2.0) or very weak (rank > 2.0) (Top). Mutations were classified as derived from single nucleotide variants (SNV) or insertions/deletions (INDEL). **d.** Summary of vaccine target mutations for each patient, including HLA binding strength (top) and mutation type (bottom). **e.** Swimmers plot depicting the clinical outcomes for 10 patients treated with NeoVax plus nivolumab. Platinum free interval (PFI) and maintenance therapy prior to trial enrollment are indicated, as well as SOC maintenance therapy during the course of vaccination (left). "CA125 rising" reflects the first date that CA125 was > ULN or > 2x from nadir. **f.** Detection of SNV vaccine target

mutations by cell free (cf)DNA analysis at vaccine priming (D1 and/or D15) or during the duration of the clinical trial.

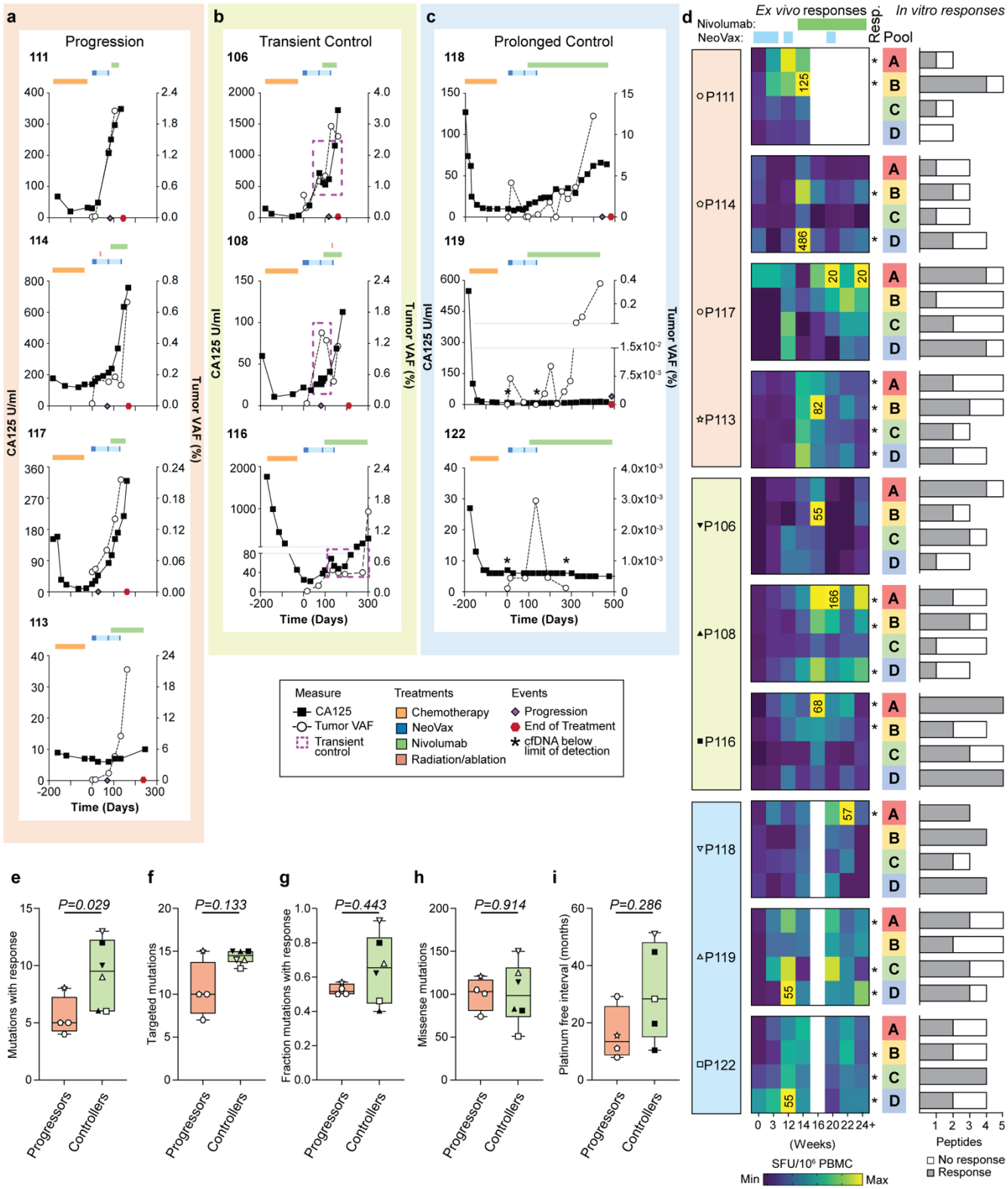


Figure 2: Clinical benefit defined by serum biomarkers and associated with peripheral immune responses. a-c. For each patient, serum CA125 (closed squares; left y axis) and cfDNA

mean tumor variant allele frequency (VAF) (open circles; right y axis; plotted as %) are plotted vs. time relative to vaccine day 0 (x axis). Mean cfDNA VAFs calculated from 150-900 coding and non-coding allele frequencies generated from WGS. Treatments are indicated above each graph and described in the figure legend key. Patients were assigned to one of three groups based on biomarker trends: (**a**) progression, (**b**) transient disease control, and (**c**) prolonged disease control. **d.** Heatmaps (left) represent the relative IFN-γ ELISpot count (normalized by patient) of serial post-vaccination PBMC re-stimulated *ex vivo* with Immunizing peptide (IMP) pools (middle); the maximum ELISpot count per patient is indicated and pools with responses passing response threshold are indicated by an asterisk (> 30 SFU/10^6, >3x over DMSO control, $P < 0.05$ by Distribution Free Resampling (DFR(EQ))[17]; See **Extended Data Fig. 3**). (Right) Fraction of IMPs per vaccine pool inducing T cell responses in each patient as assessed by deconvolution of vaccine peptide pools by *in vitro* IFN-γ ELISpot (See **Extended Data Fig. 4**). **e-i**. Comparison of progression (red; n = 4) vs. transient response and prolonged disease controllers (green; n=6 (**e-h**) and n = 5 (**i**)), with regards to total number of mutations targeted (**e**), fraction of target mutations with immune response (**f**), total number of mutations with induced immune response (**g**), tumor missense mutation count (**h**) and first platinum free interval (**i**). Individual patient values are graphed and box plots represent median +/- 1 quartile and error bars represent the minimum and maximum values; *P* values reflect two-tailed, Mann-Whitney test.

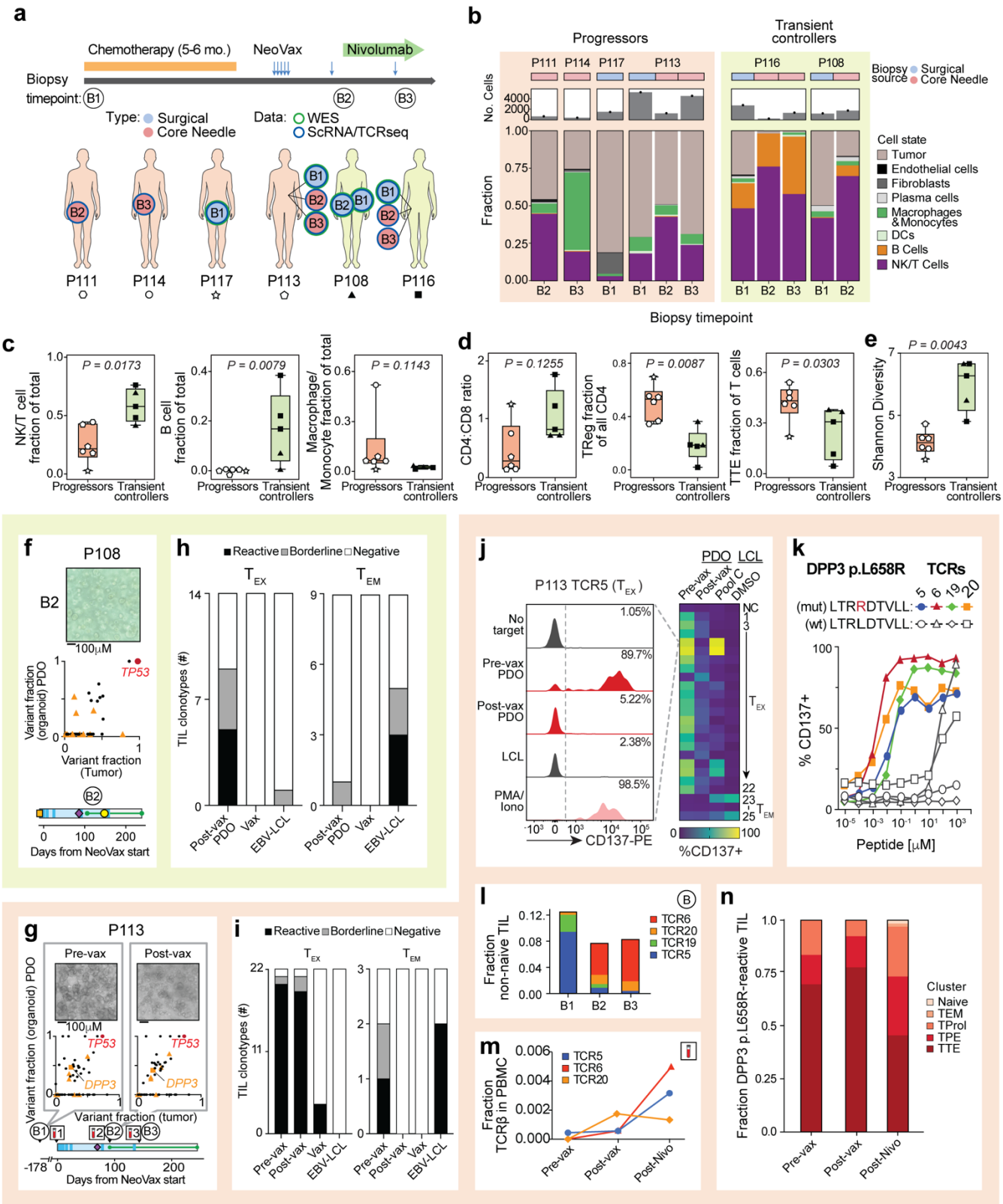


Figure 3: Evaluation of tumor microenvironment and TIL specificities from tumor biopsies.

a. Schema of tumor sample collection and processing in 7 patients. **b**. Cell populations identified by scRNAseq. Time point, biopsy type and clinical group are indicated. See also **Extended Data Fig 5**. **c.** Fraction of the indicated cell types in controllers (n = 6 biopsies) vs. progressors (n = biopsies) **d.** Fraction of the indicated T cell fractions in controllers vs. progressors **e**. TIL TCR Shannon Diversity for progressor and transient controller T cell clonotypes. For **c-e,** patient specific symbols are as indicated in **a**, box plots represent median +/- 1 quartile and whiskers extend to the minimum and maximum values, and, *P* values reflect two tailed Mann-Whitney tests. **f**. P108 Biopsy B2 (post-vax) PDO line validation: Top, PDO bright field images; middle, graphs comparing *TP53* (red), vaccine (orange), and non-vaccine (black) missense mutation variants in RNAseq from the B1 tumor biopsy (x axis) and the PDO line (y axis) (one sequencing sample, each); bottom, treatment timeline. **g**. Validation of P113 Pre-Vax B1 and Post-Vax B2 PDO, as in (**f**). **h**. Summary of CD137 expression screening of TCR reactivity against the indicated targets for 14 T_{EX} (left) and 9 T_{EM} (right) expanded TIL clones from P108. Reactivity defined as > 2 standard deviations above all controls (see also **Methods**, **Supplementary Table 4**, **Extended Data Fig 6a-b**); "borderline" indicates weak reactivity resulting in CD137 expression of < 10% or < 3x that induced by an irrelevant control TCR. Representative of 2 independent experiments. **d**. Summary of TCR reactivity screening for P113 T_{EX} (left) and T_{EM} (right) TIL clones as in (**b**) (see also **Supplementary Table 4**, **Extended Data Fig 7a, c-d**); **e**. Example of CD137 upregulation for vaccine reactive T_{EX} TCR 5 (left) vs. the indicated targets, and as well as for other tested TIL clonotypes vs. the indicated targets (heatmap, right). **d-e** representative of 2 independent experiments (B1 PDO) and 3 independent experiments (B2 PDO, vaccine pools). **f.** Avidity plots for four vaccine reactive TCRs from P113 TIL, for the DPP3 p.L458R epitope T<u>R</u>RDTVLL, as well as the wildtype sequence; Healthy donor T cells transduced with the indicated TCRs, were incubated with P113 autologous EBV-LCL pulsed with WT or mutant DPP3 peptide at the indicated concentrations, and % CD137 expression is graphed. Representative of 3 independent experiments. **g**. DPP3 p.L458R specific TIL as a fraction of non-naïve TIL (T_{EX}, T_{PE}, T_{Prol}, T_{EM}) in P113 tumor biopsy scRNAseq. **h**. Fraction peripheral blood *TCRB* clonotypes matching the indicated vaccine specific TCR clonotypes (TCR19 beta chain was not detected) are graphed from W1 (pre-vaccine), W14 (after boost 1), and W 22 (after boost 2 and nivolumab). **i.** Proportion of DPP3 p.L458R specific TIL belonging to the indicated clusters.

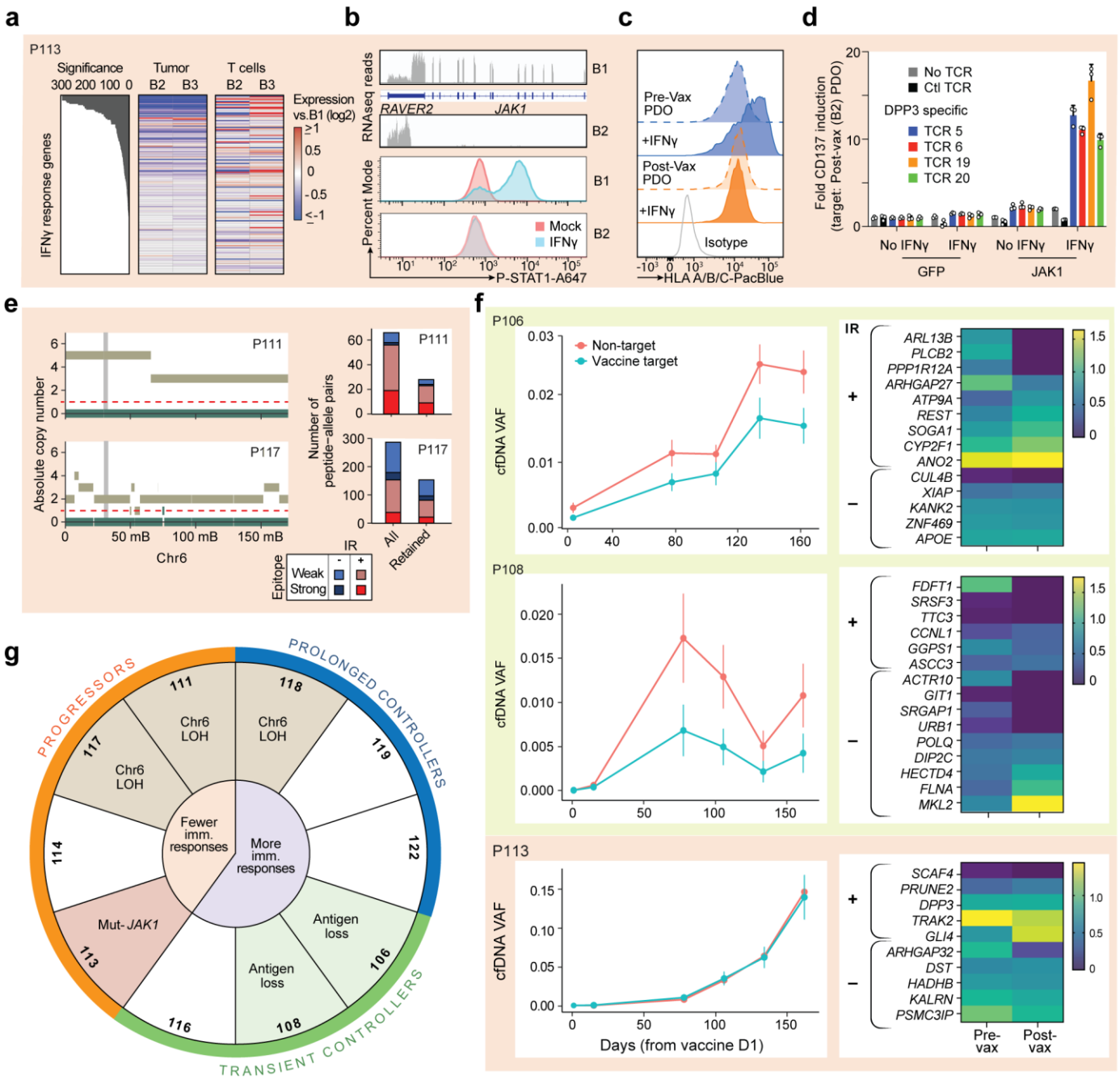


Figure 4: Mechanisms of immune evasion associated with progression.

a. Heatmaps representing the average expression of Hallmark IFNγ response geneset genes from tumor cells (middle) and T cells (right) from post-vax P113 B2 and B3, relative to pre-vax B1. Genes are ordered (top to bottom) by the most significant differential expression in tumor cells (Wilcoxan rank sum test with Bonferroni correction, calculated with FindMarkers in Seurat); significance is summarized on the far left [-log10(p-Adj + $1e^{-300}$]). **b**. Bulk RNAseq reads from pre-vax B1 and post-vax B2 organoids across the JAK1 locus (top), and phospho-STAT1

intracellular staining of pre-vax B1 and post-vax B2 PDO with or without 45 minutes IFNγ stimulation (bottom; representative of > 3 independent experiments). **c**. HLA-A/B/C expression by flow cytometry, with and without 24h IFNγ treatment for P113 pre-vax (B1) and post-vax (B2) PDO. Representative of > 3 experiments. **d**. Fold CD137 induction for T cells expressing DPP3 reactive TCRs or controls, following incubation with post-vax (B2) transduced with empty vector (GFP) or vector encoding *JAK1* cDNA (JAK1) and pre-treated or not with IFNγ. Analysis was performed in triplicate and values are normalized to mean percent $CD137^{+}$ after incubation with GFP-PDO without IFNγ (bars show mean + S.D.; see also **Extended Data Fig. 8**; representative of 2 independent experiments). **e**. ABSOLUTE copy number across chromosome 6 for P111 and P117 (left). (Right) Graphs depict predicted weak (HLAthena rank < 2.0) and strong (HLAthena rank < 0.5) epitope-HLA binding pairs for short epitopes within vaccine synthetic long-peptides, taking into account germline HLA alleles ("All"), and those HLA alleles retained in the tumor at biopsy B1, prior to vaccination ("Retained"; see **Extended Data Fig. 10**). **f.** cfDNA VAF of vaccine target (blue; n = 15 [P106], 9 [P108] or 8 [P113]) and non-target (pink; n = 36 [P106], 26 [P108], or 41 [P113]) missense mutations at the indicated time points (left; mean +/- S.E.), and normalized biopsy B1 vs. progression biopsy WES VAF for vaccine target genes (right). To account for variable tumor fraction, vaccine target VAFs are normalized to the mean VAF of truncal non-target mutations. **g**. Summary response and resistance mechanisms. From outer circle to inner circle, the following are indicated: biomarker group (progression, transient control, prolonged control), patient ID, putative resistance mechanism and number of vaccine-induced immune responses.

Main Text References

1. Zhang, L., et al. Intratumoral T cells, recurrence, and survival in epithelial ovarian cancer. N Engl J Med 348, 203-213 (2003).
2. Sato, E., et al. Intraepithelial CD8+ tumor-infiltrating lymphocytes and a high CD8+/regulatory T cell ratio are associated with favorable prognosis in ovarian cancer. Proc Natl Acad Sci U S A 102, 18538-18543 (2005).
3. Varga, A., et al. Pembrolizumab in patients with programmed death ligand 1-positive advanced ovarian cancer: Analysis of KEYNOTE-028. Gynecol Oncol 152, 243-250 (2019).
4. Hamanishi, J., et al. Safety and Antitumor Activity of Anti-PD-1 Antibody, Nivolumab, in Patients With Platinum-Resistant Ovarian Cancer. J Clin Oncol 33, 4015-4022 (2015).
5. Colombo, N., et al. Pembrolizumab plus weekly paclitaxel in platinum-resistant recurrent ovarian cancer (ENGOT-ov65/KEYNOTE-B96): a multicentre, randomised, double-blind, phase 3 study. Lancet 407, 1525-1537 (2026).
6. Cancer Genome Atlas Research, N. Integrated genomic analyses of ovarian carcinoma. Nature 474, 609-615 (2011).
7. Liu, M., et al. Improved T-cell Immunity Following Neoadjuvant Chemotherapy in Ovarian Cancer. Clin Cancer Res 28, 3356-3366 (2022).
8. Kandalaft, L.E., Dangaj Laniti, D. & Coukos, G. Immunobiology of high-grade serous ovarian cancer: lessons for clinical translation. Nat Rev Cancer 22, 640-656 (2022).
9. Vazquez-Garcia, I., et al. Ovarian cancer mutational processes drive site-specific immune evasion. Nature 612, 778-786 (2022).
10. Hornburg, M., et al. Single-cell dissection of cellular components and interactions shaping the tumor immune phenotypes in ovarian cancer. Cancer Cell 39, 928-944 e926 (2021).
11. Keskin, D.B., et al. Neoantigen vaccine generates intratumoral T cell responses in phase Ib glioblastoma trial. Nature 565, 234-239 (2019).
12. Braun, D.A., et al. A neoantigen vaccine generates antitumour immunity in renal cell carcinoma. Nature 639, 474-482 (2025).
13. Rojas, L.A., et al. Personalized RNA neoantigen vaccines stimulate T cells in pancreatic cancer. Nature 618, 144-150 (2023).
14. Sarkizova, S., et al. A large peptidome dataset improves HLA class I epitope prediction across most of the human population. Nat Biotechnol 38, 199-209 (2020).
15. Jurtz, V., et al. NetMHCpan-4.0: Improved Peptide-MHC Class I Interaction Predictions Integrating Eluted Ligand and Peptide Binding Affinity Data. J Immunol 199, 3360-3368 (2017).
16. Parsons, H.A., et al. Sensitive Detection of Minimal Residual Disease in Patients Treated for Early-Stage Breast Cancer. Clin Cancer Res 26, 2556-2564 (2020).
17. Moodie, Z., Huang, Y., Gu, L., Hural, J. & Self, S.G. Statistical positivity criteria for the analysis of ELISpot assay data in HIV-1 vaccine trials. J Immunol Methods 315, 121-132 (2006).
18. Oliveira, G., et al. Phenotype, specificity and avidity of antitumour CD8(+) T cells in melanoma. Nature 596, 119-125 (2021).
19. Caushi, J.X., et al. Transcriptional programs of neoantigen-specific TIL in anti-PD-1-treated lung cancers. Nature 596, 126-132 (2021).
20. Anadon, C.M., et al. Ovarian cancer immunogenicity is governed by a narrow subset of progenitor tissue-resident memory T cells. Cancer Cell 40, 545-557 e513 (2022).

21. Martinez-Jimenez, F., et al. Genetic immune escape landscape in primary and metastatic cancer. Nat Genet 55, 820-831 (2023).
22. Filip, I., et al. Pervasiveness of HLA allele-specific expression loss across tumor types. Genome Med 15, 8 (2023).
23. Takaya, H., Nakai, H., Takamatsu, S., Mandai, M. & Matsumura, N. Homologous recombination deficiency status-based classification of high-grade serous ovarian carcinoma. Sci Rep 10, 2757 (2020).
24. Knijnenburg, T.A., et al. Genomic and Molecular Landscape of DNA Damage Repair Deficiency across The Cancer Genome Atlas. Cell Rep 23, 239-254 e236 (2018).
25. Center, B.I.T.G.D.A. Firehose (stddata__2016_01_28). (Broad Institute of MIT and Harvard, 2016).
26. Sethna, Z., et al. RNA neoantigen vaccines prime long-lived CD8(+) T cells in pancreatic cancer. Nature 639, 1042-1051 (2025).
27. Huber, F. & Bassani-Sternberg, M. Defects in antigen processing and presentation: mechanisms, immune evasion and implications for cancer vaccine development. Nat Rev Immunol (2025).
28. Huber, F., et al. A comprehensive proteogenomic pipeline for neoantigen discovery to advance personalized cancer immunotherapy. Nat Biotechnol 43, 1360-1372 (2025).

METHODS

Study Design

This phase I study (https://clinicaltrials.gov/study/NCT04024878; Registered 7/16/2019) was conducted at the Dana-Farber Cancer Institute. Key eligibility criteria included: age ≥ 18 years, histologically confirmed epithelial ovarian, primary peritoneal or fallopian tube cancer (EOC), Eastern Cooperative Oncology Group (ECOG) performance status ≤ 2, candidacy for platinum-based chemotherapy, and disease that was either amenable to biopsy, or recently biopsied. Cohort A required newly diagnosed, untreated Stage IIIC or IV EOC; Cohort B required platinum sensitive first recurrence of EOC, with platinum sensitivity defined as disease progression > 6 months after the last dose of first line platinum-based chemotherapy. All treated patients had *TP53* mutant tumors with high grade serous (n=9) or endometroid (n=1; P122) histology. The study excluded mucinous or low grade histologies, prior immunotherapy, known central nervous system metastases, or prior or active autoimmune disease.

The study was designed with a two-stage consent process. Following initial "pre-screening" informed consent, patients underwent tumor biopsy (B1; surgical or core), followed by tumor DNA and RNA sequencing, clinical HLA typing and the initiation of SOC chemotherapy. If tissue sampling and sequencing was adequate for vaccine design and patients did not progress on SOC platinum chemotherapy, patients were offered "treatment" consent. The primary objective of the study was to evaluate the safety and feasibility of administering NeoVax with nivolumab in patients with epithelial ovarian cancer. The protocol, amendment summaries, deviations, and summaries of primary, secondary and exploratory endpoints are available in **Supplementary Information**.

Ethical approval and consent

The study was conducted in accordance with the Declaration of Helsinki and with approval by the Dana-Farber/Harvard Cancer Center (DFHCC) Institutional Review Board. Written informed consent was obtained for all patients.

Patient samples

Peripheral blood samples were obtained for HLA typing and for germline DNA sequencing. Clinical HLA class I and II typing was performed by the BWH Tissue Typing laboratory (**Supplementary Table 4**). For immune monitoring of peripheral blood mononuclear cells (PBMCs), leukaphereses were performed prior to vaccination (within 1 week), at week 14 (+/- 1 week; after boost 1) and at week 22 (+/- 1 week; after boost 2). Peripheral blood samples (K2-EDTA tubes) were collected serially. PBMCs were isolated by Ficoll (GE Healthcare) density centrifugation and cryopreserved. Plasma pooled from peripheral blood draws was frozen for cfDNA analysis. Tumor biopsies were collected in DMEM media. Viable tumor cell suspensions were prepared by mincing with a scalpel, then dissociating with PBS containing collagenase (0.4mg/mL), hyaluronidase (0.4mg/mL) and DNase, for 20-60 min at 37 degrees while rocking; cells were then washed in PBS, counted and cryopreserved in 90% heat inactivated FCS/10% DMSO.

Personalized neoantigen vaccine generation and treatment

The workflow of personalized cancer vaccine generation included whole exome sequencing (WES) of tumor tissue and peripheral blood, RNA-sequencing of tumor, somatic mutation

calling, identification and selection of target neoantigens, and peptide synthesis similar to our previously completed trials[12,29], with notable points detailed below. Briefly, for WES of tumor and normal blood to identify neoantigens, FFPE tumor scrolls and a peripheral blood sample were processed for nucleic acid extraction and sequencing at the Broad Institute Clinical Research Sequencing Platform, LLC (CRSP), a CLIA licensed (#22D2055652) and CAP accredited (#8707596) laboratory for standard Somatic WES. Libraries were sequenced on paired 76 cycle runs on Illumina HiSeq or NovaSeq instruments with two 8 cycle index reads, to a goal depth of > 150x mean target coverage. Tumor tissue RNA-sequencing (FFPE scrolls) was performed to confirm putative neoantigen expression, at the non-CLIA/CAP Broad Institute Genomics Platform. RNAseq libraries were sequenced with 76bp paired-end with an eight-base index barcode read with Illumina HiSeq or NovaSeq S2 instruments. Alignment was completed using the STAR alignment algorithm against human reference hg19.

A cloud-based Cancer Genome Analysis WES Characterization Pipeline was used to identify somatic mutations. Mutations were categorized as “green” (high-quality read support in WES and RNA-seq), “yellow” (high quality in WES; not identified in RNA-seq), or “red” (likely artifact). Green, and then yellow, mutations were prioritized. Antigen prediction was performed using HLAthena[14] and NetMHCpan version 4.0 (P106 - 113) and NetMHC pan 4.1 (P114 – 122) [15] (eluted ligand rank). NetMHC prediction scores were ranked using HLAthena's ranking models. Antigens were then ranked favoring agreement between the two prediction scores.

An Epitope Selection Board selected up to 20 short epitopes based on mutation quality, antigen rank, cancer driver status (favoring driver over passenger mutations), clonality (favoring clonal over subclonal mutations), and whether the somatic alteration was a frameshift indel capable

of producing a novel open reading frame. The driver genes list for this cohort was based on known cancer genes and significantly mutated genes in the Cancer Genome Atlas – Ovarian cohort (TCGA-OV)[30] and PanCancer lists from the TumorPortal[31] (http://www.tumorportal.org/). For the selected short epitopes, the ESB designed synthetic long peptides (SLPs; 15 – 33 amino acids in length) containing the short epitope, with a length and sequence intended to maximize synthesizability and solubility.

GMP peptides were synthesized by standard solid phase synthetic peptide chemistry and purified by reverse-phase high-performance liquid chromatography (RP-HPLC; Almac Sciences (UK)). Each peptide was assessed for appearance (visual), purity (RP-HPLC), identity (mass spectrometry), and quantity. Peptide pools were sterile-filtered and tested for sterility and endotoxin prior to vaccination.

NeoVax consisted of up to 20 neoantigen containing synthetic long peptides (SLPs) split into four personalized vaccine pools, each containing up to 5 SLPs (300µg per peptide) in 0.5ml, admixed with 0.25ml polyinosinic polycytidylic acid polylysine carboxymethylcellulose (poly ICLC; Hiltonol; 450µg). Vaccine priming doses were administered into the extremities on days 1, 4 and 8 (+/- 1 day), and 15 and 22 (+/- 3 days); Booster vaccinations were given in weeks 12 and 20 (days 78 and 134, +/- 7 days). Individual pools were injected into the same anatomical site throughout treatment. Starting at week 14 (day 92 +/- 3 days), Nivolumab was administered every 2 weeks at 240mg flat dose for up to 2 years, or until progression or intolerable toxicity. Amendments allowed the administration of standard of care maintenance therapies (e.g. PARPi, bevacizumab) and nivolumab 480mg every 4 weeks after the completion of all vaccine booster doses.

Clinical assessments and outcomes

Clinical outcome and safety data were reported until the clinical data cutoff of December 1, 2025. Adverse events, laboratory values, and vital signs were assessed regularly and graded according to the National Cancer Institute Common Terminology Criteria for Adverse Events, version 5.0. Imaging assessments were performed prior to starting vaccination and subsequently every 12 weeks according to Response Evaluation Criteria in Solid Tumors (RECIST), version 1.1. Biomarker groups were delineated as follows: Prolonged controllers were defined as those patients who exhibited (i) stable disease (RECIST) or no evidence of disease and (ii) CA125 < the ULN, throughout the entire course of vaccination. Transient controllers did not meet prolonged controller criteria due to RECIST progression or CA125 levels > ULN; however, after an initial period of increasing CA125 and cfDNA, they exhibited a decrease or change in slope in at least one biomarker for >1 assessed time point, without alternative explanation. Progressors exhibited (i) RECIST progression prior to boosting and either (iia) increases in CA125 and/or cfDNA VAF at all assayed timepoints over the course of vaccination, or (iib) any decreases in CA125 or cfDNA VAF between assayed timepoints were only associated with alternative therapies (e.g. radiation or ablation).

Organoid generation and culture

Organoids were generated and cultured as previously described[32]. PDO lines tested negative for mycoplasma contamination at late passages. For phospho-STAT1 staining, PDO cells were digested to single cells with TrypLE, rested for one-hour in organoid media at 37˚C and then treated or not with IFN-γ (20ng/ml; Peprotech) for 1 hour. Cells were fixed with 2%

paraformaldehyde (10 min, room temperature). After washing, cells were permeabilized (90% ice cold methanol, on ice, 30 min). After washing, cells were stained with Alexa Fluor 647 anti-phospho-STAT1 (BioLegend Cat. 666409) or isotype control (BioLegend Cat. 400130). For HLA flow cytometry, Matrigel encased PDOs were treated or not with IFN-γ (20ng/ml) for 24 hours. Single cells were isolated via TrypLE digestion and stained with Pacific Blue anti-human HLA-A/B/C (Biolegend Cat. 311426) or matched isotype (Biolegend Cat.400235). To rescue *JAK1* expression, the *JAK1* CDS was PCR-amplified from plasmid pDONR223-JAK1 (gift of W. Hahn & D. Root; Addgene plasmid # 23932) and inserted into a pLKO lentiviral-backbone with a P2A-GFP cassette using the NEBuilder® HiFi DNA Assembly kit. Virus was produced as below (**TCR screening**) using Lenti-X 293T cells (Takara Bio Cat. 632180). Sucrose gradient concentrated lentivirus (Lenti-X concentrator; Takara Bio Cat. 631231) was used to transduce single cell suspensions of PDO cells (spinoculation at 2000RPM x 1h with 10ug/mL Polybrene (Millipore)), and transduced cells were subsequently enriched via fluorescence activated cell sorting. Plasmids are available upon request.

Assessment of vaccine immunogenicity by IFNγ ELISpot

PBMCs containing circulating T cells were assessed for immune reactivity to vaccine peptide pools immediately upon thawing and rest (*ex vivo*) and to individual vaccine peptides following *in vitro* stimulation with pools of peptides. All T cell culture and ELISpot methods (including plate development and analysis) were previously described[33,34]. Briefly, to assess *ex vivo* immunogenicity, PBMCs were screened against neoantigen vaccine peptide pools by *ex vivo* IFNγ ELISpot assays. Opaque ELISpot plates with 0.45 mm hydrophobic high protein binding immobilon-p membranes (Millipore) were wetted with 35% ethyl alcohol, washed 3x with

distilled water and coated with anti-IFNγ antibody at 4°C (1-DK1 Mabtech) for final washes with PBS. Cryopreserved PBMC were thawed in complete DMEM media supplemented with 10% human serum and rested overnight. The PBMCs were then plated at 2×10^5 cells per well and stimulated with 10µg of peptide pool. Controls included DMSO, peptide pools derived from HIV or CEF (CMV, EBV, and influenza) (Mabtech), and phytohemagglutinin (PHA, Gibco). PBMC were stimulated in triplicate for 18-24 hours at 37°C. Plates were developed using manufacturer's protocols.

In vitro IFNγ ELISpot assays were used to assess individual peptide immunogenicity[29]. Briefly, PBMCs were plated in 24 well plates at 5×10^6 to 1×10^7 cells per well and stimulated with 10µg/mL of vaccine peptide pools in DMEM media supplemented with 10% human serum and 20 ng/mL of IL-7 (PeproTech). On day 3, cultures were supplemented with 20 U/mL of IL-2 (PeproTech). *In vitro* IFNγ ELISpot assays were performed 10-14 days post-stimulation, after an overnight rest in cytokine-free media. 2×10^5 cells were plated with 10µg of individual vaccine peptides, as well as negative controls, DMSO and 10µg of HIV, and positive controls, CEF peptides and PHA. For all ELISpot analyses, responses were considered positive if the mean spot count was > 6 (LOD: 3x the median DMSO), 3x matched DMSO control and significant by distribution free resampling (DFR(EQ) $P < 0.05$; https://rundfr.fredhutch.org/)[17] without adjustments for multiple comparisons.

scRNA-seq and scTCRseq data generation and analysis

The samples processed for scRNAseq were obtained following tumor digestion and cryopreservation. Upon thawing, dead cells were depleted via the Miltenyi Dead Cell Removal Kit. Tumor cells were washed and resuspended in PBS with UltraPure 0.04% BSA for

downstream 10x analysis. Cells were loaded onto a 10× Genomics Chromium™ instrument (10x Genomics) according to the manufacturer's recommendations. The scRNAseq libraries were processed using Chromium Next GEM Single Cell 5' Kit v2, and the scTCRseq libraries were made using Chromium Single Cell Human TCR Amplification Kit (10x Genomics). cDNA and library quality was confirmed by Bioanalyzer High Sensitivity DNA Kit (Agilent). Sequencing libraries were normalized to 4nM concentration and pooled before sequencing on an Illumina NovaSeq S4 300 cycle platform: Read 1 of 26bp, Read 2 of 90bp, Index 1 of 10bp and Index 2 of 10bp.

Single-cell RNA-seq processing and analyses

Following CellRanger (v 7.1.0) processing, scRNAseq data were read into R v4.2.1 and processed with Seurat v5.1.0[35] where they were filtered to remove mitochondrial genes and debris by eliminating cells with low RNA counts (min.cells = 3 & min.features = 200 and nCount_RNA > 1500 & nFeature_RNA > 750). Additional filtering of low-quality cells was completed with miQC v1.6.0[36] (posterior.cutoff 0.6). Data were subsequently normalized, variable features were identified, and data were scaled prior to running Principal Component Analysis (PCA). Visualization via Uniform Manifold Approximation and Projection (UMAP) revealed data stratification by batch, timepoint, and patient, which led to the use of Harmony v1.2.3[37] to integrate samples. Doublets were removed with scDblFinder v1.12.0[38]. A shared nearest-neighbor graph was constructed that was used to cluster the Seurat object with the Louvain algorithm at low resolution to identify broad cell types. To label the clusters, the top differentially expressed genes were analyzed for each cluster via FindAllMarkers. Additionally, canonical cell lineage markers were assessed for their expression across clusters. Gene set

928 signatures from Oliveira *et al*. 2023[39] were scored with AddModuleScore. Separate tumor and
929 T cell objects were subsetted from the main Seurat object. FindMarkers was used to identify
930 differential gene expression for the tumor or T cell objects over time. The CD4 and CD8 T cell
931 objects each underwent PCA and re-clustering. Cluster resolution was determined using
932 Clustree v0.5.1[40]. T cell subtypes were identified by analyzing the top differentially expressed
933 genes for each cluster found from FindAllMarkers. Additionally, gene set signatures for
934 cytotoxicity, exhaustion, memory, and proliferation from Oliveira *et al*. 2023[39] were scored with
935 AddModuleScore. Comparisons to previous studies[18,41] aided in the annotation of T cell
936 subclusters. Gene set enrichment analysis (GSEA) on the tumor cells per patient was
937 conducted using the Human MSigDB Hallmark Gene Sets[42]. A Wilcoxon rank sum test was
938 executed using presto v1.0.0 to find differentially expressed genes across time points, which
939 was then used with msigdbr v7.5.1 and fgsea v1.24.0[43] to identify enriched and depleted
940 pathways. Plots in R were generated with ggplot2 v3.5.1[44], cowplot v1.1.3, pheatmap 1.0.12,
941 and paletteer v1.6.0. Data analysis utilized tidyr v1.3.1, tidyverse v2.0.0, and dplyr v1.1.4.
942
943 Single-cell TCRseq data were filtered for low-quality and low-confidence reads after CellRanger
944 (v7.1.0) processing. TCRs were labeled as one of six categories based on the number of alpha
945 and beta chains that paired together: (1) 1 alpha 1 beta, (2) 2 alpha 1 beta, (3) 1 alpha 2 beta,
946 (4) 1 or 2 alpha and 0 beta, (5) 0 alpha and 1 or 2 beta, and (6) more than 2 alpha and/or beta
947 chains. TCRs labeled as category 6 were removed from further analysis. Single-cell TCRseq
948 data were merged with the scRNAseq Seurat object based on exact sample barcode matching.
949
950 **Bulk RNAseq analysis**

Gene expression was quantified using RSEM. Genes of interest expressed (>=1 TPM) in at least one patient tumor sample, were plotted.

TCR reconstruction and expression in T cells for vaccine and PDO specificity screening.

TCRs were cloned, expressed in human T cells and screened for specificity of neoantigen peptides using our protocols[45]. Briefly, the full-length *TCRA* and *TCRB* chains with murinized constant domains were synthesized in the *TCRB/TCRA* orientation, separated by Furin SGSG P2A linker (Integrated DNA Technologies). Gene fragments were cloned into a lentiviral vector under the control of the pEF1α promoter using Gibson assembly (New England Biolabs Inc).

Healthy donor T cells enriched from PBMCs using PanT cell selection kit (Miltenyi) were activated with antiCD3/CD28 dynabeads (ThermoFisher Scientifics) in the presence of 5ng/mL of IL-7 and IL-15 (Peprotech) in 96 well plates. On days 2-4, activated cells were transduced with a lentiviral vectors encoding TCRB-TCRA chains. Lentiviral particles were generated by Transit LT-1 (Mirus) transient transfection of Lenti-X 293T cells (Takara) in 96 well plates, using TCR encoding plasmids and packaging plasmids (VSVg and PSPAX2[45]). Lentiviral supernatant was harvested on days 1, 2 and 3, supplemented with Polybrene (10mg/mL; Millipore) and immediately used to transduce activated T cells, including one spinoculation of the virus at 2,000 rpm and 37°C for 2 hours on the second transduction day. Six days after activations, dynabeads were removed and T cells were expanded in G-REX 24 well plates in media enriched with IL-7 and IL-15.

TCR-transduced T cells were used at 14-21 days post-transduction for TCR reactivity tests. Briefly up to 28 TCR-transduced T cell lines were separately stained with up to 4 concentrations

of CellTrace Far Red (FR), CellTrace Violet, and/or CFSE (Life Technology), and pooled. $2.5x10^5$ pooled T cell effectors were incubated with either ~ 5 $x10^4$ PDO cells liberated from Matrigel via TRYPLE digestion or $2.5x10^5$ patient-derived, EBV immortalized B cells (EBV lymphoblastoid cell lines, EBV-LCL). EBV-LCLs were pulsed with 10^8 pg/mL of vaccine peptide pools, or the indicated concentrations of individual neoantigen and wildtype peptides (Almac, Genscript). After an overnight incubation, TCR reactivity was measured via detection of CD137 surface expression on CD8+, TCR transduced (murine TCRB+) T cells using a Fortessa flow cytometer equipped with a high-throughput system acquisition (BD Biosciences). Data were analyzed on Flowjo (v10.8). Criteria for determining TCR reactivity were (must meet all three): Target average % CD137+ > 2 standard deviations higher than (1) Average of untransduced T cells across all targets; (2) Matched background (average of the TCR without target); (3) Average of an irrelevant control TCR across all targets. Borderline reactivity was defined as meeting the above criteria, but with average CD137 < 10% or < 3 fold the irrelevant TCR average across targets

Whole Genome Sequencing (WGS) of tumor and normal samples for cfDNA and SV analysis.

DNA was obtained as above. WGS of tumor DNA (median depth 84x; range: 61x–103x), and normal DNA (median depth 41x; range: 30x–53x) was performed using NovaSeq S4. For cfDNA analysis, patient-specific MRD Tracker panels were designed as previously described from tumor and normal WGS[16,46]. Neoantigen variants identified in the CGA pipeline were expressly included in the MRD Tracker panels.

Structural variants (SVs) were identified using the Manta structural variant caller[47] (v1.6.0). Aligned tumor WGS BAM format data was used as input, with the *GRCh37/hg19* reference genome. Manta was executed with default parameters, and candidate SVs were filtered to retain high-confidence calls passing internal quality filters (i.e., FILTER == PASS in the VCF). Integrative Genomics Viewer (IGV) was used to examine supporting split reads and discordant read pairs at candidate both breakpoints. PCR primers were designed to amplify *chr1* break points and adjacent DNA and sanger sequencing was used to confirm the chr1 structural variant. Primers are provided in the **Supplementary Iinformation.**

Plasma sample processing for cfDNA

cfDNA was extracted from median 4.5 ml (range 0.6 – 78.5 ml) plasma using the QIAsymphony Circulating DNA kit and quantified using the Quant-iT PicoGreen assay on a Hamilton STAR-line liquid handling system. cfDNA libraries were constructed using the Kapa Hyper Prep kit with custom dual index duplex UMI adapters (IDT)[16]. Libraries were quantified via the Quant-iT PicoGreen assay on a Hamilton STAR-line liquid handling system. MRD Tracker assay was performed[16]. Briefly, patient specific probe panels (IDT) and the xGen hybridization and wash kit with xGen Universal blockers (IDT) were used for hybrid capture (HC). For each HC reaction, libraries were pooled up to 8-plex with a library mass equivalent to 25 times DNA mass into library construction for each sample, and 4 pmol of probe panel (IDT) was applied. Following round one of HC, libraries were PCR amplified (16 cycles) and then carried through a second HC using half amounts of human Cot-1 DNA, xGen Universal blockers and probes. Libraries were again PCR amplified (8-10 cycles) before sequencing to a target raw depth of 10,000 x per site, per 20 ng input DNA mass.

MRD data analysis

FASTQs were first aligned, deduplicated, and recalibrated by following the GATK Best Practices “Data pre-processing for variant discovery” workflow. Next, UMIs were extracted using *fgbio*, raw sequencing reads were converted into duplex consensus molecules. Then tumor fractions and tumor VAFs were estimated[16].

Visualization of HLA haplotype loss

cDNA sequences from patient HLA alleles were retrieved from IDP-IMGT/HLA database (https://www.ebi.ac.uk/ipd/imgt/hla/; v3.61) and aligned locally to identify allele specific SNPs. cDNA coordinates were converted to hg19 coordinates and samtools mpileup was used to collect base calls from WES BAM files. SNP VAFs were graphed in prism.

Data Availability

Bulk WES, RNA-seq, WGS and TCR-seq, and single-cell RNA and single-cell TCR-seq data is deposited and available on dbGaP under the accession phs004380.v1.

Code Availability

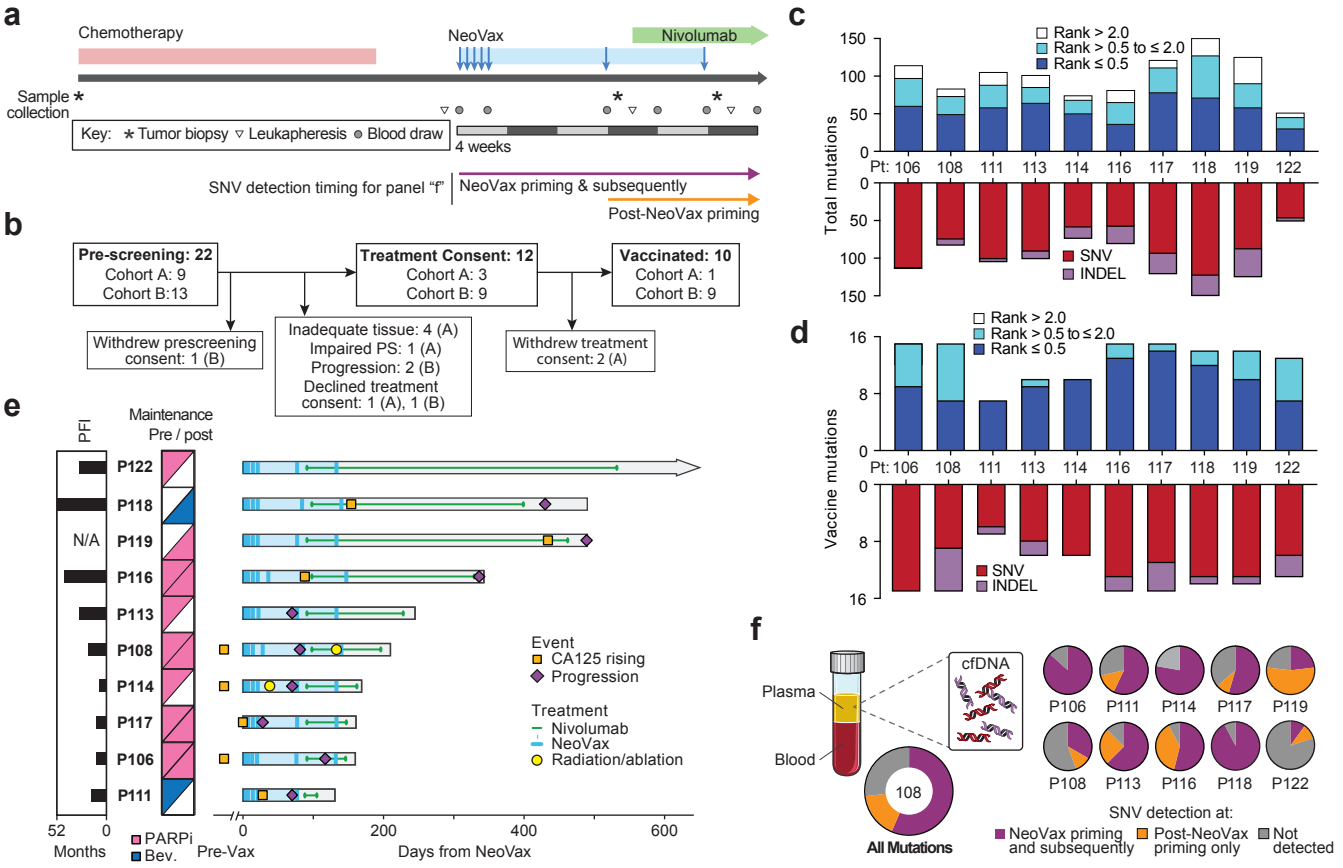
All code used in the processing and analysis of bulk TCRseq data is available on GitHub at https://github.com/jeremymsimon/. Other code using established tools will be made available within 30 days upon request to the corresponding authors

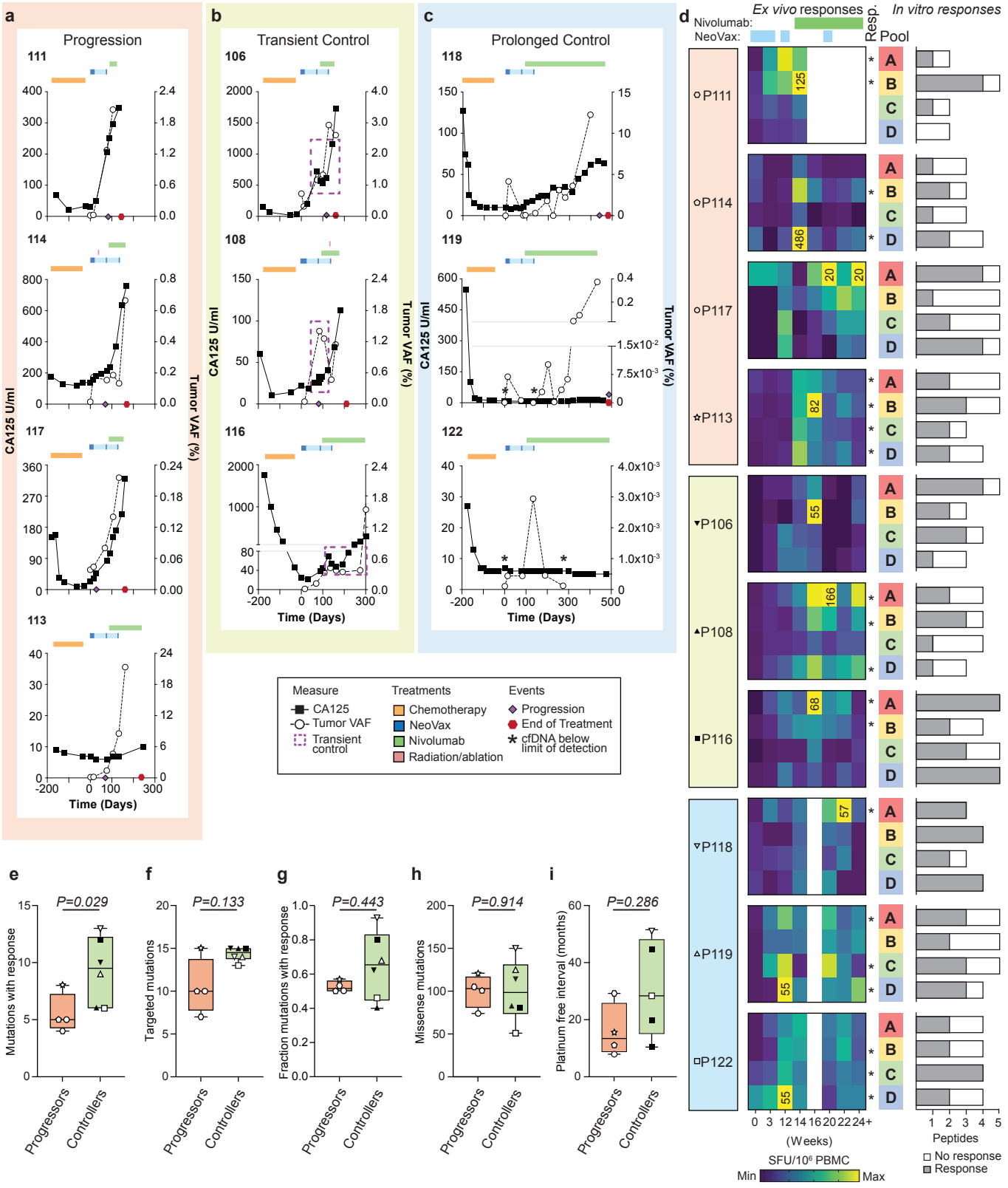
Complete References

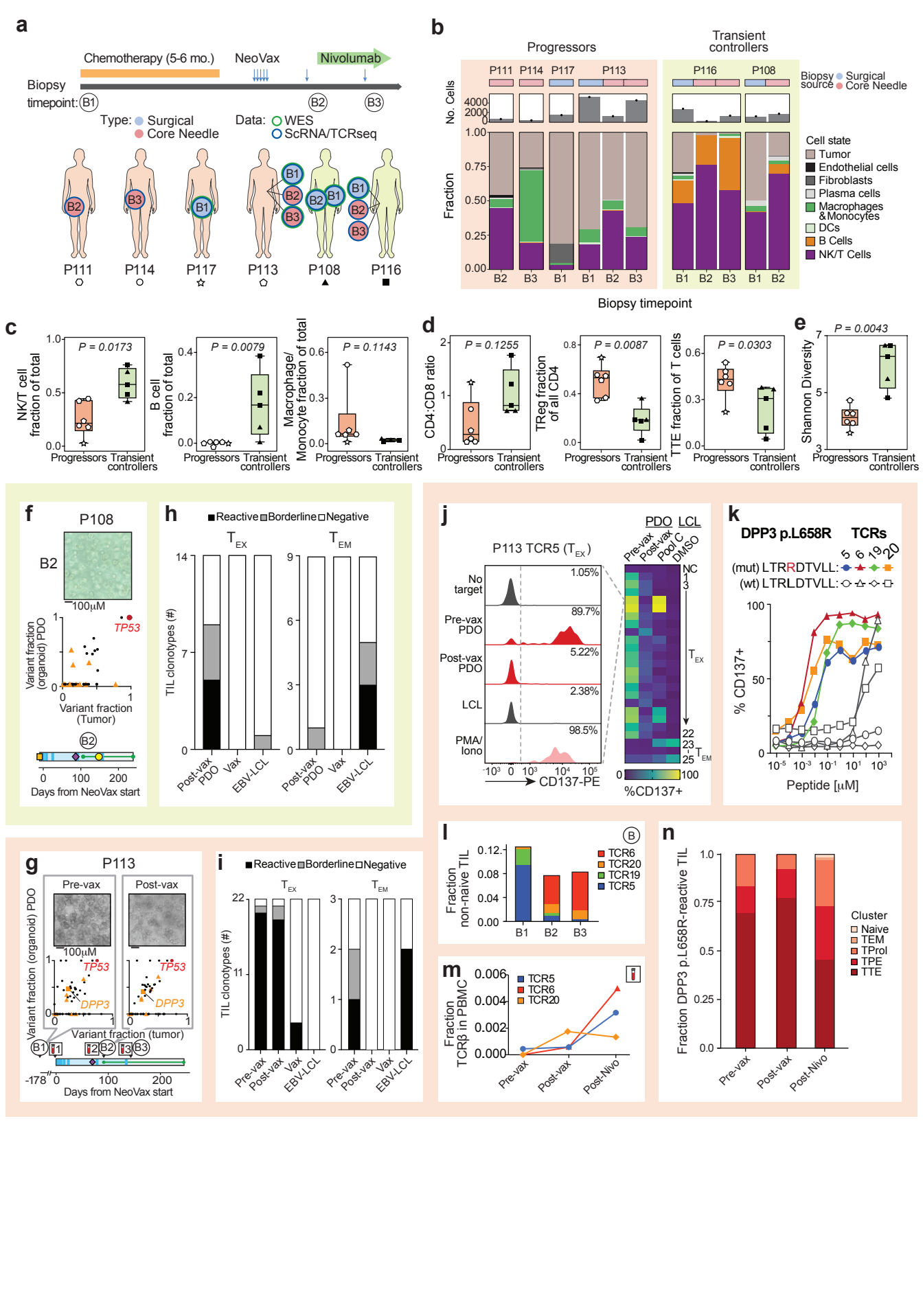
1. Zhang, L.*, et al.* Intratumoral T cells, recurrence, and survival in epithelial ovarian cancer. *N Engl J Med* **348**, 203-213 (2003).
2. Sato, E.*, et al.* Intraepithelial CD8+ tumor-infiltrating lymphocytes and a high CD8+/regulatory T cell ratio are associated with favorable prognosis in ovarian cancer. *Proc Natl Acad Sci U S A* **102**, 18538-18543 (2005).
3. Varga, A.*, et al.* Pembrolizumab in patients with programmed death ligand 1-positive advanced ovarian cancer: Analysis of KEYNOTE-028. *Gynecol Oncol* **152**, 243-250 (2019).
4. Hamanishi, J.*, et al.* Safety and Antitumor Activity of Anti-PD-1 Antibody, Nivolumab, in Patients With Platinum-Resistant Ovarian Cancer. *J Clin Oncol* **33**, 4015-4022 (2015).
5. Colombo, N.*, et al.* Pembrolizumab plus weekly paclitaxel in platinum-resistant recurrent ovarian cancer (ENGOT-ov65/KEYNOTE-B96): a multicentre, randomised, double-blind, phase 3 study. *Lancet* **407**, 1525-1537 (2026).
6. Cancer Genome Atlas Research, N. Integrated genomic analyses of ovarian carcinoma. *Nature* **474**, 609-615 (2011).
7. Liu, M.*, et al.* Improved T-cell Immunity Following Neoadjuvant Chemotherapy in Ovarian Cancer. *Clin Cancer Res* **28**, 3356-3366 (2022).
8. Kandalaft, L.E., Dangaj Laniti, D. & Coukos, G. Immunobiology of high-grade serous ovarian cancer: lessons for clinical translation. *Nat Rev Cancer* **22**, 640-656 (2022).
9. Vazquez-Garcia, I.*, et al.* Ovarian cancer mutational processes drive site-specific immune evasion. *Nature* **612**, 778-786 (2022).
10. Hornburg, M.*, et al.* Single-cell dissection of cellular components and interactions shaping the tumor immune phenotypes in ovarian cancer. *Cancer Cell* **39**, 928-944 e926 (2021).
11. Keskin, D.B.*, et al.* Neoantigen vaccine generates intratumoral T cell responses in phase Ib glioblastoma trial. *Nature* **565**, 234-239 (2019).
12. Braun, D.A.*, et al.* A neoantigen vaccine generates antitumour immunity in renal cell carcinoma. *Nature* **639**, 474-482 (2025).
13. Rojas, L.A.*, et al.* Personalized RNA neoantigen vaccines stimulate T cells in pancreatic cancer. *Nature* **618**, 144-150 (2023).
14. Sarkizova, S.*, et al.* A large peptidome dataset improves HLA class I epitope prediction across most of the human population. *Nat Biotechnol* **38**, 199-209 (2020).
15. Jurtz, V.*, et al.* NetMHCpan-4.0: Improved Peptide-MHC Class I Interaction Predictions Integrating Eluted Ligand and Peptide Binding Affinity Data. *J Immunol* **199**, 3360-3368 (2017).
16. Parsons, H.A.*, et al.* Sensitive Detection of Minimal Residual Disease in Patients Treated for Early-Stage Breast Cancer. *Clin Cancer Res* **26**, 2556-2564 (2020).
17. Moodie, Z., Huang, Y., Gu, L., Hural, J. & Self, S.G. Statistical positivity criteria for the analysis of ELISpot assay data in HIV-1 vaccine trials. *J Immunol Methods* **315**, 121-132 (2006).
18. Oliveira, G.*, et al.* Phenotype, specificity and avidity of antitumour CD8(+) T cells in melanoma. *Nature* **596**, 119-125 (2021).
19. Caushi, J.X.*, et al.* Transcriptional programs of neoantigen-specific TIL in anti-PD-1-treated lung cancers. *Nature* **596**, 126-132 (2021).

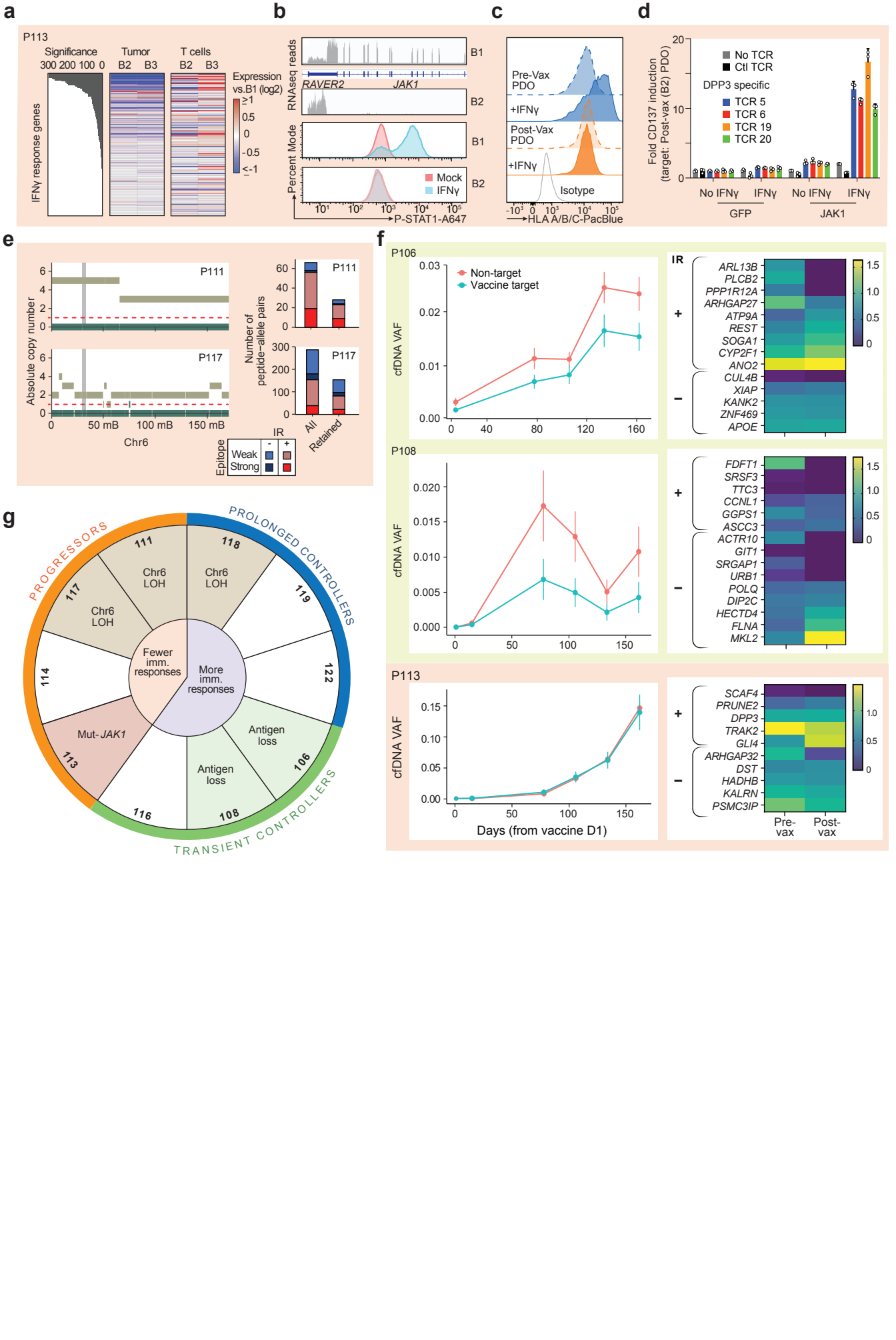
20. Anadon, C.M.*, et al.* Ovarian cancer immunogenicity is governed by a narrow subset of progenitor tissue-resident memory T cells. *Cancer Cell* **40**, 545-557 e513 (2022).
21. Martinez-Jimenez, F.*, et al.* Genetic immune escape landscape in primary and metastatic cancer. *Nat Genet* **55**, 820-831 (2023).
22. Filip, I.*, et al.* Pervasiveness of HLA allele-specific expression loss across tumor types. *Genome Med* **15**, 8 (2023).
23. Takaya, H., Nakai, H., Takamatsu, S., Mandai, M. & Matsumura, N. Homologous recombination deficiency status-based classification of high-grade serous ovarian carcinoma. *Sci Rep* **10**, 2757 (2020).
24. Knijnenburg, T.A.*, et al.* Genomic and Molecular Landscape of DNA Damage Repair Deficiency across The Cancer Genome Atlas. *Cell Rep* **23**, 239-254 e236 (2018).
25. Center, B.I.T.G.D.A. Firehose (stddata__2016_01_28). (Broad Institute of MIT and Harvard, 2016).
26. Sethna, Z.*, et al.* RNA neoantigen vaccines prime long-lived CD8(+) T cells in pancreatic cancer. *Nature* **639**, 1042-1051 (2025).
27. Huber, F. & Bassani-Sternberg, M. Defects in antigen processing and presentation: mechanisms, immune evasion and implications for cancer vaccine development. *Nat Rev Immunol* (2025).
28. Huber, F.*, et al.* A comprehensive proteogenomic pipeline for neoantigen discovery to advance personalized cancer immunotherapy. *Nat Biotechnol* **43**, 1360-1372 (2025).
29. Blass, E.*, et al.* A multi-adjuvant personal neoantigen vaccine generates potent immunity in melanoma. *Cell* (2025).
30. Cancer Genome Atlas Research, N. Comprehensive molecular characterization of clear cell renal cell carcinoma. *Nature* **499**, 43-49 (2013).
31. Lawrence, M.S.*, et al.* Discovery and saturation analysis of cancer genes across 21 tumour types. *Nature* **505**, 495-501 (2014).
32. Hill, S.J.*, et al.* Prediction of DNA Repair Inhibitor Response in Short-Term Patient-Derived Ovarian Cancer Organoids. *Cancer Discov* **8**, 1404-1421 (2018).
33. Lee, P.C.*, et al.* Reversal of viral and epigenetic HLA class I repression in Merkel cell carcinoma. *J Clin Invest* **132**(2022).
34. Keskin, D.B.*, et al.* Direct identification of an HPV-16 tumor antigen from cervical cancer biopsy specimens. *Front Immunol* **2**, 75 (2011).
35. Hao, Y.*, et al.* Dictionary learning for integrative, multimodal and scalable single-cell analysis. *Nat Biotechnol* **42**, 293-304 (2024).
36. Hippen, A.A.*, et al.* miQC: An adaptive probabilistic framework for quality control of single-cell RNA-sequencing data. *PLoS Comput Biol* **17**, e1009290 (2021).
37. Korsunsky, I.*, et al.* Fast, sensitive and accurate integration of single-cell data with Harmony. *Nat Methods* **16**, 1289-1296 (2019).
38. Germain, P.L., Lun, A., Garcia Meixide, C., Macnair, W. & Robinson, M.D. Doublet identification in single-cell sequencing data using scDblFinder. *F1000Res* **10**, 979 (2021).
39. Oliveira, G.*, et al.* Preexisting tumor-resident T cells with cytotoxic potential associate with response to neoadjuvant anti-PD-1 in head and neck cancer. *Sci Immunol* **8**, eadf4968 (2023).
40. Zappia, L. & Oshlack, A. Clustering trees: a visualization for evaluating clusterings at multiple resolutions. *Gigascience* **7**(2018).

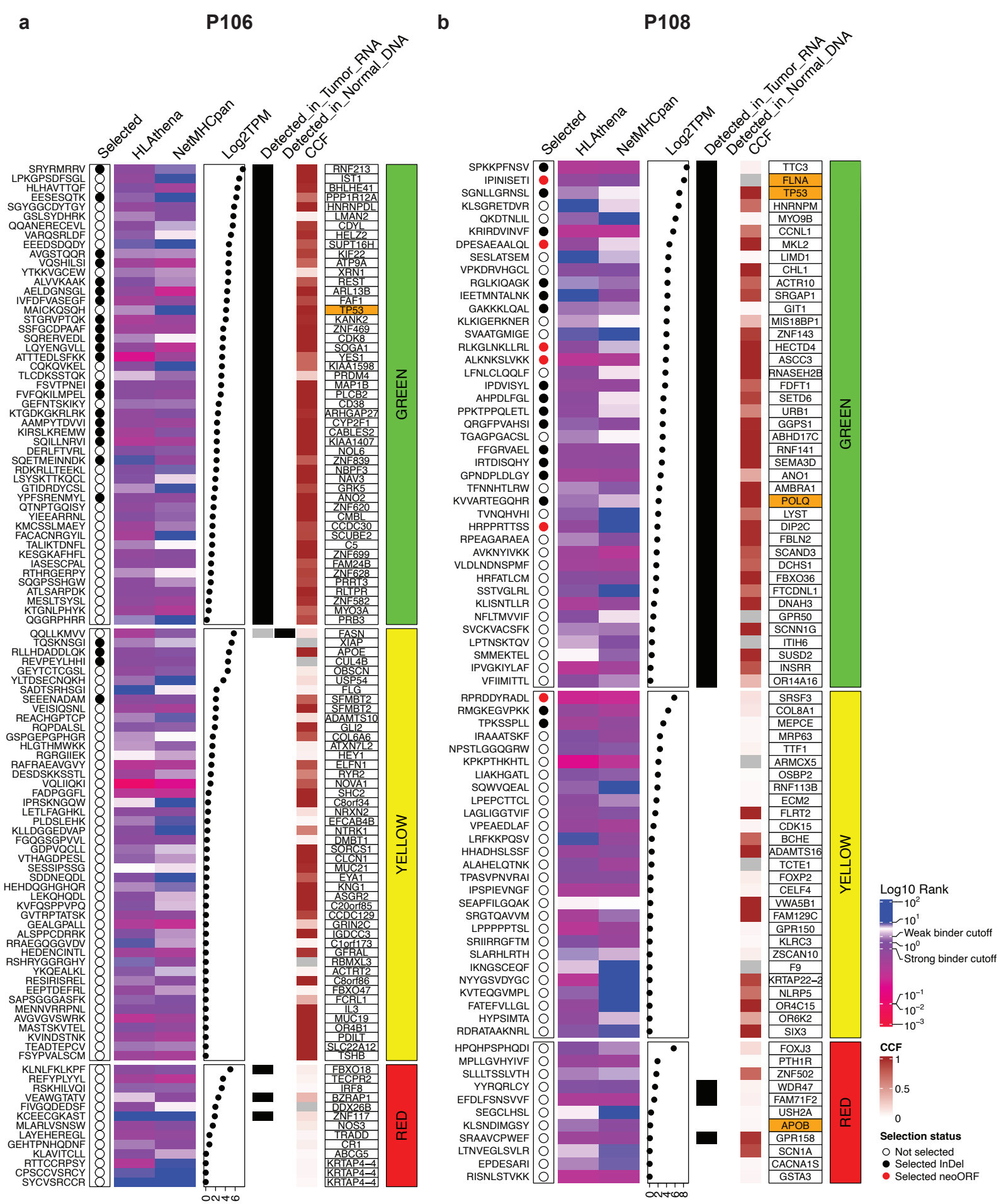
41. Oliveira, G., *et al.* Landscape of helper and regulatory antitumour CD4(+) T cells in melanoma. *Nature* **605**, 532-538 (2022).
42. Liberzon, A., *et al.* The Molecular Signatures Database (MSigDB) hallmark gene set collection. *Cell Syst* **1**, 417-425 (2015).
43. Korotkevich, G., *et al.* Fast gene set enrichment analysis. *bioRxiv*, 060012 (2021).
44. Wickham, H. ggplot2 : Elegant Graphics for Data Analysis. in *Use R!,* 1 online resource (XVI, 260 pages 232 illustrations, 140 illustrations in color (Springer International Publishing : Imprint: Springer,, Cham, 2016).
45. Afeyan, A.B., Wu, C.J. & Oliveira, G. Rapid parallel reconstruction and specificity screening of hundreds of T cell receptors. *Nat Protoc* (2024).
46. Parsons, H.A., *et al.* Circulating tumor DNA association with residual cancer burden after neoadjuvant chemotherapy in triple-negative breast cancer in TBCRC 030. *Ann Oncol* **34**, 899-906 (2023).
47. Chen, X., *et al.* Manta: rapid detection of structural variants and indels for germline and cancer sequencing applications. *Bioinformatics* **32**, 1220-1222 (2016).

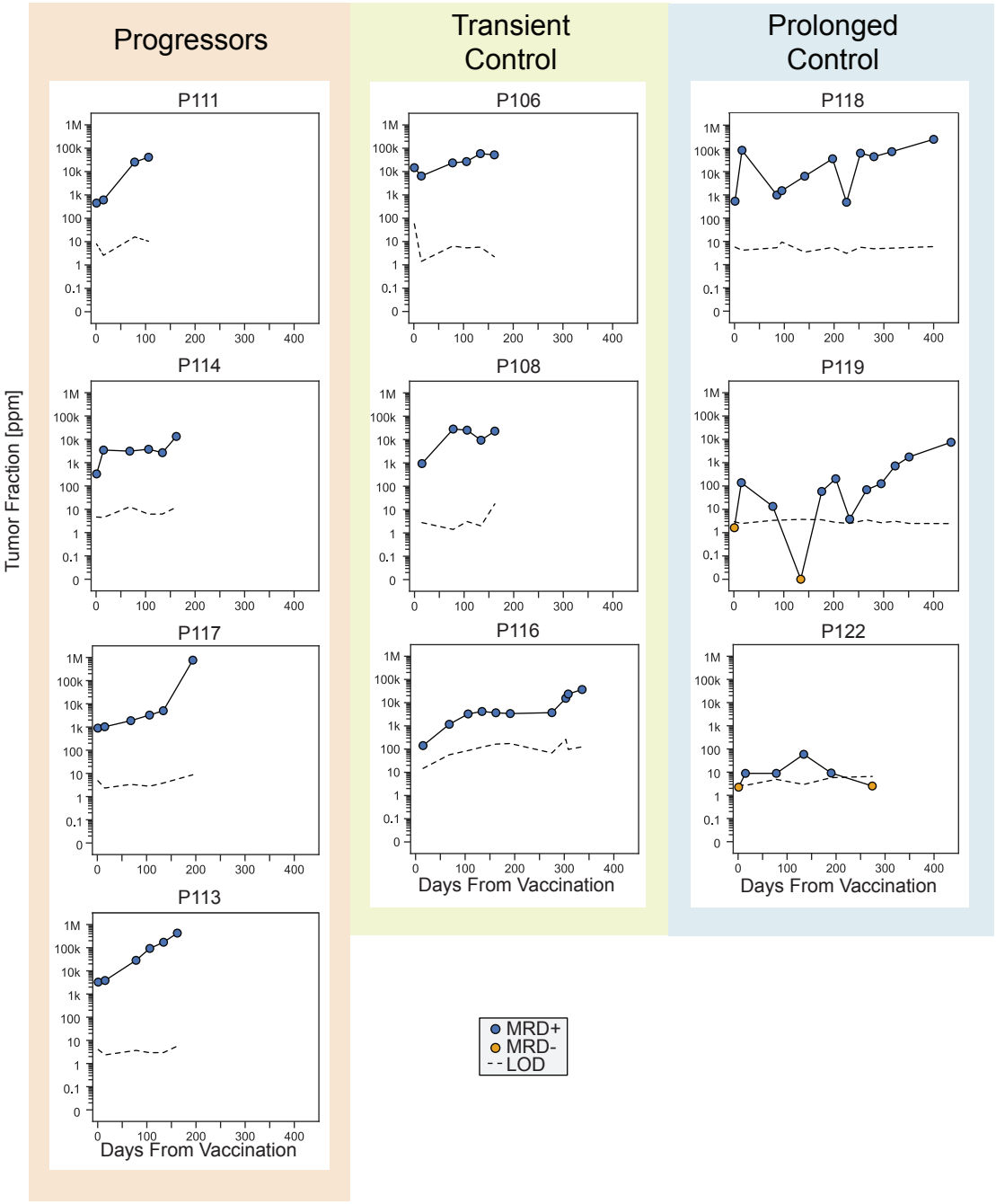

a
Chemotherapy
NeoVax
Nivolumab
Sample collection
Key: Tumor biopsy Leukapheresis Blood draw
4 weeks
SNV detection timing for panel "f"
NeoVax priming & subsequently
Post-NeoVax priming
b
Pre-screening: 22
Cohort A: 9
Cohort B:13
Treatment Consent: 12
Cohort A: 3
Cohort B: 9
Vaccinated: 10
Cohort A: 1
Cohort B: 9
Withdrew prescreening consent: 1 (B)
Inadequate tissue: 4 (A)
Impaired PS: 1 (A)
Progression: 2 (B)
Declined treatment consent: 1 (A), 1 (B)
Withdrew treatment consent: 2 (A)
c
Rank > 2.0
Rank > 0.5 to ≤ 2.0
Rank ≤ 0.5
Total mutations
Pt: 106 108 111 113 114 116 117 118 119 122
SNV
INDEL
d
Vaccine mutations
e
PFI
Maintenance
Pre / post
P122
P118
P119
P116
P113
P108
P114
P117
P106
P111
N/A
Event
CA125 rising
Progression
Treatment
Nivolumab
NeoVax
Radiation/ablation
Months
PARPi
Bev.
Pre-Vax
Days from NeoVax
f
Plasma
Blood
cfDNA
108
All Mutations
P106 P111 P114 P117 P119
P108 P113 P116 P118 P122
SNV detection at:
NeoVax priming and subsequently
Post-NeoVax priming only
Not detected

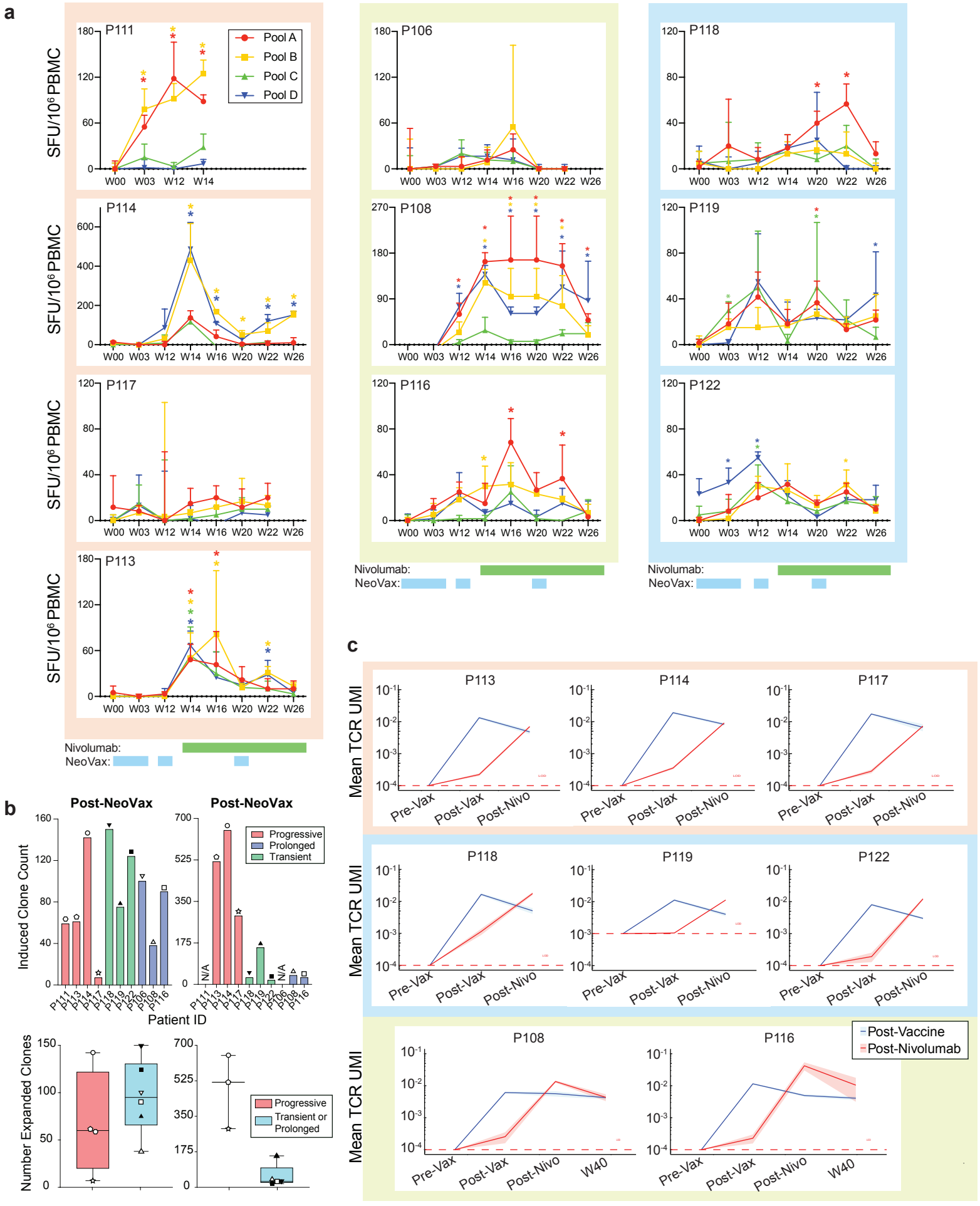

a
Progression
111
114
117
113
CA125 U/ml
Tumor VAF (%)
Time (Days)
b
Transient Control
106
108
116
CA125 U/ml
Tumor VAF (%)
Time (Days)
c
Prolonged Control
118
119
122
CA125 U/ml
Tumor VAF (%)
Time (Days)
Measure
CA125
Tumor VAF
Transient control
Treatments
Chemotherapy
NeoVax
Nivolumab
Radiation/ablation
Events
Progression
End of Treatment
cfDNA below limit of detection
d
Ex vivo responses
In vitro responses
Nivolumab:
NeoVax:
Resp.
Pool
P111
P114
P117
P113
P106
P108
P116
P118
P119
P122
A
B
C
D
(Weeks)
SFU/10⁶ PBMC
Min
Max
Peptides
No response
Response
e
P=0.029
Mutations with response
Progressors
Controllers
f
P=0.133
Targeted mutations
Progressors
Controllers
g
P=0.443
Fraction mutations with response
Progressors
Controllers
h
P=0.914
Missense mutations
Progressors
Controllers
i
P=0.286
Platinum free interval (months)
Progressors
Controllers

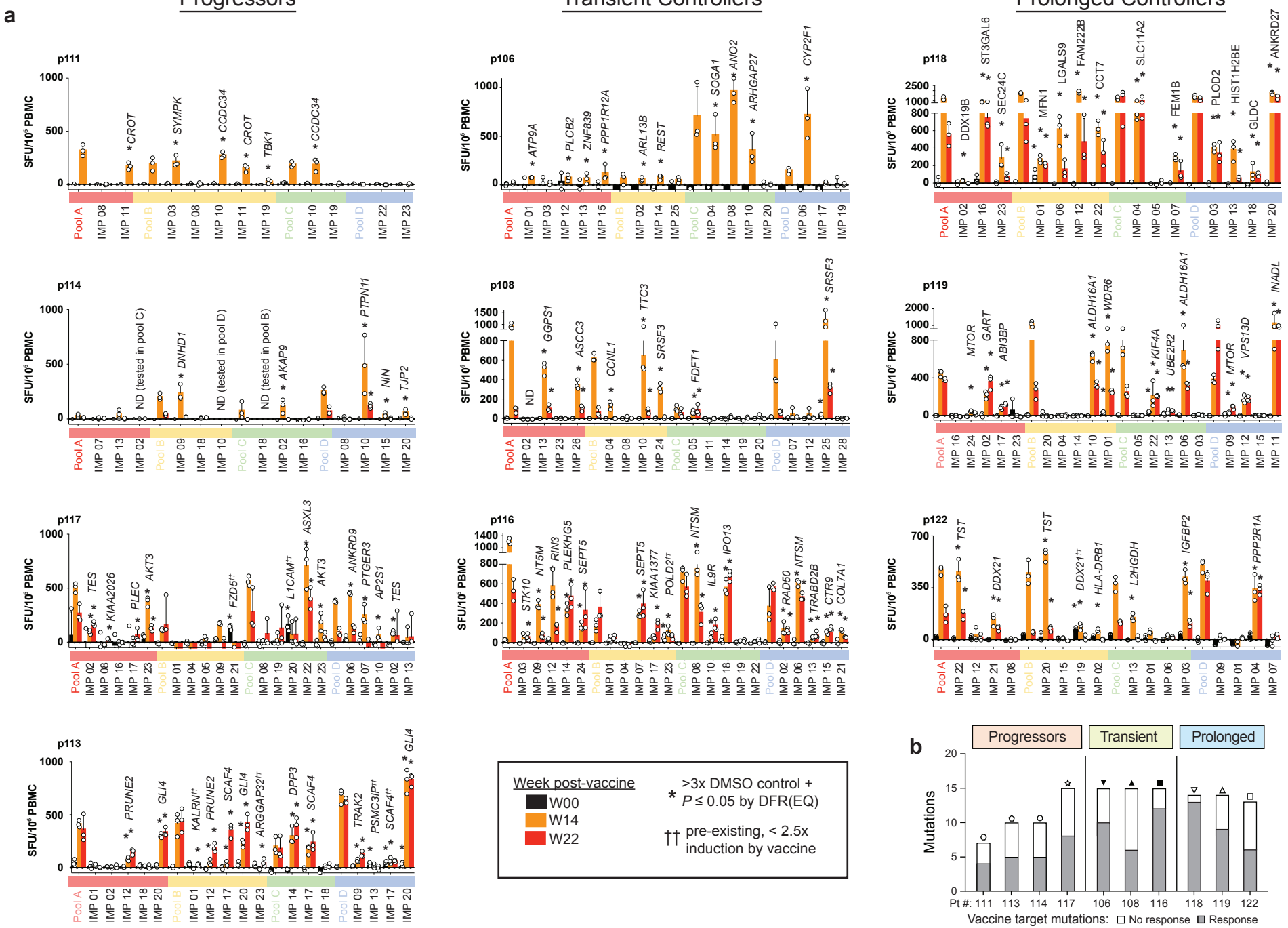

a
Chemotherapy (5-6 mo.)
NeoVax
Nivolumab
Biopsy timepoint:
Type: Surgical Core Needle
Data: WES ScRNA/TCRseq
P111
P114
P117
P113
P108
P116
b
Progressors
Transient controllers
No. Cells
Fraction
Biopsy source Surgical Core Needle
Cell state
Tumor
Endothelial cells
Fibroblasts
Plasma cells
Macrophages & Monocytes
DCs
B Cells
NK/T Cells
Biopsy timepoint
c
NK/T cell fraction of total
B cell fraction of total
Macrophage/ Monocyte fraction of total
P = 0.0173
P = 0.0079
P = 0.1143
Progressors
Transient controllers
d
CD4:CD8 ratio
TReg fraction of all CD4
TTE fraction of T cells
P = 0.1255
P = 0.0087
P = 0.0303
e
Shannon Diversity
P = 0.0043
f
P108
B2
100μM
TP53
Variant fraction (organoid) PDO
Variant fraction (Tumor)
Days from NeoVax start
h
Reactive Borderline Negative
TEX
TEM
TIL clonotypes (#)
Post-vax PDO
Vax
EBV-LCL
j
PDO LCL
P113 TCR5 (TEX)
Pre-vax
Post-vax
Pool C
DMSO
No target
Pre-vax PDO
Post-vax PDO
LCL
PMA/ Iono
1.05%
89.7%
5.22%
2.38%
98.5%
CD137-PE
%CD137+
k
DPP3 p.L658R TCRs
5 6 19 20
(mut) LTRRDTVLL:
(wt) LTRLDTVLL:
% CD137+
Peptide [μM]
g
P113
Pre-vax
Post-vax
100μM
TP53
DPP3
Variant fraction (organoid) PDO
Variant fraction (tumor)
Days from NeoVax start
i
Reactive Borderline Negative
TIL clonotypes (#)
Pre-vax
Post-vax
Vax
EBV-LCL
l
Fraction non-naive TIL
TCR6
TCR20
TCR19
TCR5
m
Fraction TCRβ in PBMC
TCR5
TCR6
TCR20
Pre-vax
Post-vax
Post-Nivo
n
Fraction DPP3 p.L658R-reactive TIL
Cluster
Naive
TEM
TProl
TPE
TTE

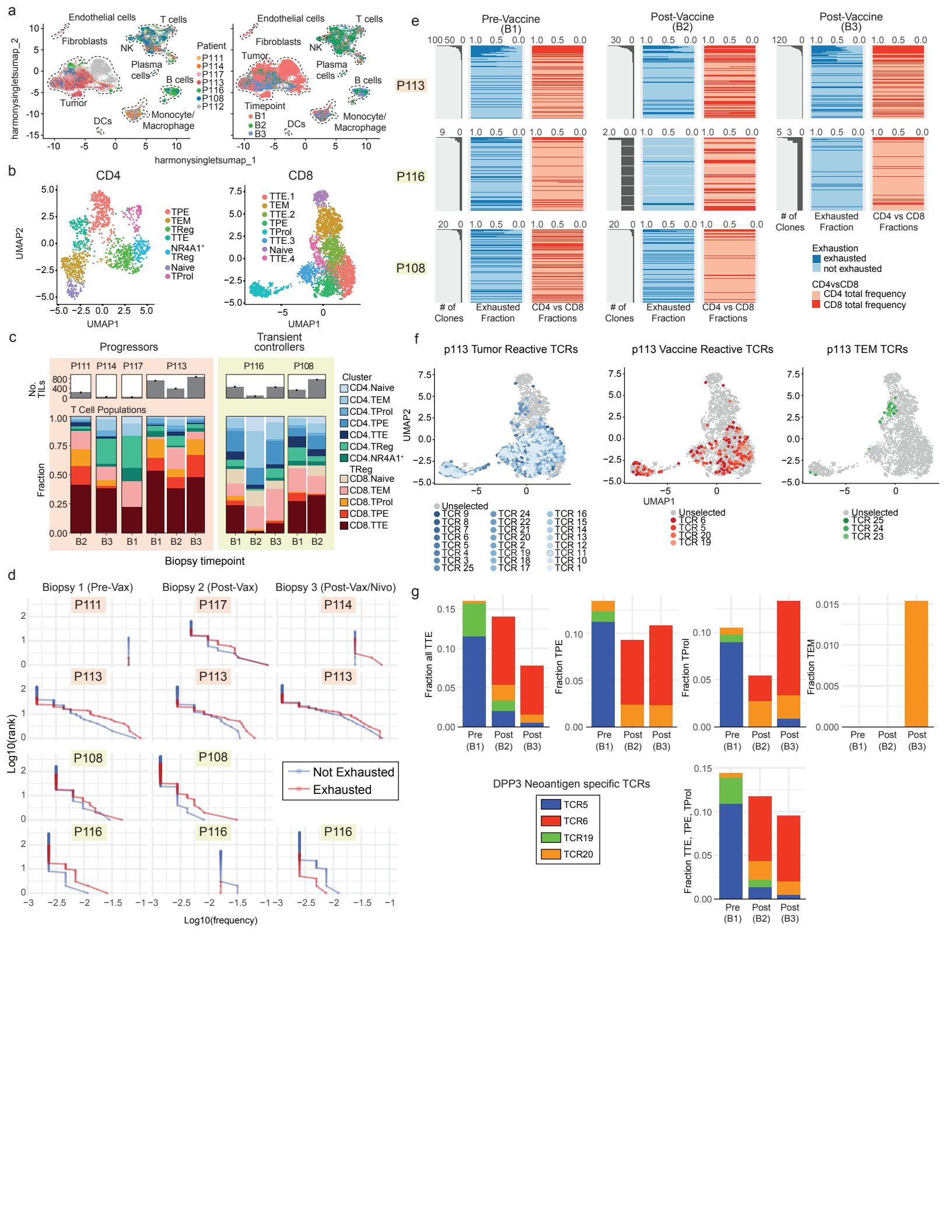

a
P113
Significance
300 200 100 0
Tumor
B2 B3
T cells
B2 B3
IFNγ response genes
Expression vs.B1 (log2)
≥1
0.5
0
-0.5
≤-1
b
RNAseq reads
RAVER2
JAK1
B1
B2
Percent Mode
Mock
IFNγ
P-STAT1-A647
c
Pre-Vax PDO
+IFNγ
Post-Vax PDO
+IFNγ
Isotype
HLA A/B/C-PacBlue
d
Fold CD137 induction (target: Post-vax (B2) PDO)
No TCR
Ctl TCR
DPP3 specific
TCR 5
TCR 6
TCR 19
TCR 20
No IFNγ
IFNγ
GFP
JAK1
e
P111
P117
Absolute copy number
Chr6
50 mB
100 mB
150 mB
Number of peptide-allele pairs
IR
All
Retained
Epitope
Weak
Strong
f
P106
Non-target
Vaccine target
cfDNA VAF
IR
ARL13B
PLCB2
PPP1R12A
ARHGAP27
ATP9A
REST
SOGA1
CYP2F1
ANO2
CUL4B
XIAP
KANK2
ZNF469
APOE
P108
FDFT1
SRSF3
TTC3
CCNL1
GGPS1
ASCC3
ACTR10
GIT1
SRGAP1
URB1
POLQ
DIP2C
HECTD4
FLNA
MKL2
P113
SCAF4
PRUNE2
DPP3
TRAK2
GLI4
ARHGAP32
DST
HADHB
KALRN
PSMC3IP
Pre-vax
Post-vax
Days (from vaccine D1)
g
PROGRESSORS
PROLONGED CONTROLLERS
TRANSIENT CONTROLLERS
Chr6 LOH
Fewer imm. responses
More imm. responses
Mut-JAK1
Antigen loss
111
118
117
119
114
122
113
106
116
108

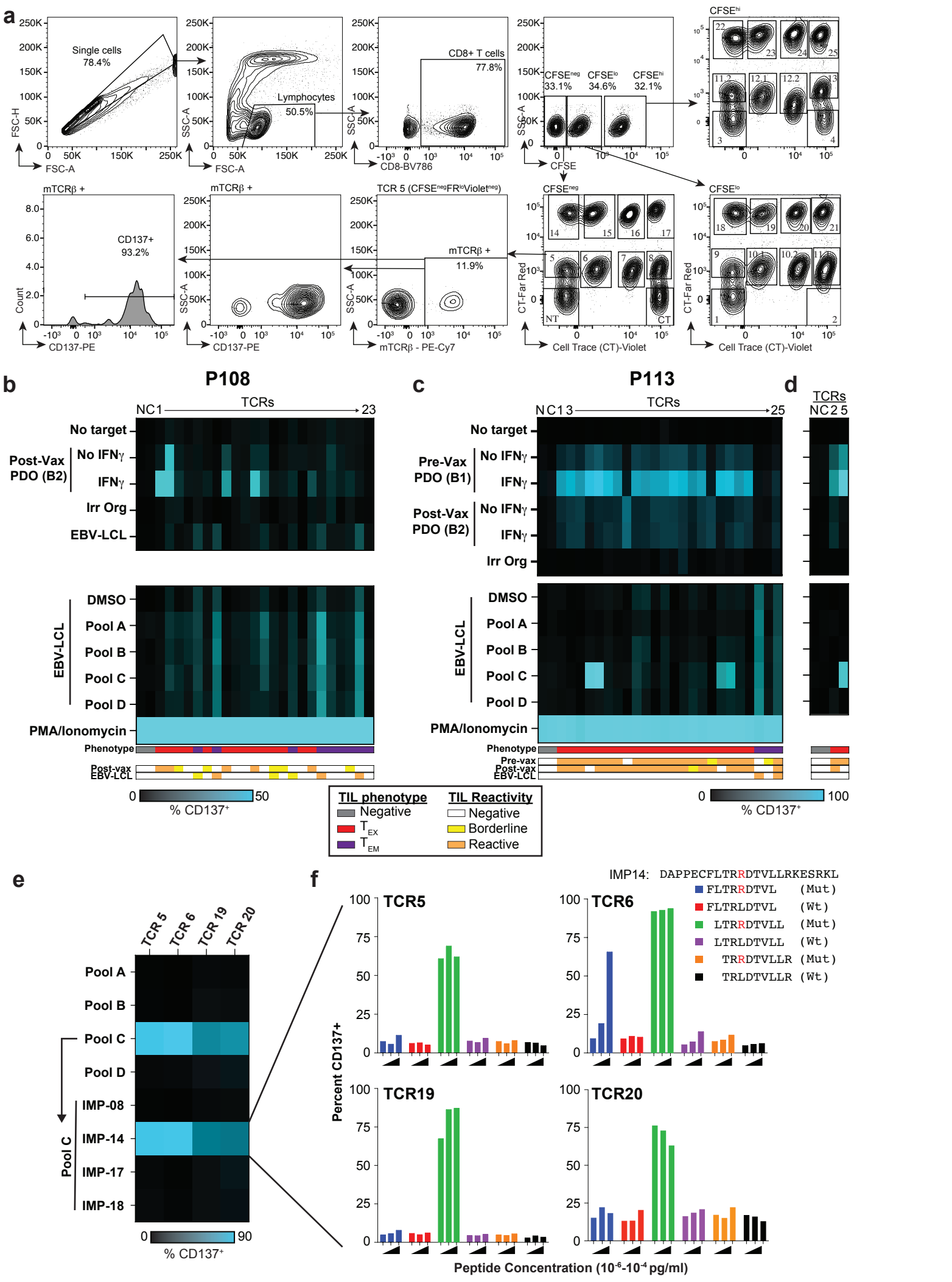

a
P106
b
P108
Selected
HLAthena
NetMHCpan
Log2TPM
Detected_in_Tumor_RNA
Detected_in_Normal_DNA
CCF
GREEN
YELLOW
RED
Log10 Rank
Weak binder cutoff
Strong binder cutoff
Selection status
Not selected
Selected InDel
Selected neoORF

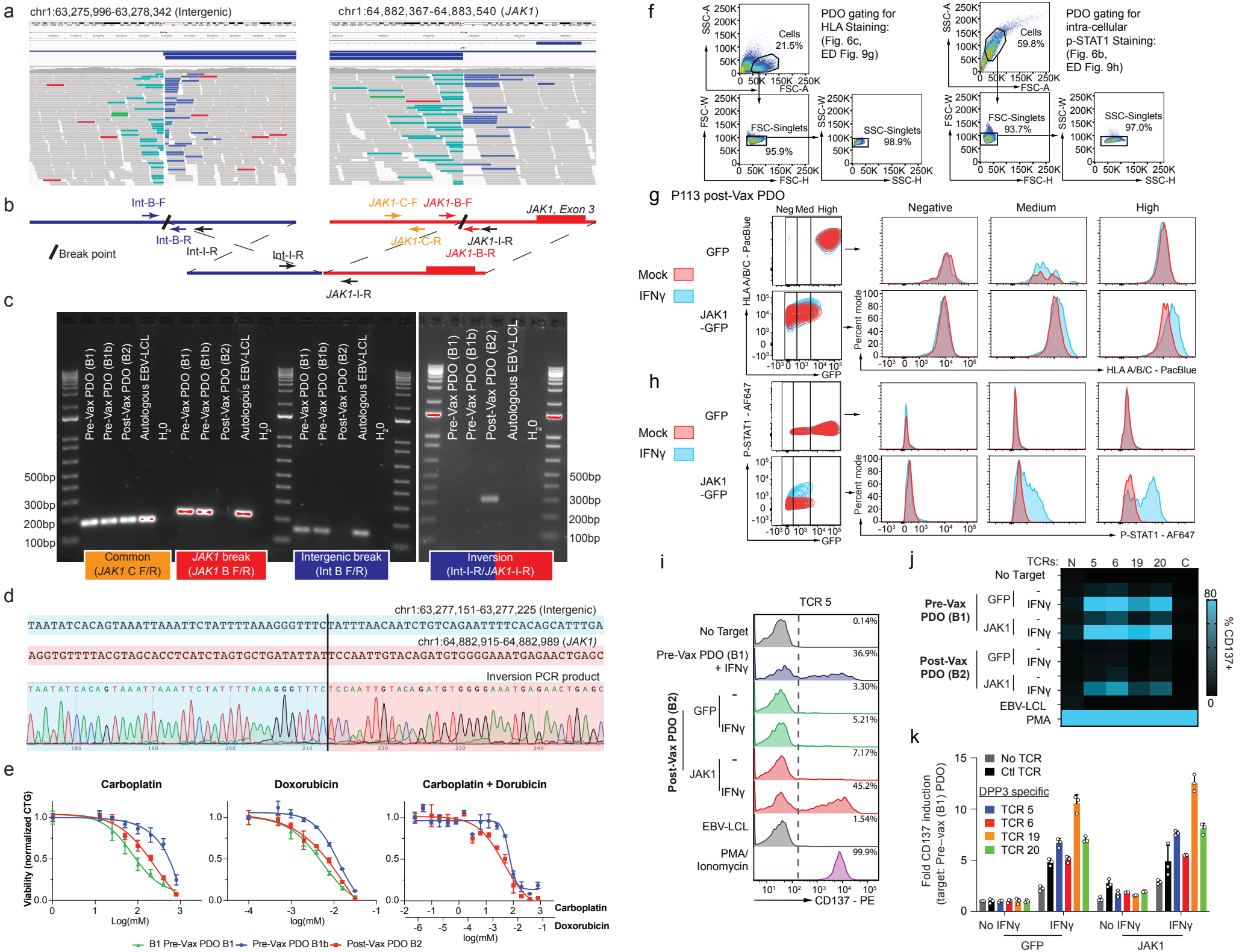

Progressors
Transient Control
Prolonged Control
Tumor Fraction [ppm]
P111
P114
P117
P113
P106
P108
P116
P118
P119
P122
1M
100k
10k
1k
100
10
1
0.1
0
0
100
200
300
400
Days From Vaccination
MRD+
MRD-
LOD

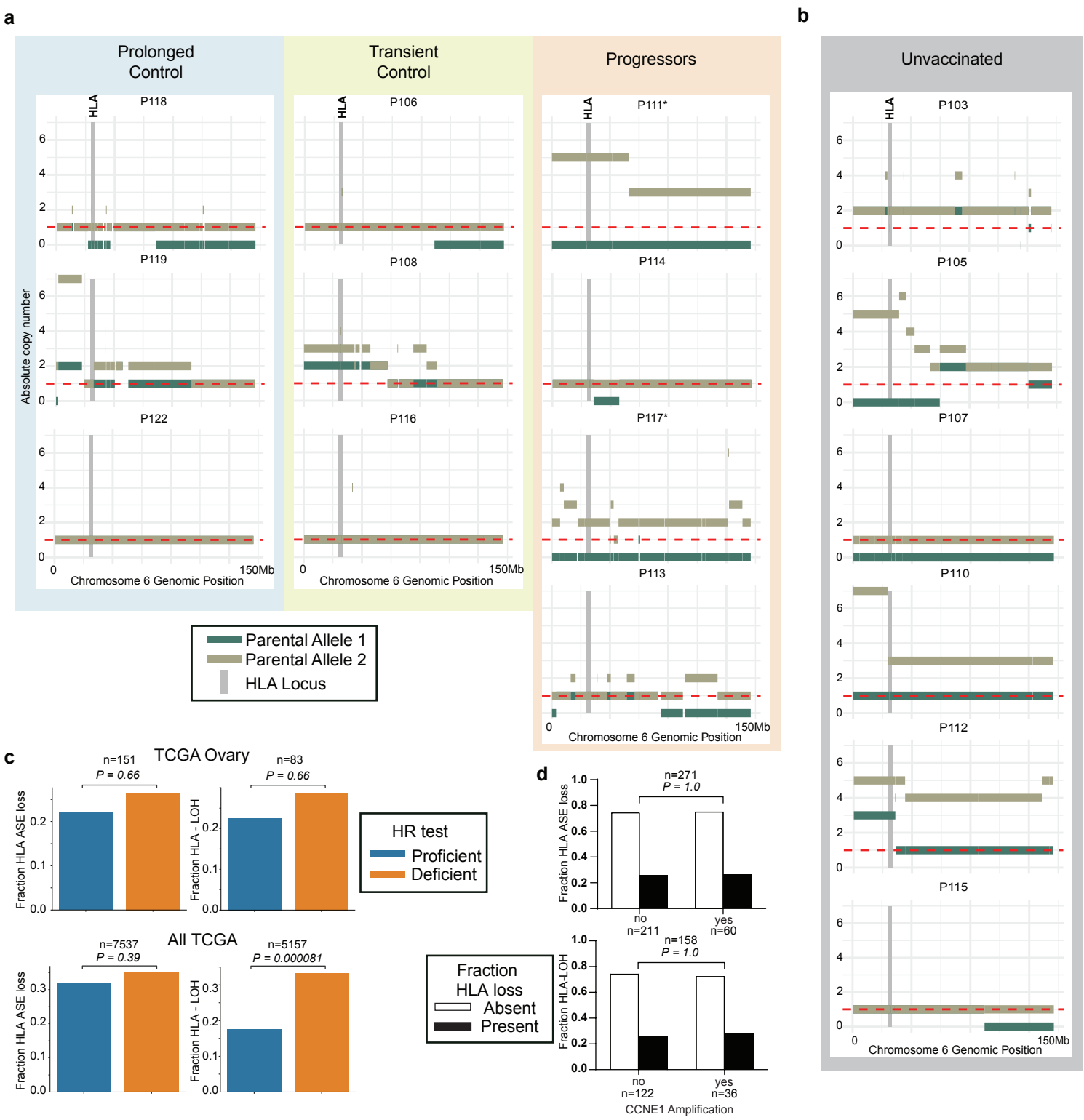

a
SFU/10^6 PBMC
P111
P114
P117
P113
P106
P108
P116
P118
P119
P122
Pool A
Pool B
Pool C
Pool D
W00 W03 W12 W14 W16 W20 W22 W26
Nivolumab:
NeoVax:
b
Post-NeoVax
Post-NeoVax
Induced Clone Count
Progressive
Prolonged
Transient
N/A
Patient ID
Number Expanded Clones
Progressive
Transient or Prolonged
c
Mean TCR UMI
Pre-Vax
Post-Vax
Post-Nivo
W40
Post-Vaccine
Post-Nivolumab

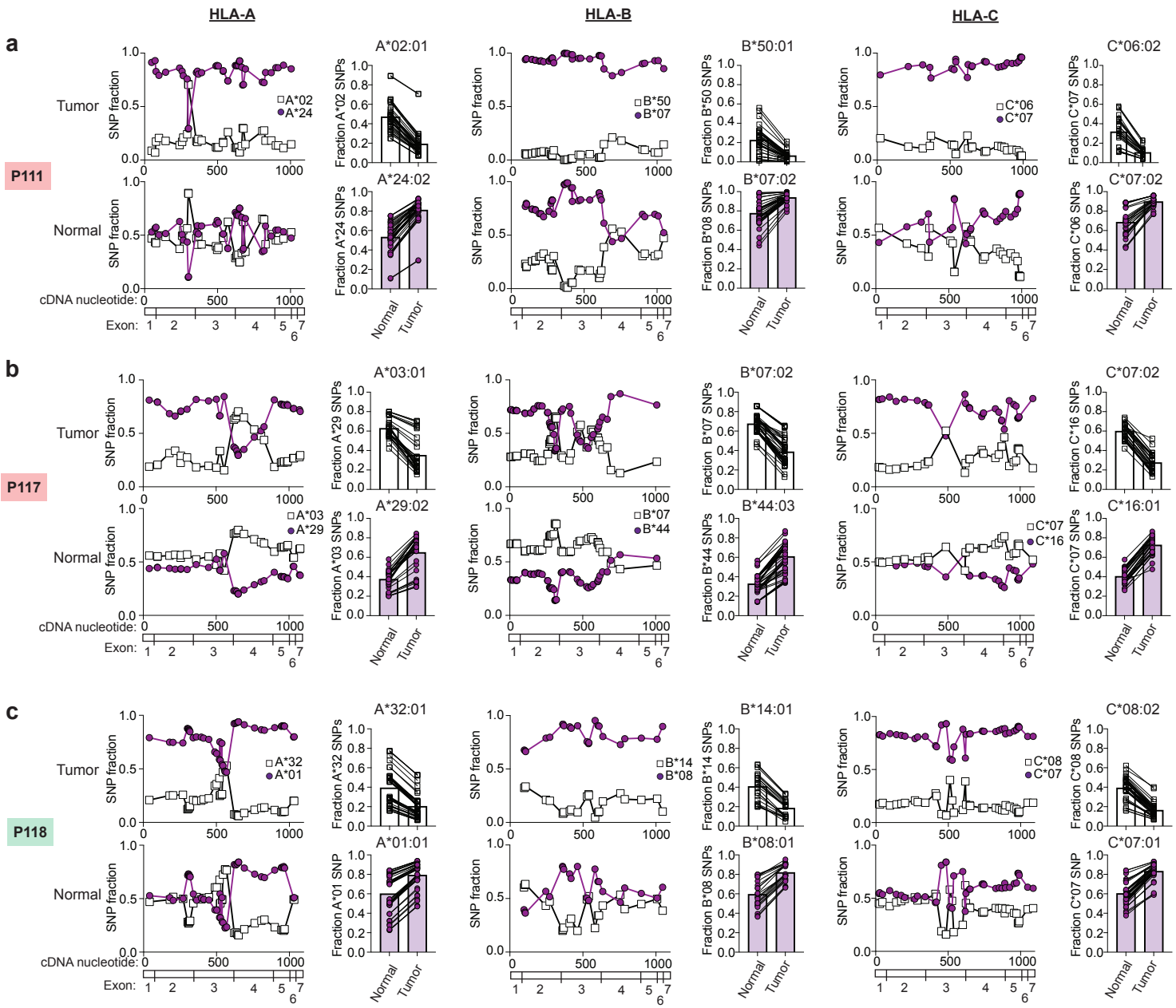

a
Progressors
Transient Controllers
Prolonged Controllers
p111
p106
p118
p114
p108
p119
p117
p116
p122
p113
SFU/10^6 PBMC
Week post-vaccine
W00
W14
W22
* >3x DMSO control + P ≤ 0.05 by DFR(EQ)
†† pre-existing, < 2.5x induction by vaccine
b
Progressors
Transient
Prolonged
Mutations
Pt #: 111 113 114 117 106 108 116 118 119 122
Vaccine target mutations: No response Response

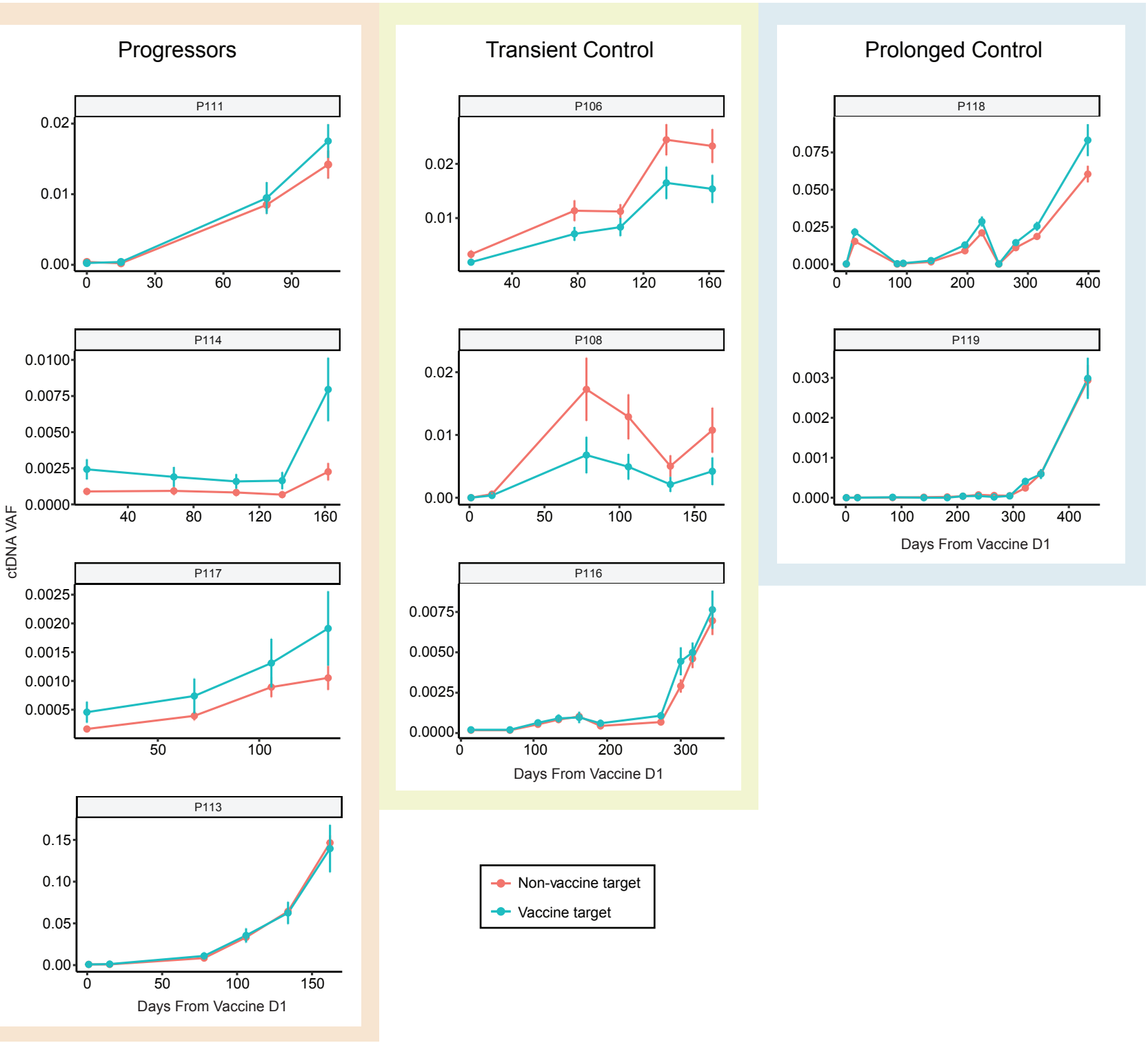

a
Endothelial cells
T cells
Fibroblasts
NK
Plasma cells
B cells
Tumor
DCs
Monocyte/ Macrophage
Patient
P111
P114
P117
P113
P116
P108
P112
Timepoint
B1
B2
B3
harmonysingletsumap_2
harmonysingletsumap_1
b
CD4
CD8
UMAP1
UMAP2
TPE
TEM
TReg
TTE
NR4A1+ TReg
Naive
TProl
TTE.1
TTE.2
TTE.3
TTE.4
c
Progressors
Transient controllers
No. TILs
T Cell Populations
Fraction
Biopsy timepoint
Cluster
CD4.Naive
CD4.TEM
CD4.TProl
CD4.TPE
CD4.TTE
CD4.TReg
CD4.NR4A1+ TReg
CD8.Naive
CD8.TEM
CD8.TProl
CD8.TPE
CD8.TTE
d
Biopsy 1 (Pre-Vax)
Biopsy 2 (Post-Vax)
Biopsy 3 (Post-Vax/Nivo)
Log10(rank)
Log10(frequency)
Not Exhausted
Exhausted
e
Pre-Vaccine (B1)
Post-Vaccine (B2)
Post-Vaccine (B3)
of Clones
Exhausted Fraction
CD4 vs CD8 Fractions
Exhaustion
exhausted
not exhausted
CD4vsCD8
CD4 total frequency
CD8 total frequency
f
p113 Tumor Reactive TCRs
p113 Vaccine Reactive TCRs
p113 TEM TCRs
Unselected
g
Fraction all TTE
Fraction TPE
Fraction TProl
Fraction TEM
Pre (B1)
Post (B2)
Post (B3)
DPP3 Neoantigen specific TCRs
TCR5
TCR6
TCR19
TCR20
Fraction TTE, TPE, TProl


a
Single cells
78.4%
FSC-H
FSC-A
Lymphocytes
50.5%
SSC-A
CD8+ T cells
77.8%
CD8-BV786
CFSE^neg 33.1%
CFSE^lo 34.6%
CFSE^hi 32.1%
CFSE
CFSE^hi
mTCRβ +
CD137+
93.2%
Count
CD137-PE
mTCRβ +
11.9%
TCR 5 (CFSE^negFR^loViolet^neg)
mTCRβ - PE-Cy7
CFSE^neg
CFSE^lo
CT-Far Red
NT
CT
Cell Trace (CT)-Violet
b
P108
NC1
TCRs
23
No target
Post-Vax PDO (B2)
No IFNγ
IFNγ
Irr Org
EBV-LCL
DMSO
Pool A
Pool B
Pool C
Pool D
PMA/Ionomycin
Phenotype
Post-vax EBV-LCL
0
50
% CD137+
c
P113
NC1 3
TCRs
25
No target
Pre-Vax PDO (B1)
No IFNγ
IFNγ
Post-Vax PDO (B2)
No IFNγ
IFNγ
Irr Org
EBV-LCL
DMSO
Pool A
Pool B
Pool C
Pool D
PMA/Ionomycin
Phenotype
Pre-vax
Post-vax
EBV-LCL
0
100
% CD137+
d
TCRs
NC2 5
TIL phenotype
Negative
T_EX
T_EM
TIL Reactivity
Negative
Borderline
Reactive
e
TCR 5
TCR 6
TCR 19
TCR 20
Pool A
Pool B
Pool C
Pool D
IMP-08
IMP-14
IMP-17
IMP-18
Pool C
0
90
% CD137+
f
IMP14: DAPPECFLTRRDTVLLRKESRKL
FLTRRDTVL (Mut)
FLTRLDTVL (Wt)
LTRRDTVLL (Mut)
LTRLDTVLL (Wt)
TRRDTVLLR (Mut)
TRLDTVLLR (Wt)
TCR5
TCR6
TCR19
TCR20
Percent CD137+
Peptide Concentration (10^-6-10^-4 pg/ml)


a
chr1:63,275,996-63,278,342 (Intergenic)
chr1:64,882,367-64,883,540 (JAK1)
b
Int-B-F
Int-B-R
Int-I-R
Int-I-R
Break point
JAK1-I-R
JAK1-C-F
JAK1-B-F
JAK1, Exon 3
JAK1-C-R
JAK1-I-R
JAK1-B-R
c
Pre-Vax PDO (B1)
Pre-Vax PDO (B1b)
Post-Vax PDO (B2)
Autologous EBV-LCL
H2O
500bp
300bp
200bp
100bp
Common (JAK1 C F/R)
JAK1 break (JAK1 B F/R)
Intergenic break (Int B F/R)
Inversion (Int-I-R/JAK1-I-R)
d
chr1:63,277,151-63,277,225 (Intergenic)
TAATATCACAGTAAATTAAATTCTATTTTAAAGGGTTTCTATTTAACAATCTGTCAGAATTTTCACAGCATTTGA
chr1:64,882,915-64,882,989 (JAK1)
AGGTGTTTTACGTAGCACCTCATCTAGTGCTGATATTATTCCAATTGTACAGATGTGGGGAAATGAGAACTGAGC
Inversion PCR product
e
Carboplatin
Doxorubicin
Carboplatin + Dorubicin
Viability (normalized CTG)
Log(mM)
log(mM)
B1 Pre-Vax PDO B1
Pre-Vax PDO B1b
Post-Vax PDO B2
f
PDO gating for HLA Staining: (Fig. 6c, ED Fig. 9g)
PDO gating for intra-cellular p-STAT1 Staining: (Fig. 6b, ED Fig. 9h)
SSC-A
FSC-A
Cells 21.5%
Cells 59.8%
FSC-W
FSC-H
FSC-Singlets 95.9%
FSC-Singlets 93.7%
SSC-W
SSC-H
SSC-Singlets 98.9%
SSC-Singlets 97.0%
g
P113 post-Vax PDO
Neg Med High
Negative
Medium
High
GFP
Mock
IFNγ
JAK1 -GFP
HLA-A/B/C - PacBlue
Percent mode
HLA A/B/C - PacBlue
h
P-STAT1 - AF647
P-STAT1 - AF647
i
TCR 5
No Target
Pre-Vax PDO (B1) + IFNγ
Post-Vax PDO (B2)
GFP
JAK1
IFNγ
EBV-LCL
PMA/ Ionomycin
0.14%
36.9%
3.30%
5.21%
7.17%
45.2%
1.54%
99.9%
CD137 - PE
j
TCRs: N 5 6 19 20 C
No Target
Pre-Vax PDO (B1)
Post-Vax PDO (B2)
EBV-LCL
PMA
% CD137+
k
No TCR
Ctl TCR
DPP3 specific
TCR 5
TCR 6
TCR 19
TCR 20
Fold CD137 induction (target: Pre-vax (B1) PDO)
No IFNγ
IFNγ
GFP
JAK1


a
Prolonged Control
Transient Control
Progressors
Unvaccinated
HLA
P118
P106
P111*
P103
P119
P108
P114
P105
P122
P116
P117*
P107
P113
P110
P112
P115
Absolute copy number
0
2
4
6
0
150Mb
Chromosome 6 Genomic Position
Parental Allele 1
Parental Allele 2
HLA Locus
b
c
TCGA Ovary
n=151
P = 0.66
n=83
P = 0.66
Fraction HLA ASE loss
Fraction HLA - LOH
HR test
Proficient
Deficient
All TCGA
n=7537
P = 0.39
n=5157
P = 0.000081
d
n=271
P = 1.0
no
n=211
yes
n=60
n=158
P = 1.0
n=122
n=36
CCNE1 Amplification
Fraction HLA-LOH
Fraction HLA loss
Absent
Present


HLA-A
HLA-B
HLA-C
a
P111
Tumor
Normal
SNP fraction
cDNA nucleotide:
Exon:
A*02
A*24
B*50
B*07
C*06
C*07
A*02:01
A*24:02
B*50:01
B*07:02
C*06:02
C*07:02
Fraction A*02 SNPs
Fraction A*24 SNPs
Fraction B*50 SNPs
Fraction B*08 SNPs
Fraction C*07 SNPs
Fraction C*06 SNPs
Normal
Tumor
b
P117
A*03
A*29
B*07
B*44
C*07
C*16
A*03:01
A*29:02
B*07:02
B*44:03
C*07:02
C*16:01
Fraction A*29 SNPs
Fraction A*03 SNPs
Fraction B*07 SNPs
Fraction B*44 SNPs
Fraction C*16 SNPs
Fraction C*07 SNPs
c
P118
A*32
A*01
B*14
B*08
C*08
C*07
A*32:01
A*01:01
B*14:01
B*08:01
C*08:02
C*07:01
Fraction A*32 SNPs
Fraction A*01 SNP
Fraction B*14 SNPs
Fraction B*08 SNPs
Fraction C*08 SNPs
Fraction C*07 SNP


Progressors
Transient Control
Prolonged Control
P111
P114
P117
P113
P106
P108
P116
P118
P119
ctDNA VAF
Days From Vaccine D1
Days From Vaccine D1
Non-vaccine target
Vaccine target